LA-11294-MS

C.3

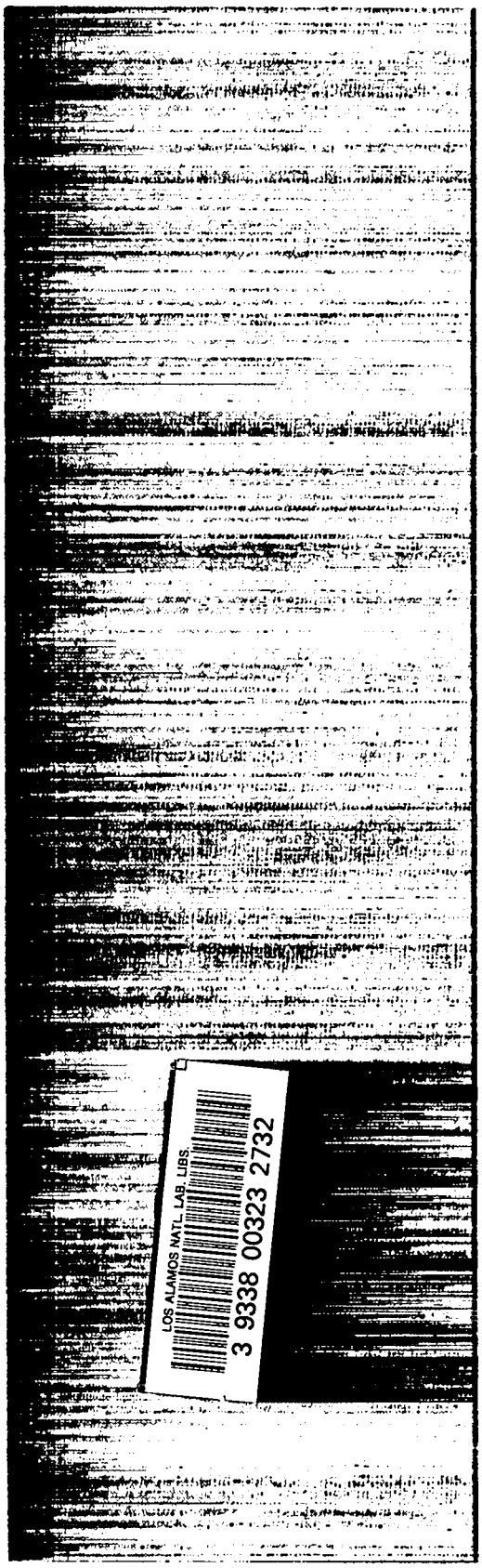

Numerical Simulation of the Simultaneous Detonation of Two Identical, Fully Contained Explosions

Los Alamos

Los Alamos National Laboratory is operated by the University of California for the United States Department of Energy under contract W-7405-ENG-36.

This work was supported by the US Department of Energy, Nuclear Weapons Applications and Planning.

An Affirmative Action/Equal Opportunity Employer

LA-11294-MS

UC-2
Issued: July 1989

Numerical Simulation of the Simultaneous Detonation of Two Identical, Fully Contained Explosions

Bruce C. Trent

Los Alamos National Laboratory
Los Alamos, New Mexico 87545

CONTENTS

NUMERICAL SIMULATION OF THE SIMULTANEOUS DETONATION OF TWO IDENTICAL, FULLY CONTAINED EXPLOSIONS

by

B. C. Trent

ABSTRACT

It has been proposed that a multiburst environment may have certain advantages over a single burst for driving a stress wave with given characteristics to a particular depth. This report describes a numerical study performed with the SHALE code to look at the simultaneous detonation of two fully contained, identical 500-kt bursts. Calculations are presented that show the distance a given peak stress is propagated in a low-porosity, saturated limestone and how this distance is enhanced if the stress waves from two bursts, with known separation, are allowed to interact.

I. INTRODUCTION

The SHALE code is an explicit finite-difference computer program for simulating stress wave propagation and interaction as described by Demuth et al. (1985). The constitutive model predicts brittle fracture and volumetric compaction of geologic materials (see Margolin and Smith, 1984). It has been used by DeVault (1987) and Margolin et al. (1988) to simulate underground nuclear explosions and the associated ground motion to the earth's surface. The detonation of two equal sources is relatively easy to model with the SHALE code. One symmetry axis and one reflection boundary condition exist, so only a single explosive source needs to be modeled.

This report gives detailed information on the calculational results in a saturated material and in a material with one-half percent air-filled voids. Zoning and boundary conditions are discussed along with time histories of various stress components. Previous simulations of a multiburst environment simply superimpose the results of single bursts. The mathematical basis for this and a discussion of some potential pitfalls are presented. One-dimensional calculations were done to apply this technique and evaluate its accuracy

with respect to fully two-dimensional calculations. Also, the stress field of a single 1-Mt burst has been compared with the peak stresses and with the "footprint" generated by two separated 500-kt bursts. The results are discussed in light of the assumptions and limitations of the modeling effort. A summary gives an overview and suggests where some additional numerical and analytic work might be worthwhile.

II. TWO-DIMENSIONAL MULTIBURST CALCULATIONS

Several simplifying assumptions were made in these first numerical simulations. The effects of the stress wave interaction should first be fully understood before considering the complications of a free surface, gravity, unequal yields, and differences in timing. This simplest case was easily performed with the existing version of SHALE since the symmetry of the problem resembles a containment calculation of an explosion above a very hard rock layer.

A. Initial Conditions

A conceptual model is shown in Fig. 1 where two explosive sources are illustrated. Clearly two axes of symmetry exist if the following conditions are satisfied: 1) both are detonated at the same time, 2) both are of equal yield, 3) the medium is homogeneous and isotropic, and 4) there is a uniform initial stress field. The explosion of two sources in two different media were considered: the baseline case is for a saturated limestone and the other case is for a limestone with one-half percent air-filled voids. The material properties are given in Table I.

Notice that the unsaturated matrix has a slightly lower bulk density. This reflects the slight decrease in water weight, resulting in a lower net bulk density. The total void volume (air plus water) remains the same. Poisson's ratio for both materials was 0.32. A crushing strength of 47.5 MPa (0.475 kbar) was also specified in both cases. Above this pressure, irreversible inelastic volume reductions occur.

B. Mesh Zoning

Figure 2 shows how a single source may be modeled such that the horizontal reflection plane causes a situation identical to Fig. 1. The mesh for a standard containment problem is shown in Fig. 3. The coordinates in this figure are radial (x) and vertical (y) where the

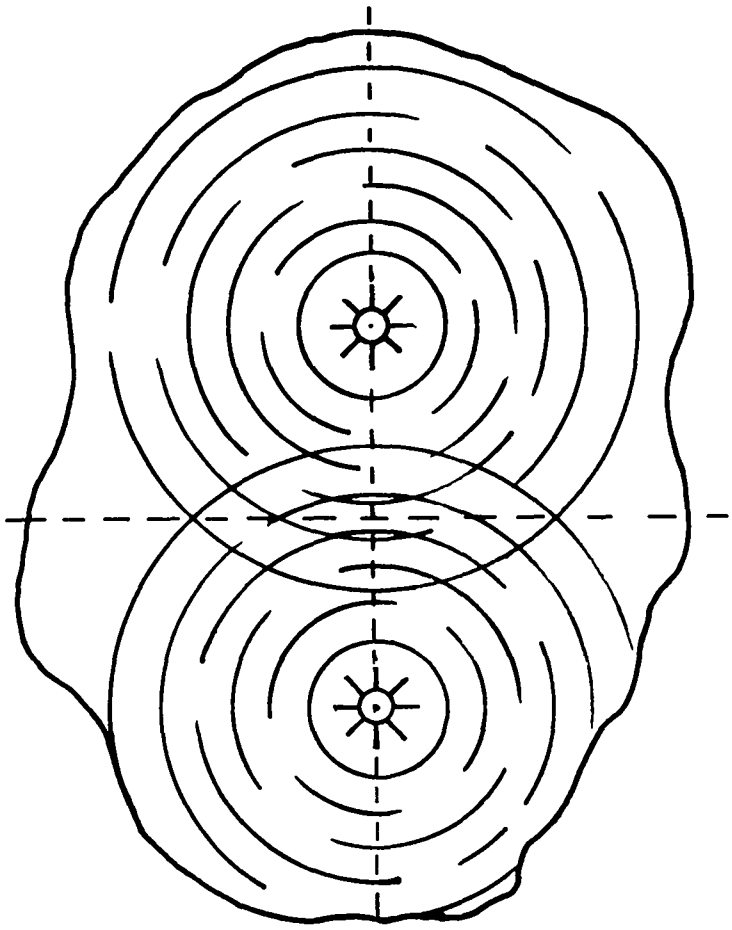

Fig. 1. Conceptual drawing of two sources detonated simultaneously.

TABLE I. Material Property Data for the Two Uniform Materials

Bulk Material	Bulk Density (g/cc)	Grain Density (g/cc)	Water Content (wt %)	Sound Speed (m/s)	Air-Filled Voids (vol %)	Total Voids (vol %)	Saturation (vol %)
Saturated	2.495	2.750	5.830	4500	0.016	14.56	99.89
0.5% air voids	2.490	2.750	5.646	4500	0.504	14.56	96.54

y-axis is a line of cylindrical symmetry. The mesh has 31 radial cell boundaries, or i-lines, and 226 tangential lines, or j-lines. Figure 3 may be mapped into a rectangular "logical" grid in i-j space, bounded by four boundaries as illustrated in Fig. 4. Typically, the logical left side is simple free slip, or roller boundary, allowing vertical but no horizontal motion.

The logical bottom is fixed such that no motion is allowed. In this case it consists of a single point where all of the radial lines converge at the center of the source. The logical right side allows vertical motion but no horizontal displacements exactly like the left side. The top, which wraps around from the farthest point directly above the source to the farthest point directly below the source, is usually unconstrained for that portion corresponding to the free surface and fixed for all points with a nonzero depth.

The calculational mesh for the simultaneous detonation case is shown in Fig. 5. A separation distance of 200 m was chosen, somewhat arbitrarily, since information was to be obtained up to 600 m away. The limits of the mesh are 100 m from the source to the horizontal axis of symmetry (one-half of the spacing), 900 m along this axis, and 800 m from the source vertically upward. The mesh is elliptical since it gives the impression of elliptical circumferential lines intersecting the two axes of symmetry. Initially there are 25 radial (i-lines) and 212 circumferential (j-lines) cell boundaries. The first i-line is vertical and allows motion only in the vertical direction. The last (i=25) is also a "free-slip" or roller boundary, but the motion is vertical along the axis of cylindrical symmetry and horizontal along the reflection axis. The stagnation point (initially j=117) is fixed. The mesh zoning consists of seven regions. The first consists of spherical zones, each spaced at 0.2-m intervals to a distance of 10 m. Then from j=51 to j=105 the zone spacing increases geometrically by a factor of 1.05 out to a distance of 60 m. This ratio continues to 100 m and j=117, but the circumferential boundary at i=17, j=117 to the stagnation point (i=25, j=117) is linear instead of circular. Additional regions are defined with radial boundaries at 150, 200, 300, and finally 800 m, all of which terminate on the reflection axis (i=25). Notice that the logical top now only extends from the top of the grid until the intersection of the horizontal axis of symmetry. That axis is now part of the logical left side. The corner directly below the source is fixed (the stagnation point), and the section above allows vertical motion and the boundary to the right allows horizontal motion. Since this is logically one continuous boundary (the left side), some minor code modifications had to be made. The aspect ratio of zones in the region of highest expected stress is very nearly one and the cell size growth is gradual. If the twofold symmetry is utilized, the implied zoning of two separate sources is shown in Fig. 6.

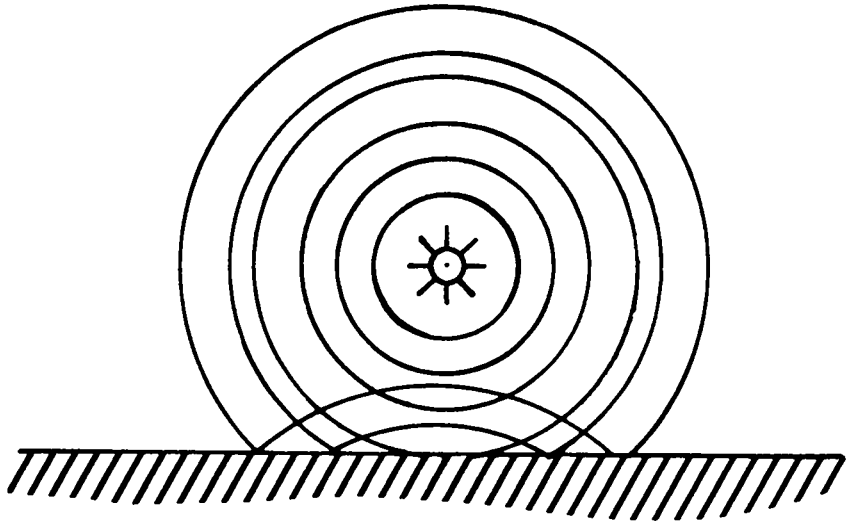

Fig. 2 Single source showing an axis of cylindrical symmetry and a reflection plane boundary condition.

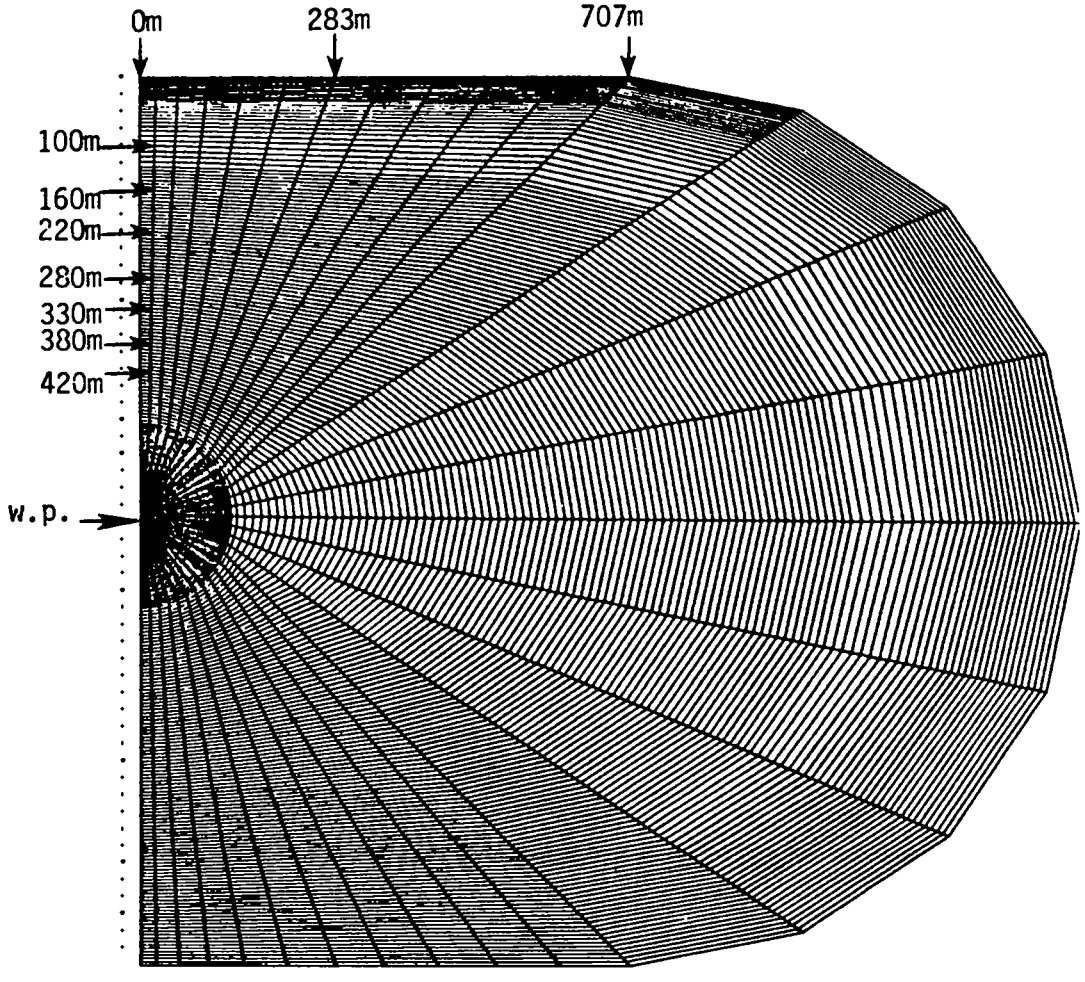

Fig. 3. Numerical mesh for a typical containment calculation.

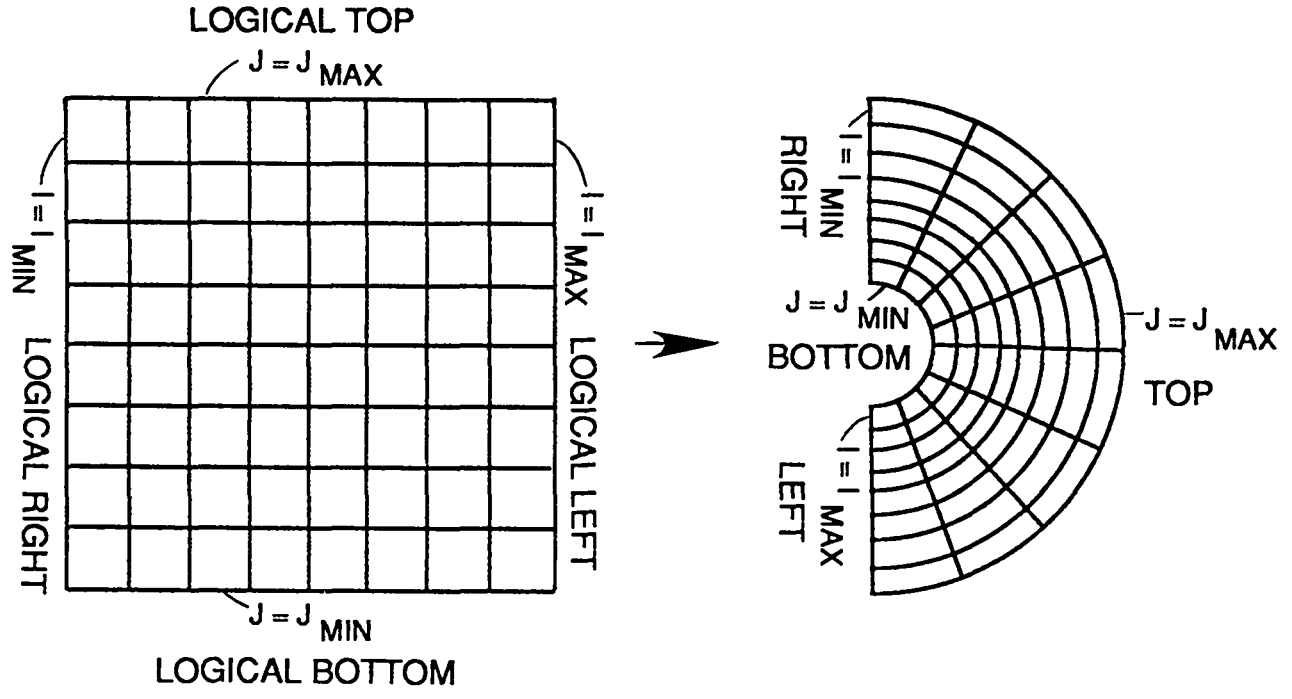

Fig. 4. Logical grid in i-j space and distortion for a grid as shown in Fig. 3.

C. Numerical Results

The yield for (each) source is 500 kt and the separation distance is twice 100 or 200 m. To make comparisons between saturated and unsaturated material and to evaluate the linear superposition technique, pressures and peak stress components were calculated and plotted. Peak overstress was also determined to measure the distance a signal of a given strength had traveled. The calculational results presented in the following sections consist of time histories at selected locations (see Fig. 7) as well as contour and surface projection plots of certain variables over selected areas of the calculational mesh.

1. Fully Saturated Limestone. Figures 8a-f show time histories of pressure along the reflection axis (y = -900 m) every 100 m. The solid lines represent the behavior in saturated material. The dashed lines are for limestone with one-half percent air-filled voids and will be discussed in the next section. Notice there is only a single pulse; at these locations the distance to each source is equal. The first station at a range from the point of double symmetry of 100 m shows a peak pressure of 2240 MPa (22.4 kbar). The rise times are similar here and at a range of 200 m, shown in Fig. 8b. A small precursor may

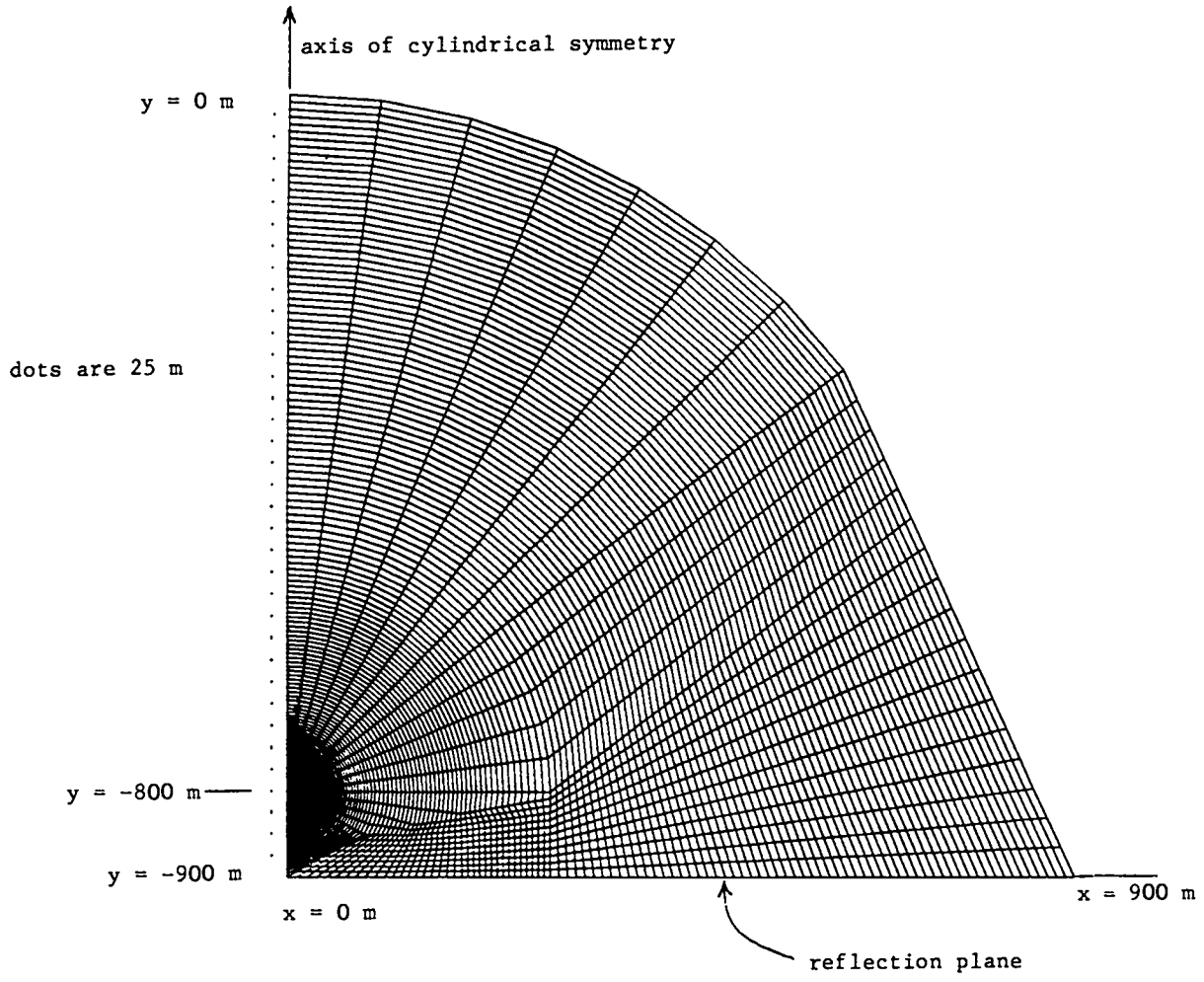

Fig. 5. Calculational mesh for the simultaneous detonation of two identical explosions. Notice the axis of symmetry, the reflection plane, and the elliptical shape of the outer circumferential lines.

be seen in Fig. 8c. This reflects the elastic range of the combined pulse that travels at a slightly faster acoustic speed. The relative magnitude of the elastic portion has increased at a range of 400 m as indicated in Fig. 8d. Figures 8e and 8f show the pulse at 500 and 600 m, respectively. The first arrival at 600 m is at 113 ms. The maximum time that the calculation could be run is 200 ms, at which time the stress wave reaches the end of the mesh. The most prominent feature of Figs. 8a-f is the smooth, continuous rise and drop-off at each location. Recall from Table I that air occupied only one hundredth of one percent

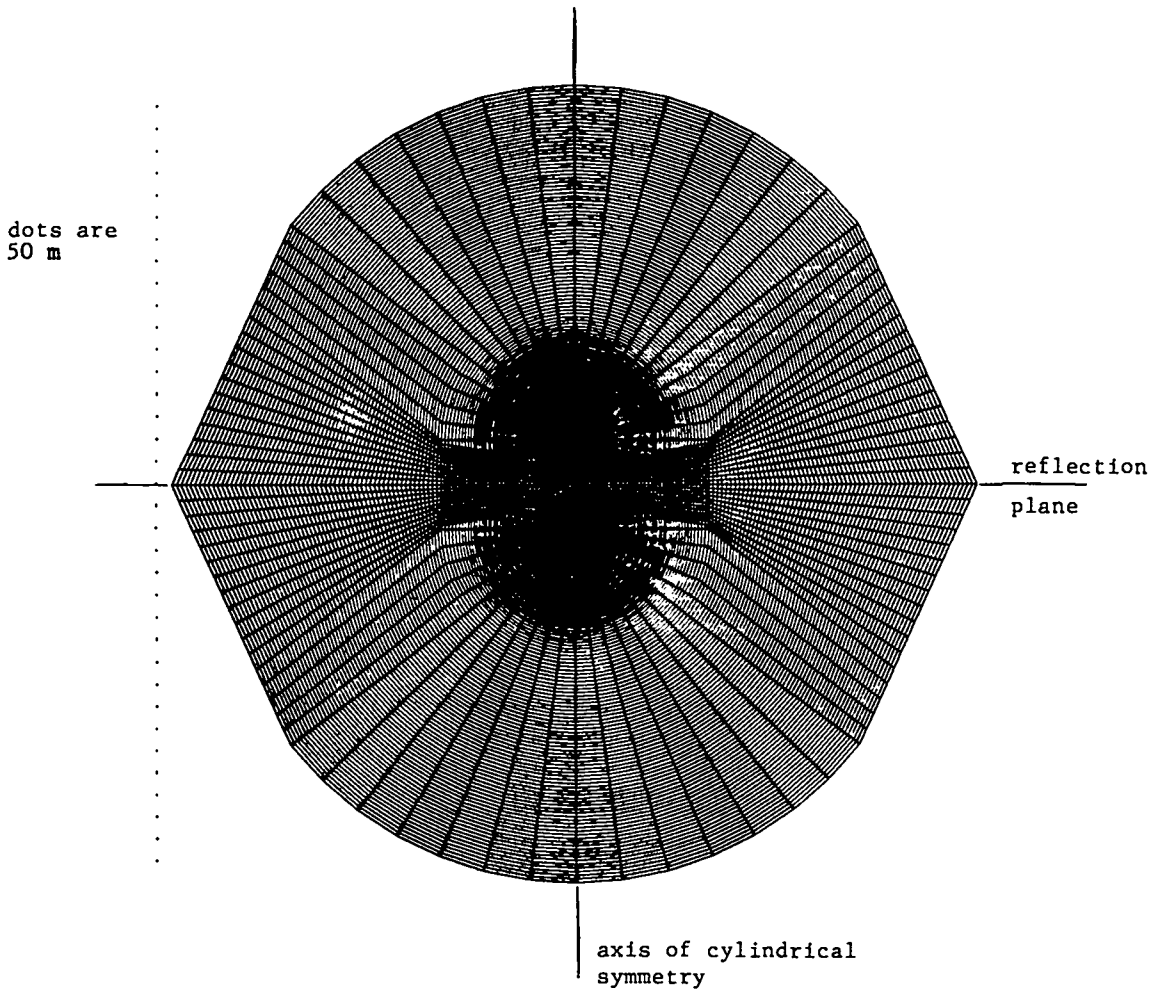

Fig. 6. The elliptical mesh in Fig. 5 plus the three images implied by the symmetry.

of the total volume, so no significant compaction could take place.

The next series of time histories is at the same elevation as one of the bursts. An angle theta is defined counterclockwise positive from a horizontal line parallel to the reflection axis and through the source. Figures 9a-f represent the response along the theta=zero line (see Fig. 7). The effects of the two distinct bursts are clearly seen in Figs. 9a and 9b, 100 and 200 m from the nearest source, respectively. The location of the cell in 9a is actually 40% closer than the zone corresponding to the record in Fig. 8a. This is reflected in the higher amplitude and the sharper pulse width. The second pulse arrives at about 20 ms and has traveled through compacted, or preconditioned, rock. The significance of this will be shown later during the discussion of superposition. The second pulse is of a similar

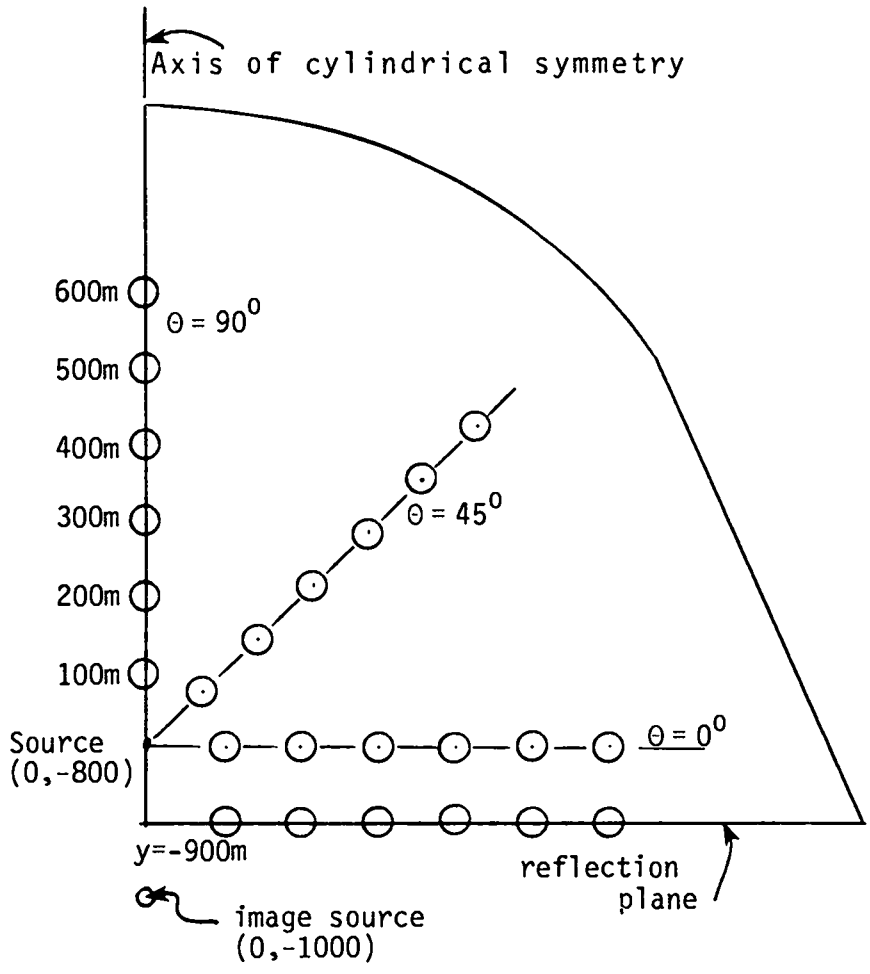

Fig. 7. Locations of the time history stations for Figs. 8, 9, 10, 11, 34, 35, 36, 39, 40, and 41.

magnitude in Fig. 9b, but at a range of 300 m in Fig. 9c both pulses have merged together. This is mainly due to the longer pulse width of the closest source at greater distances. By the time the signal has gone 400 m as illustrated in Fig. 9d, the shape looks similar to the response on the axis in Fig. 8d. In fact, the magnitude of the peak is 89.3% of that pressure profile. The distance to each source in Fig. 8d is 412 m. The responses in Figs. 9e and 9f also show single-source-like behavior.

Various histories along the theta=45° line are given in Figs. 10a-f. The responses are similar to the theta=zero data in Figs. 9a-f. Arrival of the second pulse is clearly shown up through the 500-m station (Fig. 10e) because the distance from the second (reflected) source becomes significantly greater as the range increases. Notice that the peak values at the 100- and 200- m depths agree well with the corresponding values in Figs. 8a and 8b

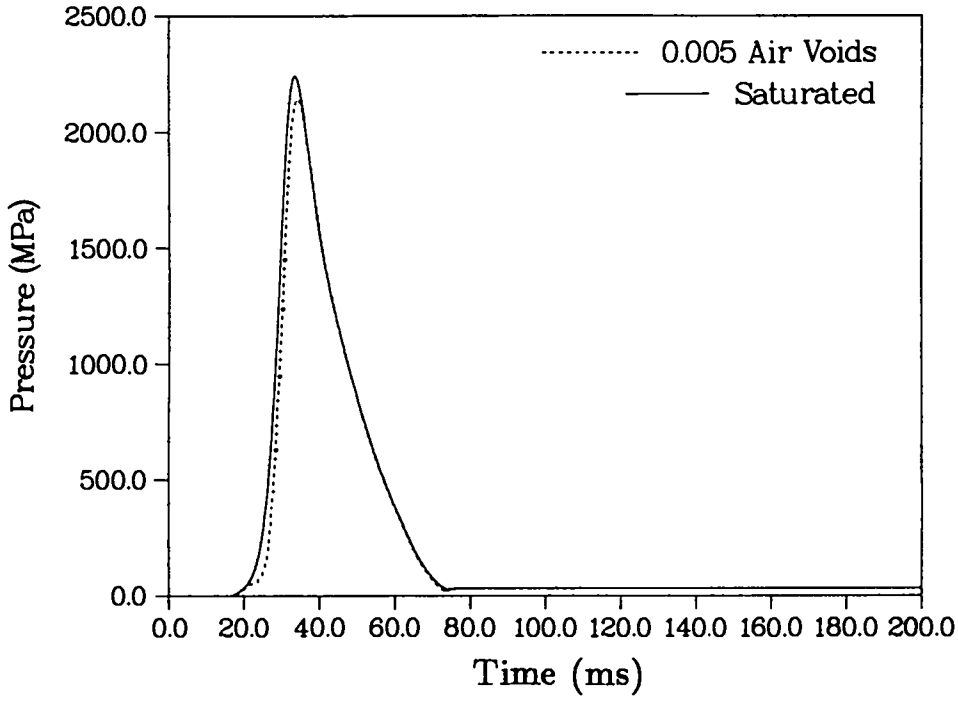

Fig. 8a. Pressure time histories for saturated and unsaturated limestone at a location of x = 100 m, y = -900 m. This is along the reflection axis. Both curves show similar response since the stresses are so great.

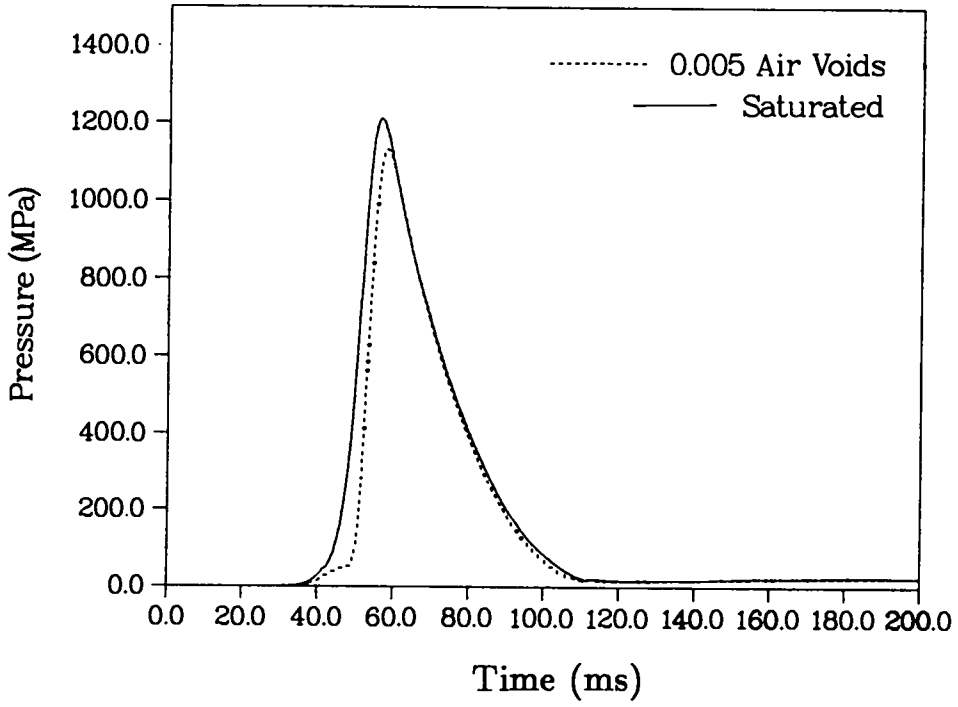

Fig. 8b. Pressure time histories for saturated and unsaturated limestone at a location of x = 200 m, y = -900 m. This is along the reflection axis. The unsaturated signal lags a bit, and the peak is slightly lower.

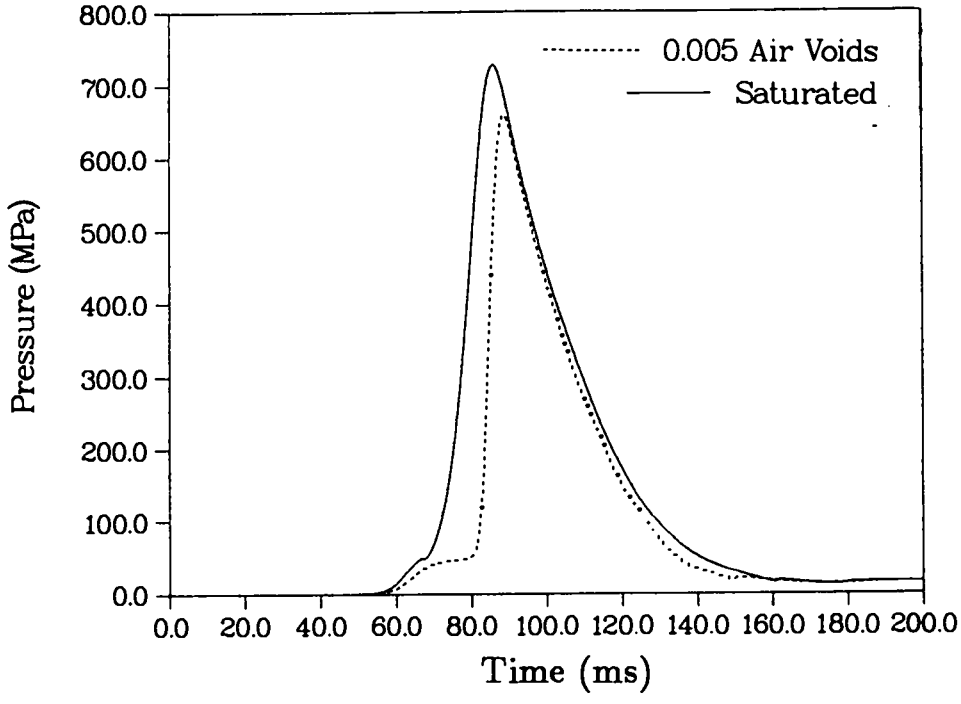

Fig. 8c. Pressure time histories for saturated and unsaturated limestone at a location of x = 300 m, y = -900 m. This is along the reflection axis. There is more pronounced material crushing in the unsaturated case.

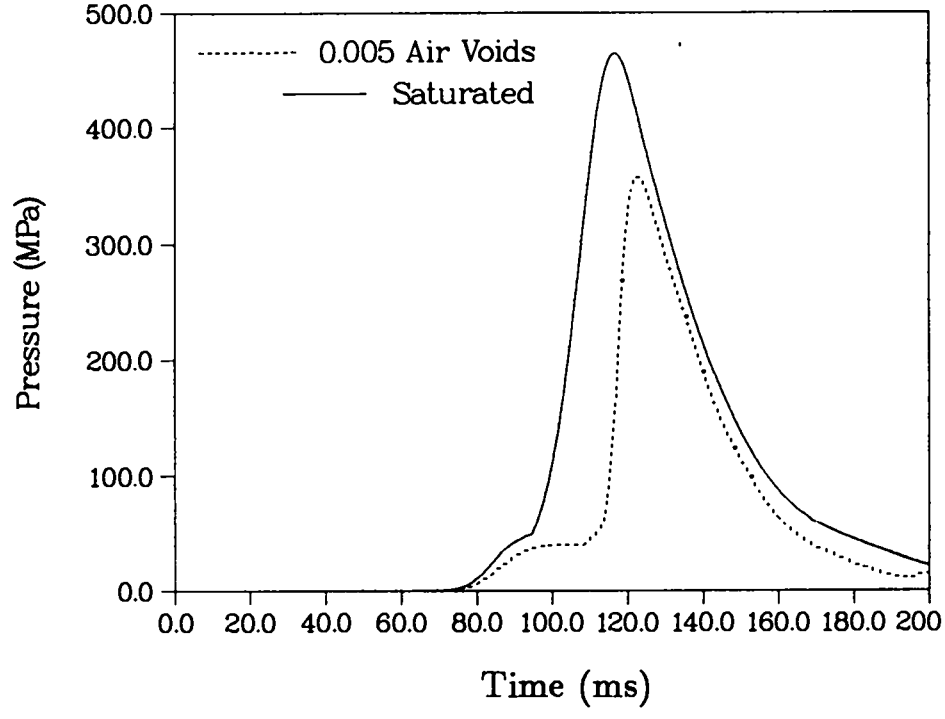

Fig. 8d. Pressure time histories for saturated and unsaturated limestone at a location of x = 400 m, y = -900 m. This is along the reflection axis. The peak pressure is much lower and it arrives later in unsaturated material.

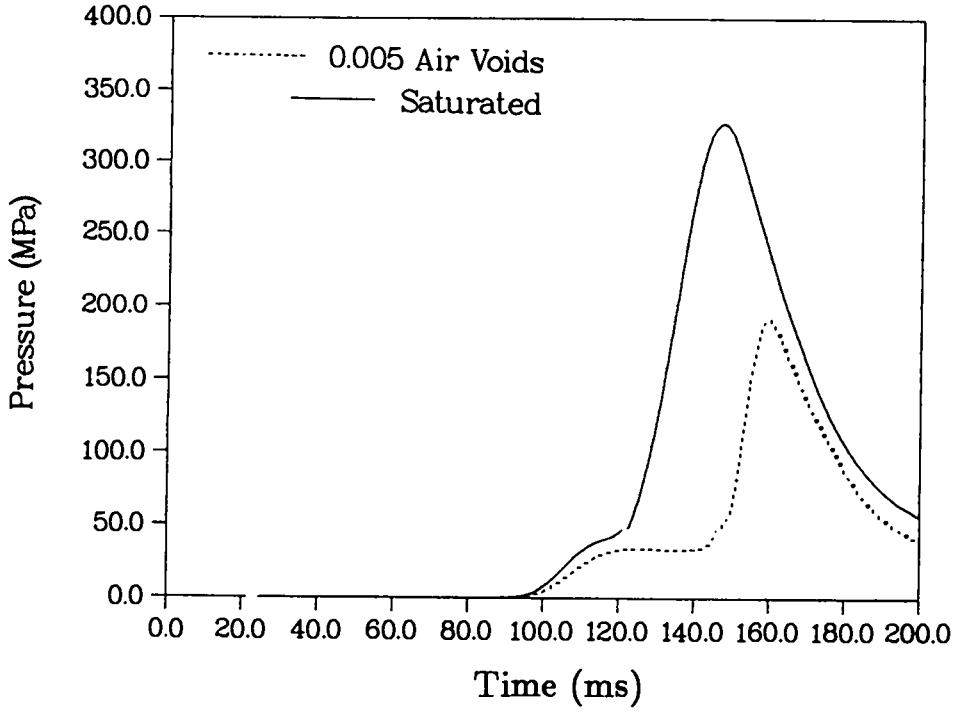

Fig. 8e. Pressure time histories for saturated and unsaturated limestone at a location of x = 500 m, y = -900 m. This is along the reflection axis. The crushing strength in unsaturated material is a significant fraction of the peak.

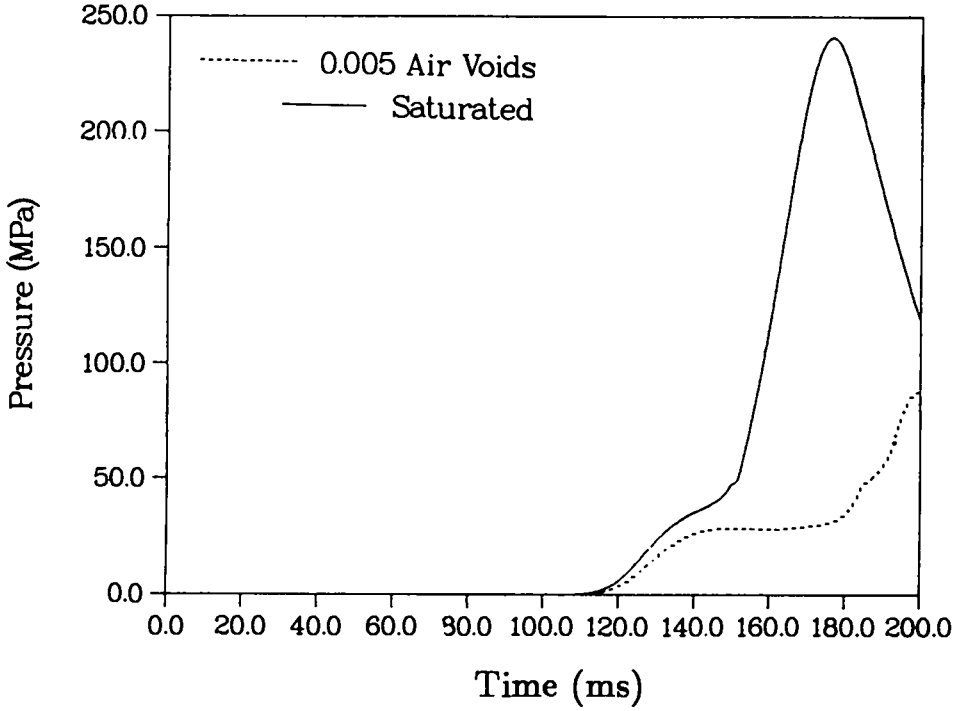

Fig. 8f. Pressure time histories for saturated and unsaturated limestone at a location of x = 600 m, y = -900 m. This is along the reflection axis. The peak pressure in the unsaturated material has not arrived, even at 200 ms.

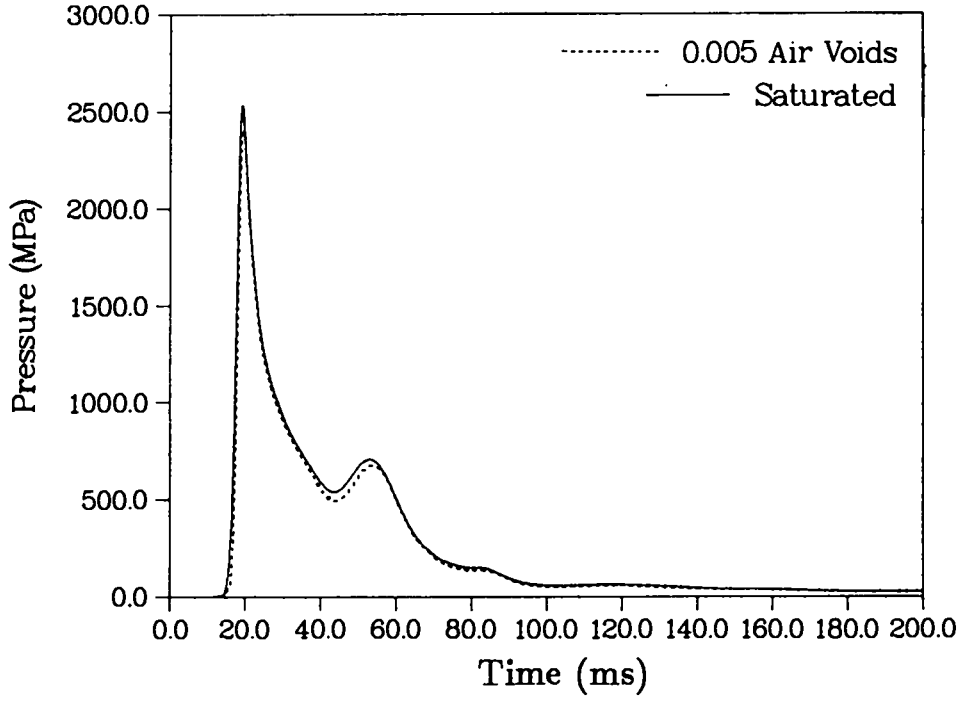

Fig. 9a. Pressure time histories for saturated and unsaturated limestone at a location of x = 100 m, y = -800 m. This is along the theta=zero line (adjacent to a source). Note the arrival of the second signal.

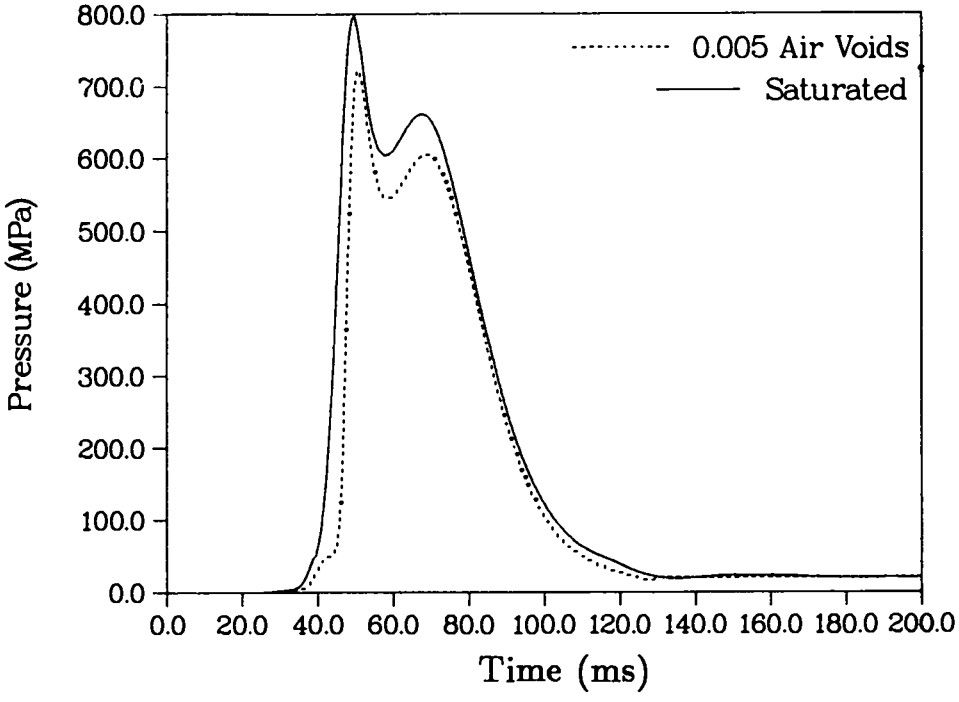

Fig. 9b. Pressure time histories for saturated and unsaturated limestone at a location of x = 200 m, y = -800 m. This is along the theta=zero line (adjacent to a source). Peak pressure is still governed by the first signal only.

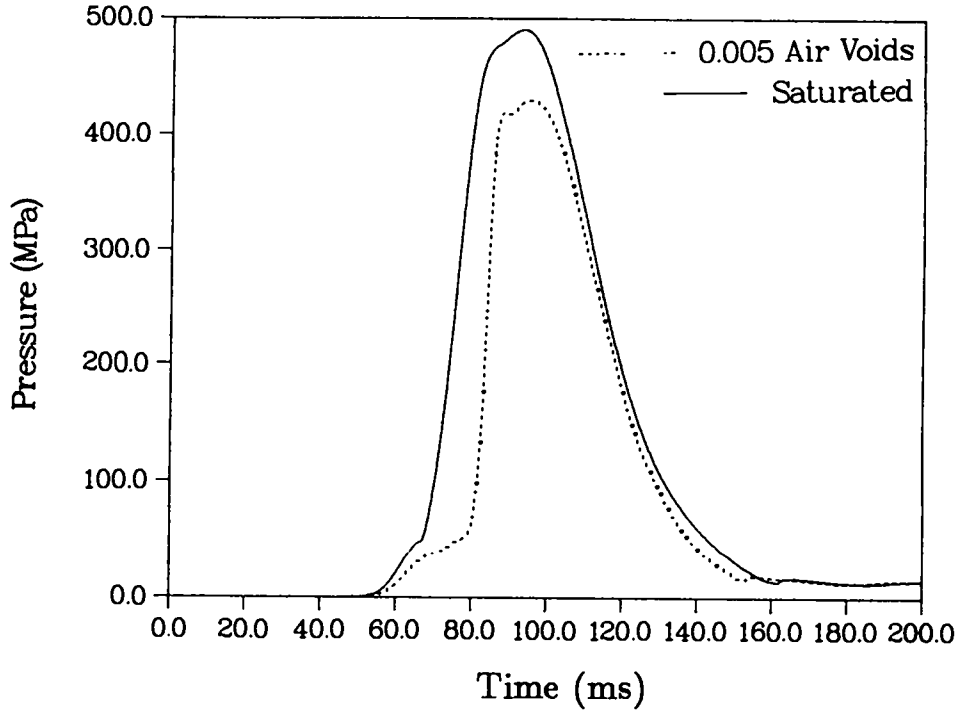

Fig. 9c. Pressure time histories for saturated and unsaturated limestone at a location of x = 300 m, y = -800 m. This is along the theta=zero line (adjacent to a source). Both signals have merged into one.

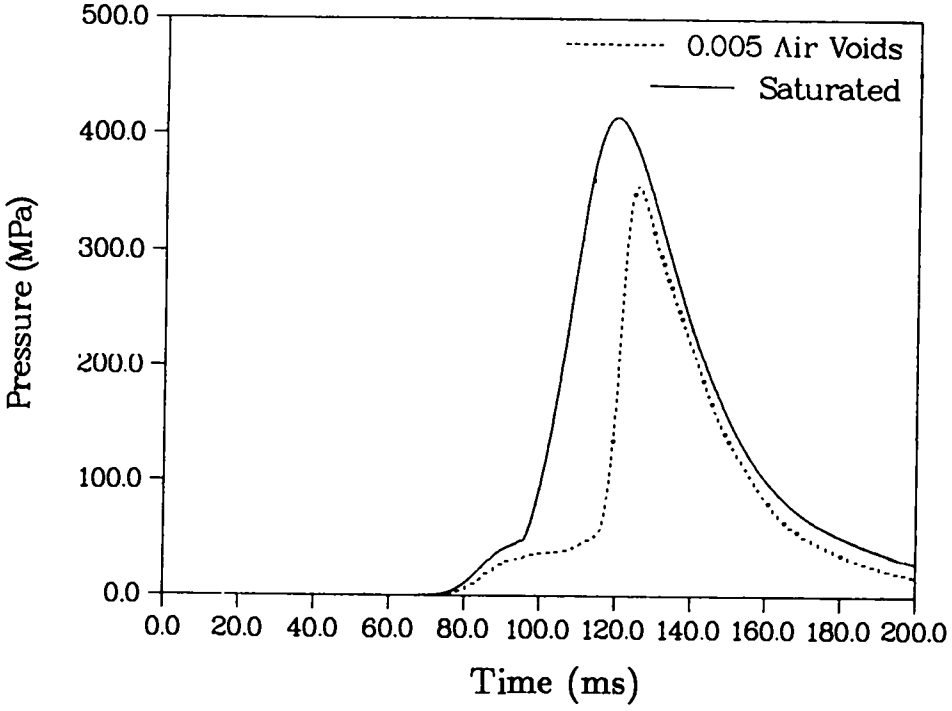

Fig. 9d. Pressure time histories for saturated and unsaturated limestone at a location of x = 400 m, y = -800 m. This is along the theta=zero line (adjacent to a source). Magnitude is lower and arrives later for unsaturated case.

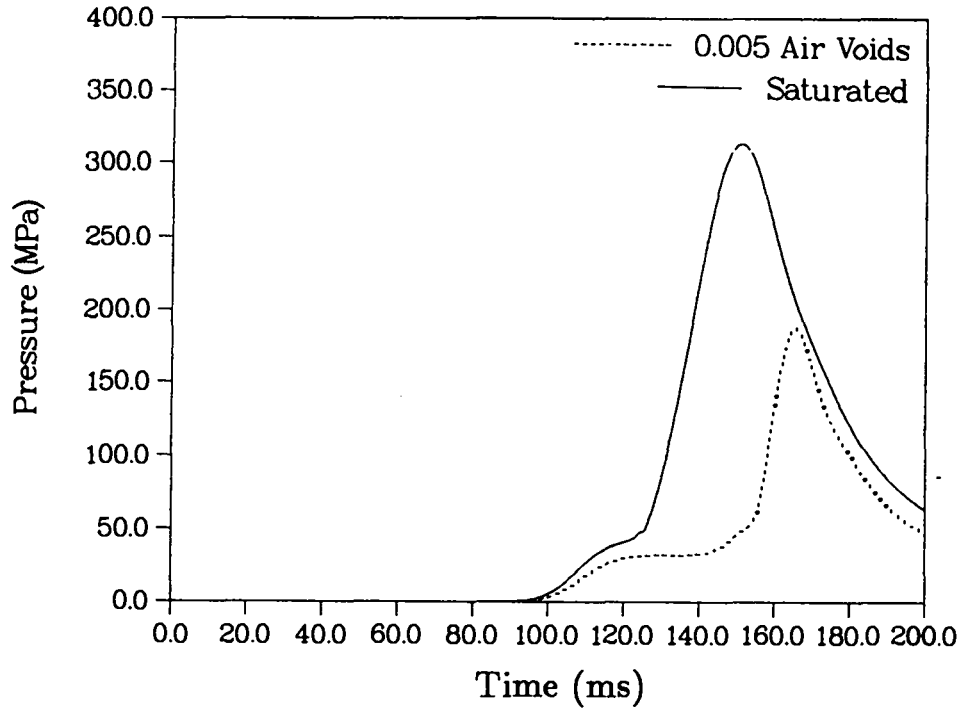

Fig. 9e. Pressure time histories for saturated and unsaturated limestone at a location of x = 500 m, y = -800 m. This is along the theta=zero line (adjacent to a source). Much smaller combined signal in unsaturated material.

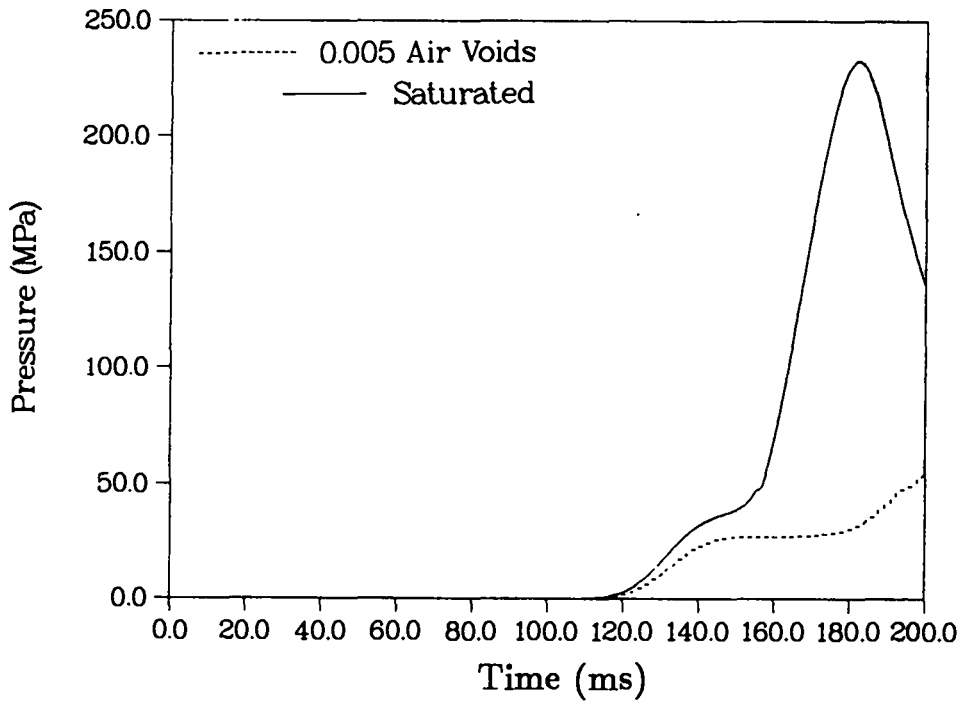

Fig. 9f. Pressure time histories for saturated and unsaturated limestone at a location of x = 600 m, y = -800 m. This is along the theta=zero line (adjacent to a source). Unsaturated peak will arrive much later than 200 ms.

since the response up to that point is from a single (one-dimensional) source. Pseudo one-dimensional response to 600 m is shown in Figs. 11a-f (theta=90°). These are time histories taken at points directly above the first source so that most of the record is due only to that burst. The distance to the second source is always 200 m farther than the first. Also, the cavity "shields" any direct reflection from the boundary, so any influence from the second source occurs from indirect refraction. Cavity growth at 200 ms was nearly complete, and the cavity was slightly elliptical because of the reflection boundary. Its semi-major and semi-minor axes were roughly 166 m (vertical) by 176 m, resulting in an average cavity radius of 86 m. The pressure record at 100 m from the closest source is shown in Fig. 11a. Notice the arrival of the signal from the second source at about 90 ms and its relatively low amplitude. The peak amplitudes of Figs. 11a-f compare well with the records from the theta=zero line in Figs. 10a-f. The differences are minor and may be attributed to slight boundary effects along the theta=90° line. The pseudo one-dimensional results in Figs. 11a-f will be compared with true one-dimensional pressure histories in a later section.

The evolution of the calculational variables is of interest since it shows how cavity growth and pore collapse proceed. Figures 12a-j show plots of the different material states at 10, 15, 25, 50, 75, 100, 125, 150, 175, and 200 ms, respectively. Similar plots for the case of one-half percent air-filled voids are shown at equivalent times for comparison in Figs. 19a-j. At 10 ms the two sources are acting independently. The stress waves first come into contact at about 15 ms. The symmetry of this calculation requires that a stagnation point exist at the point where the two axes of symmetry intersect. Since the velocity of this point is always zero, stresses accumulate rapidly and in fact become so great that this region acts like a third source as material moves laterally into less compacted material. This effect is observed at 25 and 50 ms where the shape of the crushed-out region loses its "figure 8" shape (as it would appear if the three images were shown) and becomes more elliptical. At 50 ms the region of completely crushed-out pores begins to look more circular than elliptical, and by 100 ms the stress wave has traveled nearly 500 m and significant cracking has taken place in the solid material between the two sources. The evolution of this pattern is shown to 200 ms in Figs. 12e-j. In this case of nearly 100% water saturation, the location of the boundary of crushed-out pore space is essentially the shock front.

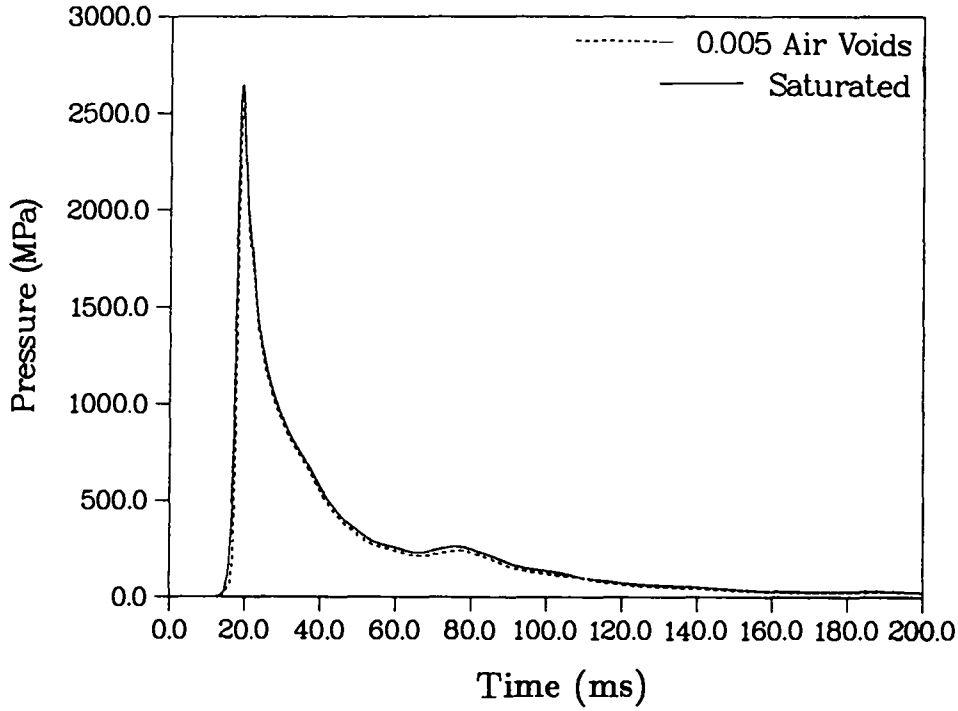

Fig. 10a. Pressure time histories for saturated and unsaturated limestone at a range of 100 m and along the theta=45° line. Nearly identical signals in both cases.

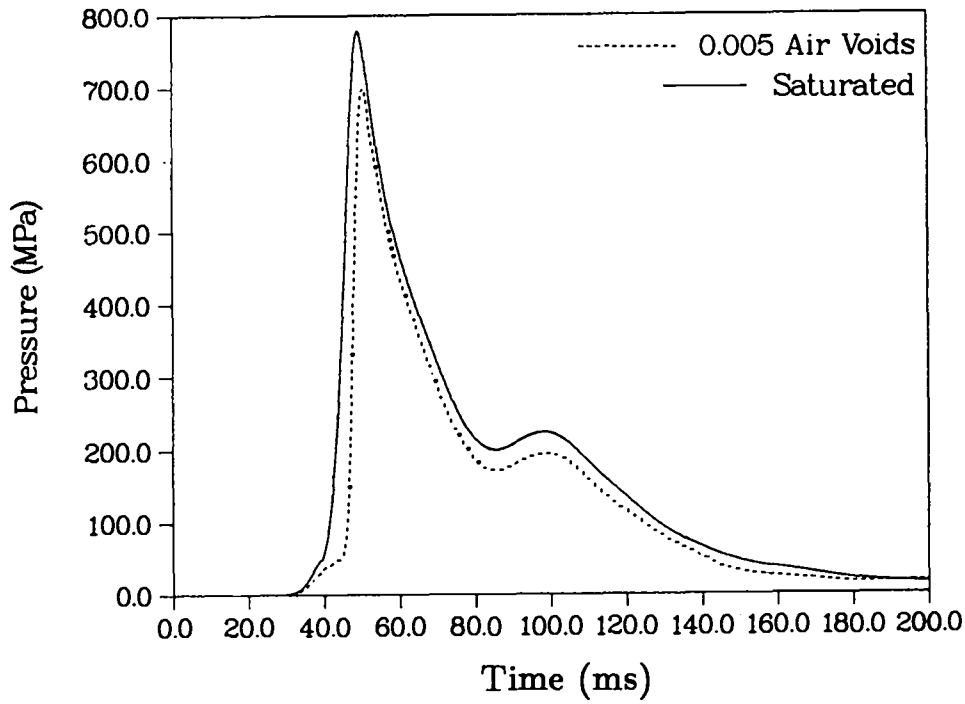

Fig. 10b. Pressure time histories for saturated and unsaturated limestone at a range of 200 m and along the theta=45° line. Notice much smaller influence of second source because of its much greater distance.

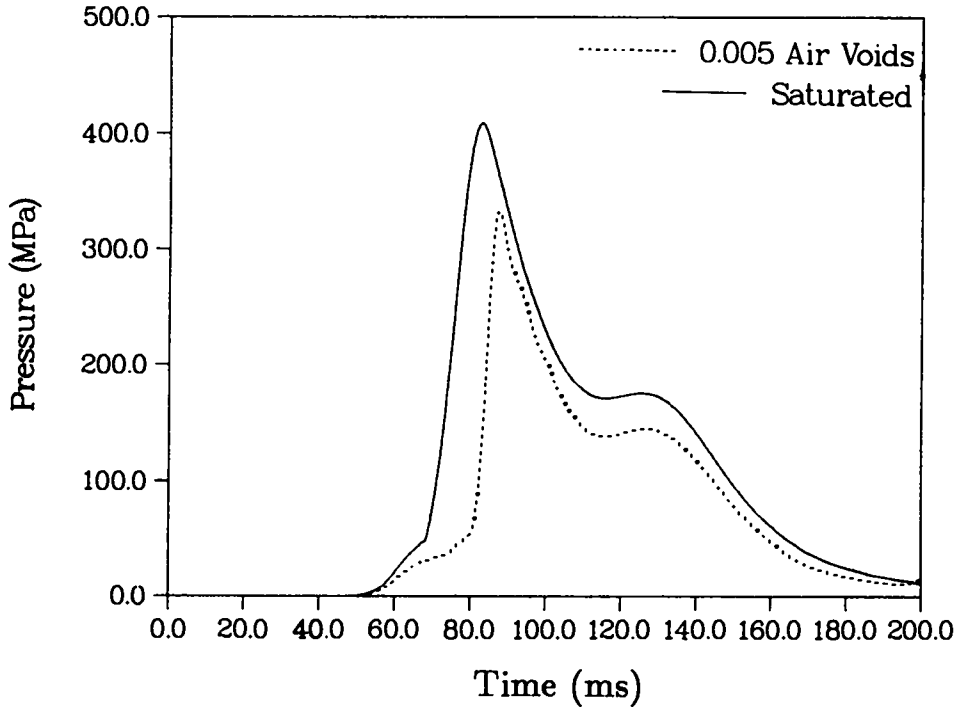

Fig. 10c. Pressure time histories for saturated and unsaturated limestone at a range of 300 m and along the theta=45° line. Peak pressures are governed only by the nearer source, indicating this point is outside the enhanced footprint.

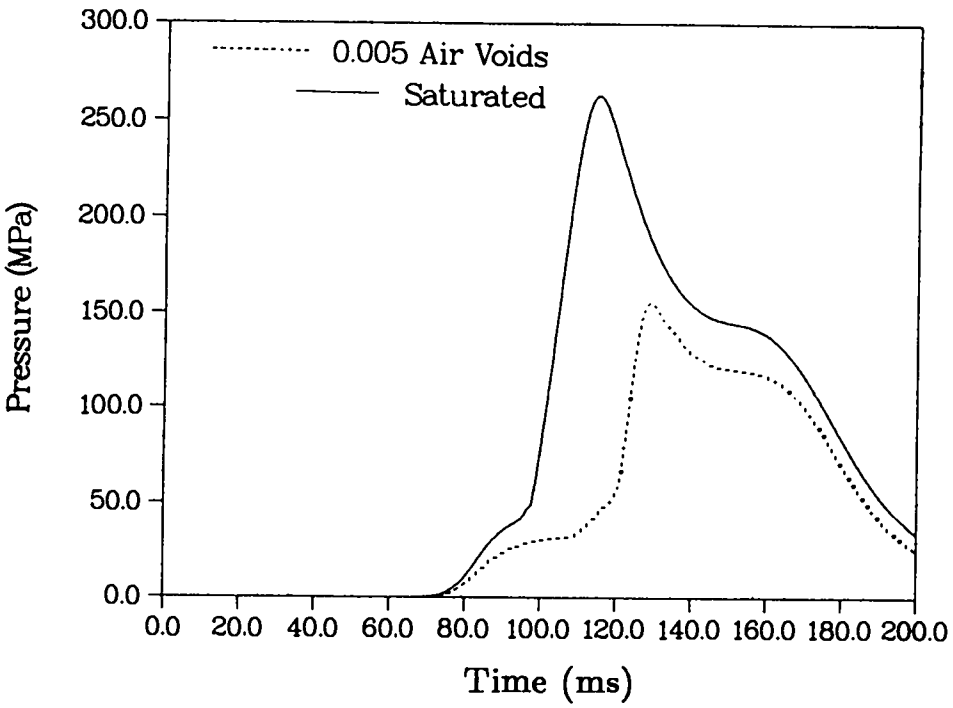

Fig. 10d. Pressure time histories for saturated and unsaturated limestone at a range of 400 m and along the theta=45° line. Essentially single-source response.

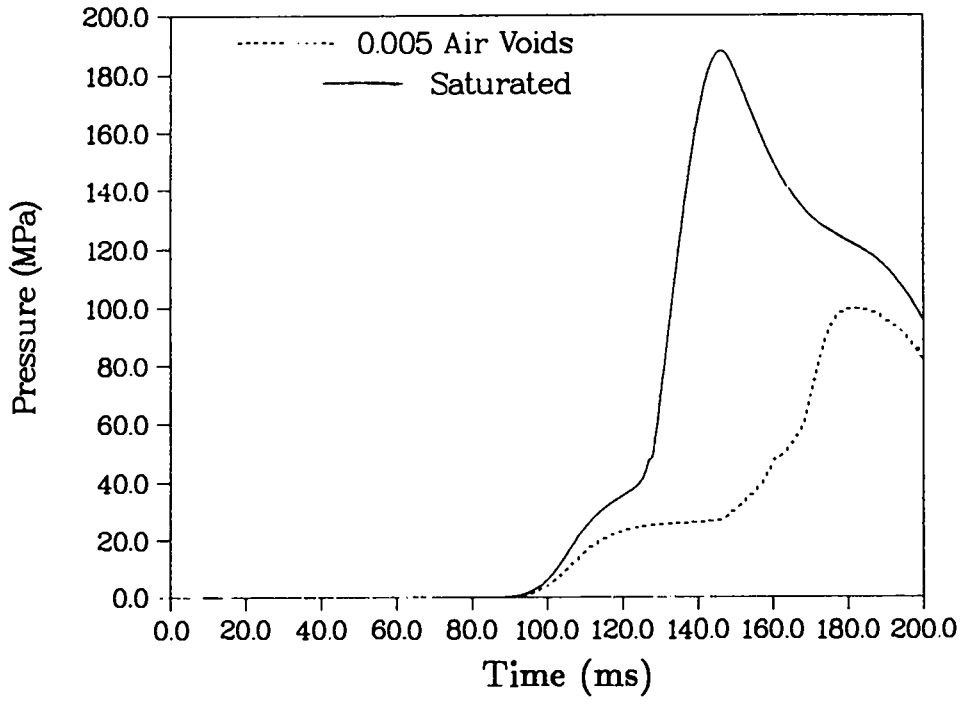

Fig. 10e. Pressure time histories for saturated and unsaturated limestone at a range of 500 m and along the theta=45° line. The arrival of the second source is now obscured.

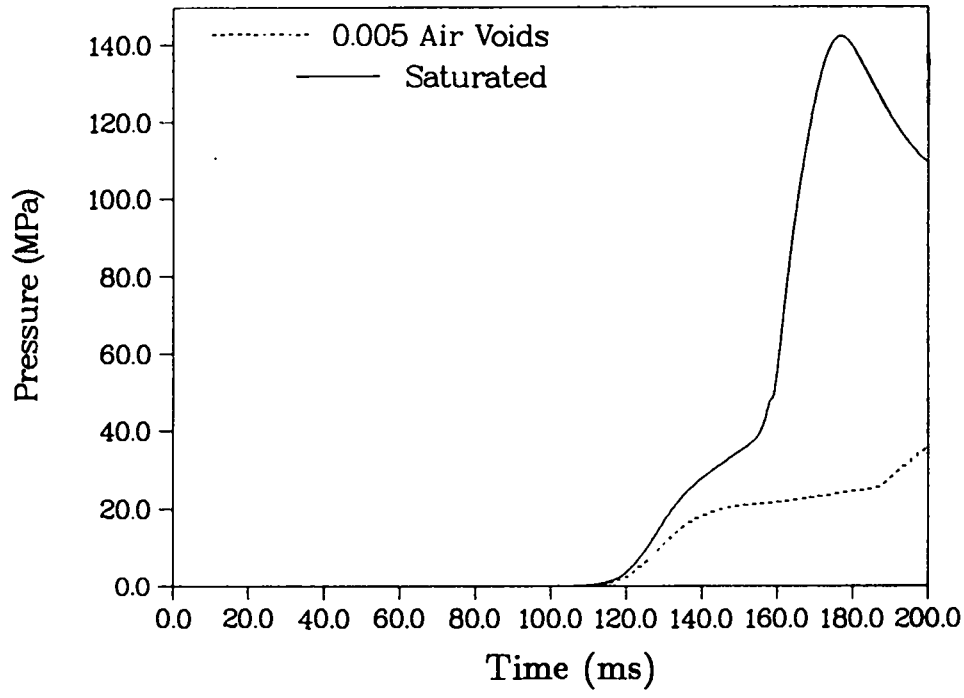

Fig. 10f. Pressure time histories for saturated and unsaturated limestone at a range of 600 m and along the theta=45° line. Significantly diminished signal in the unsaturated case.

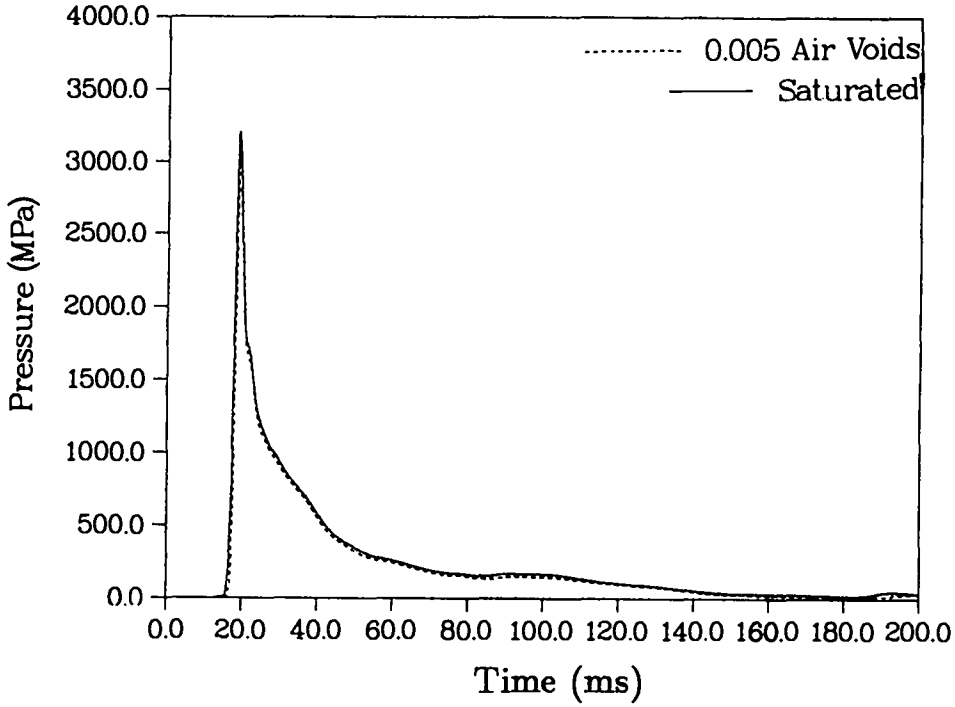

Fig. 11a. Pseudo one-dimensional pressure time histories for saturated and unsaturated limestone along the vertical axis at a range of 100 m. Difficult to see the second source arrival.

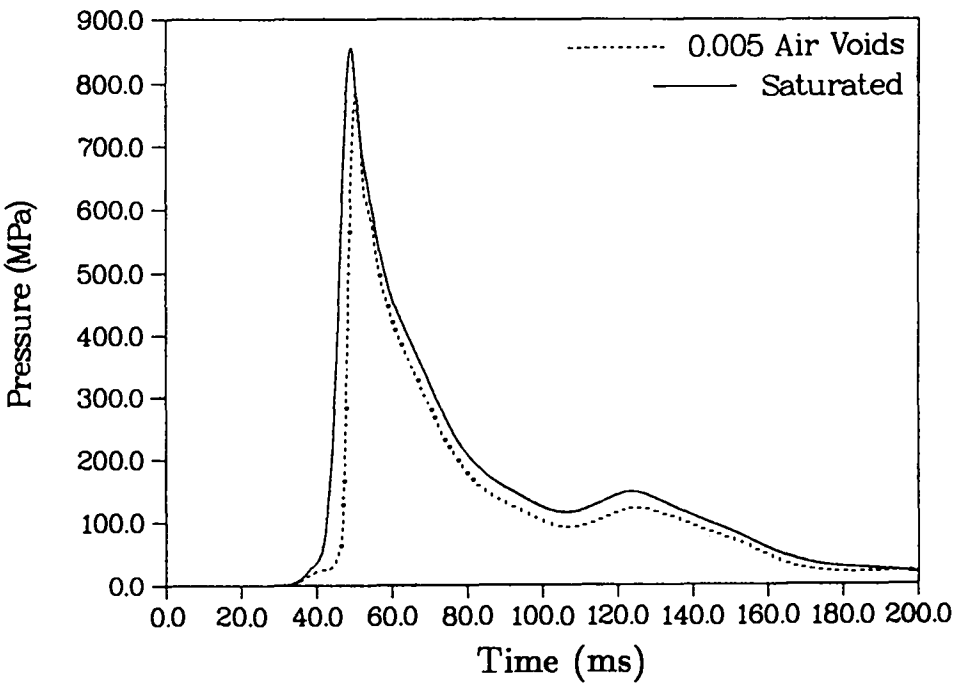

Fig. 11b. Pseudo one-dimensional pressure time histories for saturated and unsaturated limestone along the vertical axis at a range of 200 m. Second signal arrives at about 100 ms.

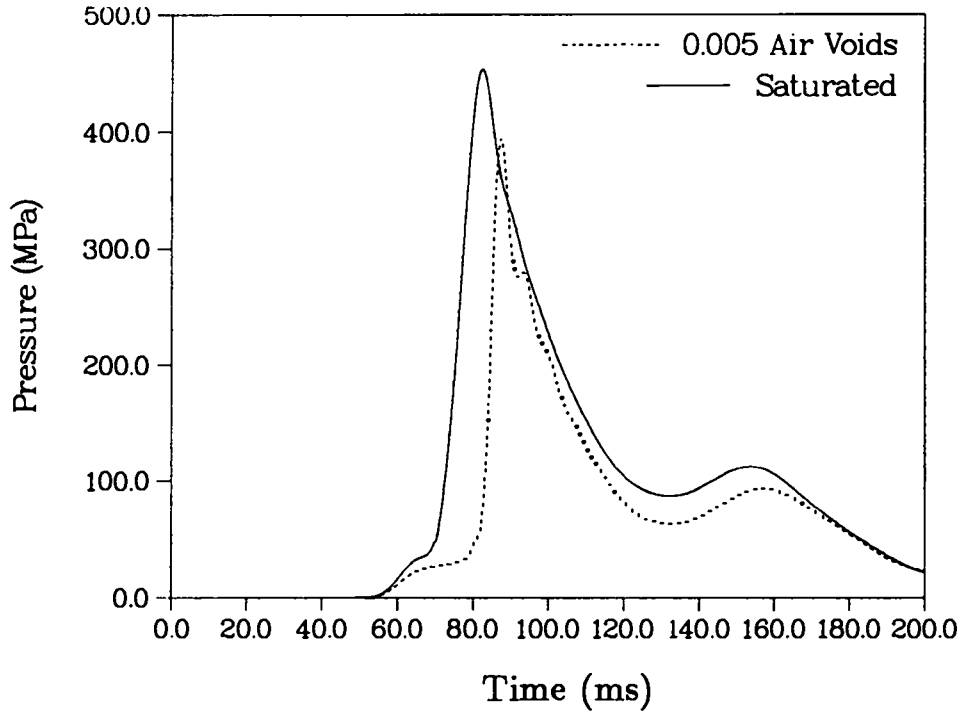

Fig. 11c. Pseudo one-dimensional pressure time histories for saturated and unsaturated limestone along the vertical axis at a range of 300 m. Delay in the peak pressure is nearly 10 ms.

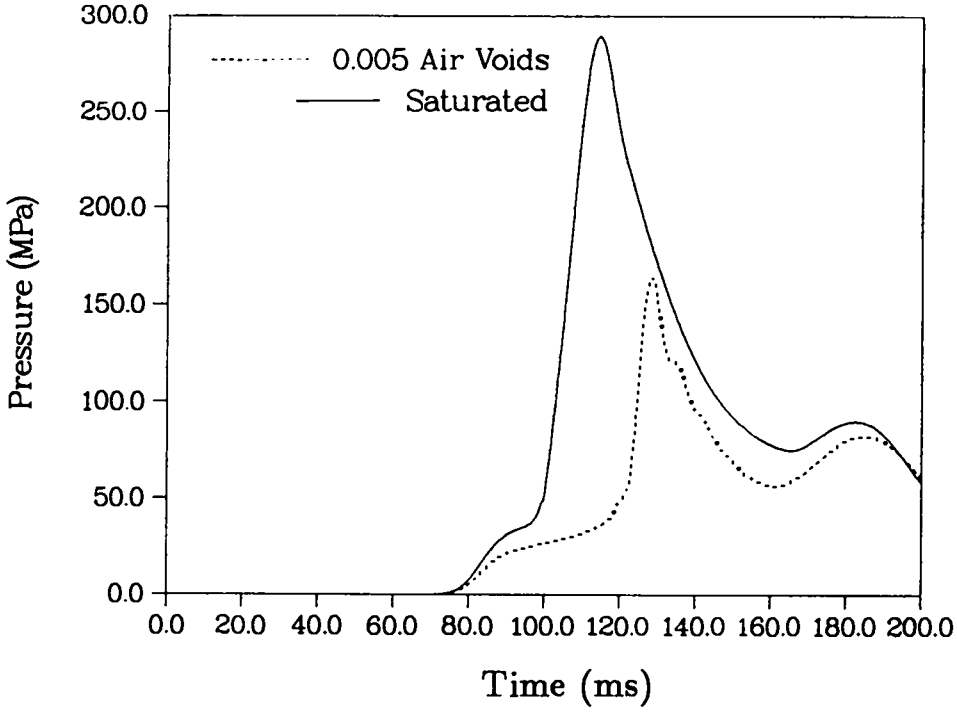

Fig. 11d. Pseudo one-dimensional pressure time histories for saturated and unsaturated limestone along the vertical axis at a range of 400 m. Significantly diminished signal in the unsaturated material.

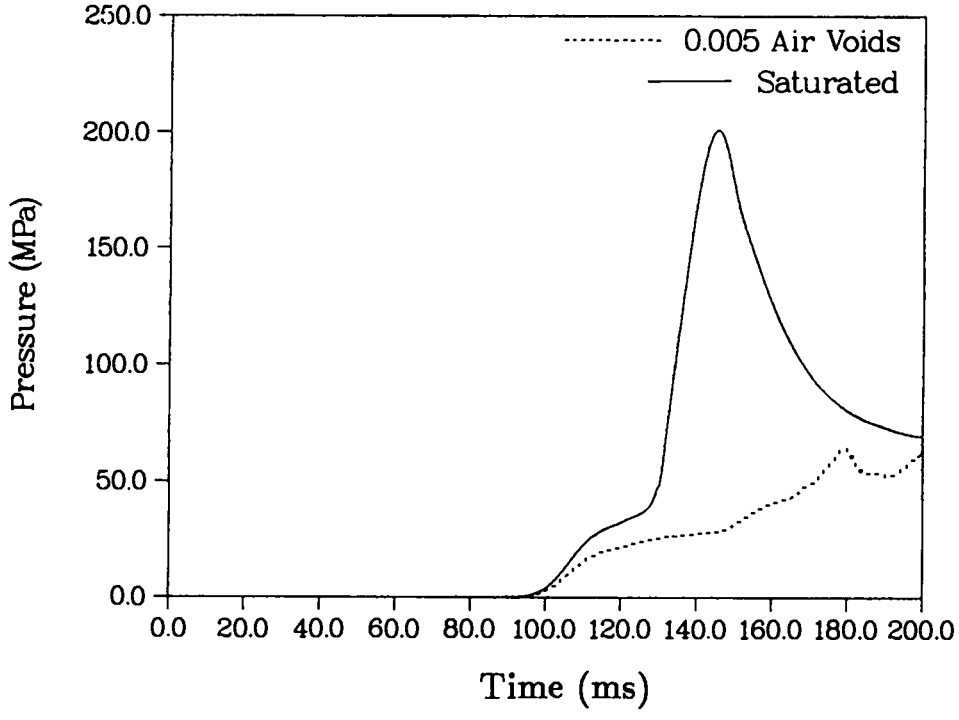

Fig. 11e. Pseudo one-dimensional pressure time histories for saturated and unsaturated limestone along the vertical axis at a range of 500 m. Truly one-dimensional response in the saturated material to 200 ms.

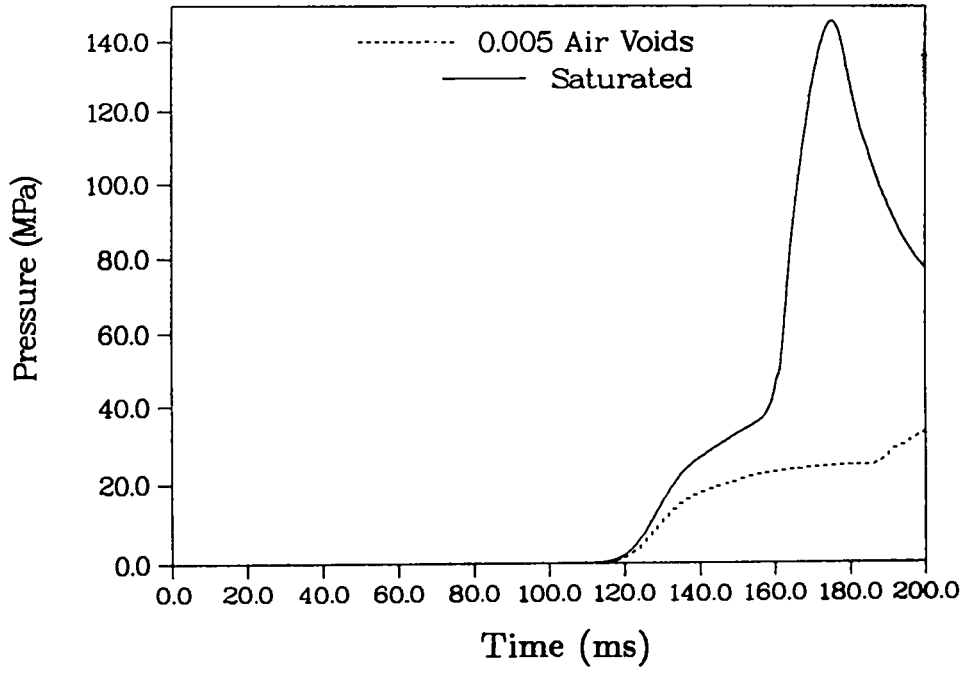

Fig. 11f. Pseudo one-dimensional pressure time histories for saturated and unsaturated limestone along the vertical axis at a range of 600 m. Mostly crushing in the unsaturated material by 200 ms. Note the second source is 800 m away from this station.

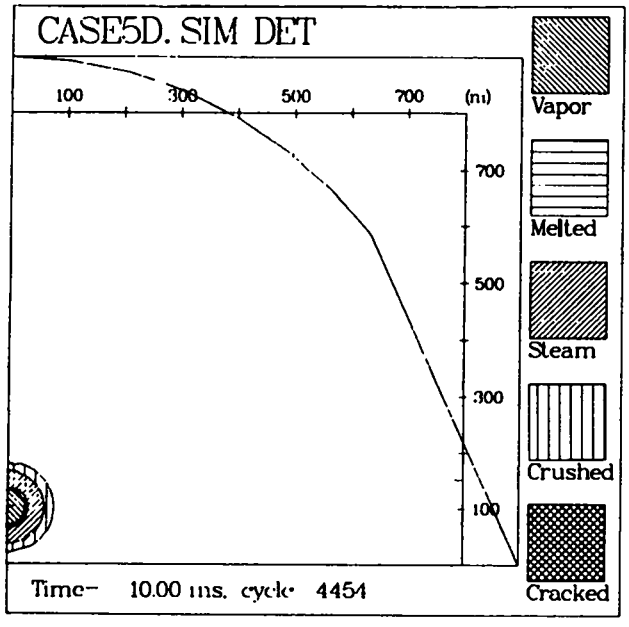

Fig. 12a. Different material states at 10 ms in saturated limestone. Each source is acting independently.

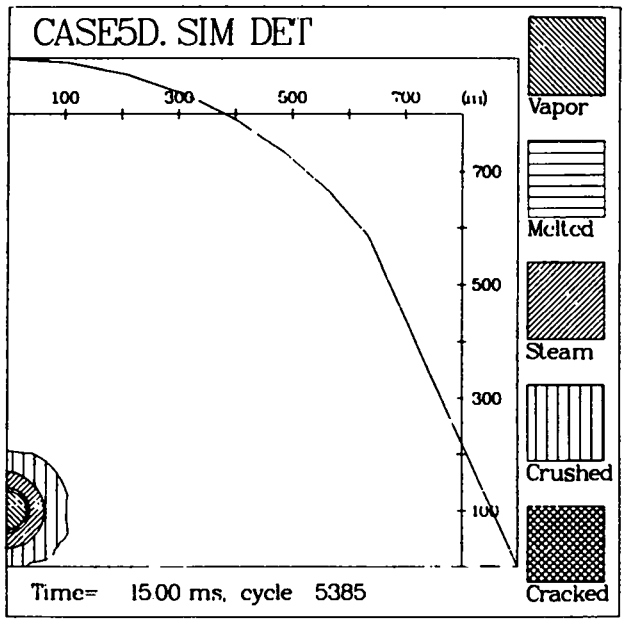

Fig. 12b. Different material states at 15 ms in saturated limestone. The stress waves have just started to interact.

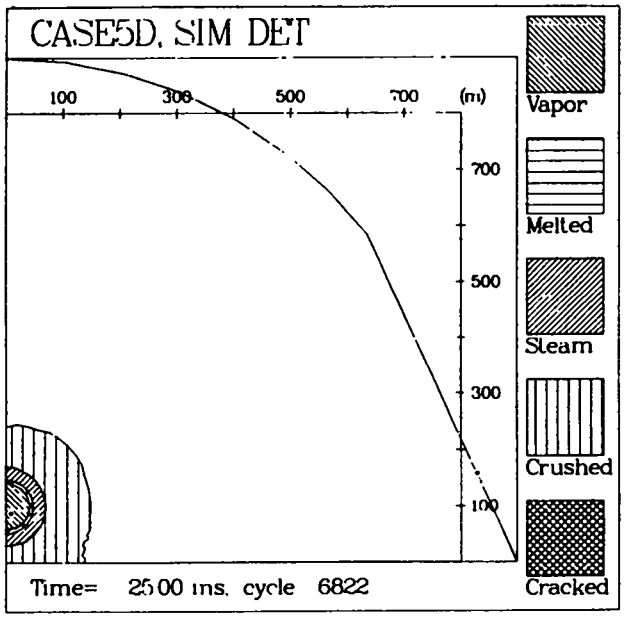

Fig. 12c. Different material states at 25 ms in saturated limestone. Influence from stagnation pressure is beginning to be seen.

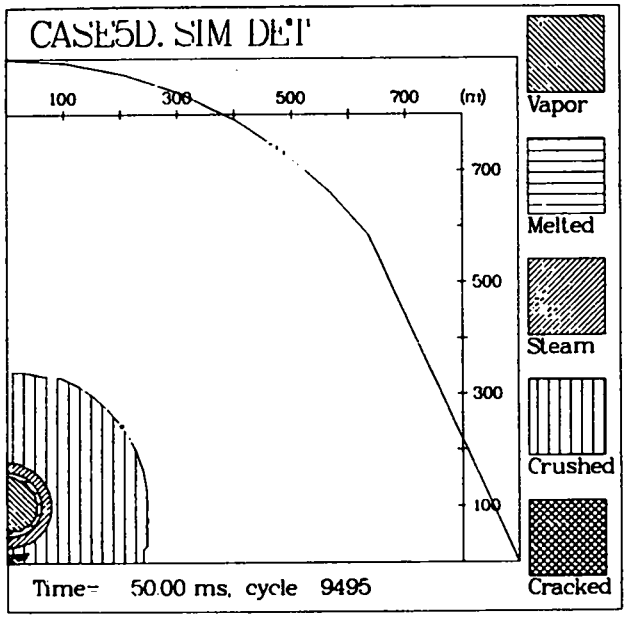

Fig. 12d. Different material states at 50 ms in saturated limestone. Region of tension is starting to form.

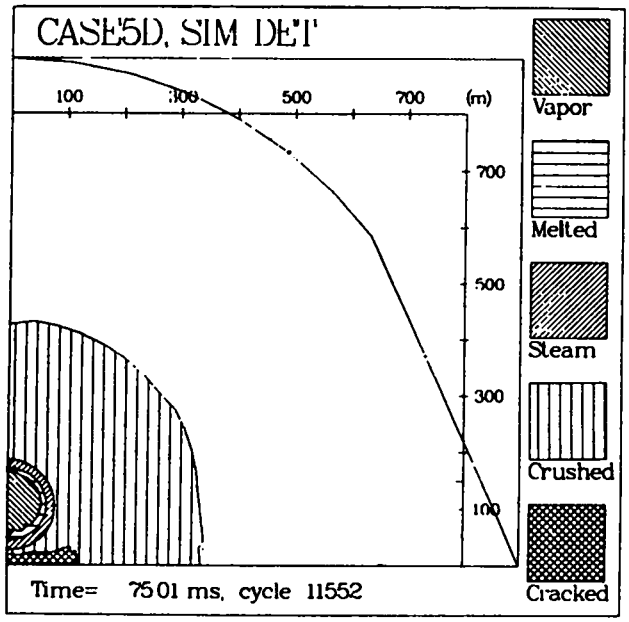

Fig. 12e. Different material states at 75 ms in saturated limestone. Crushed-out region is now ellipitcal.

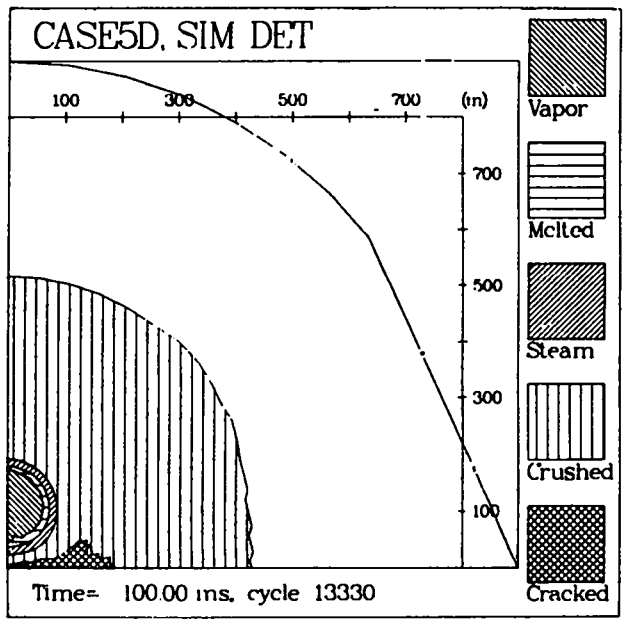

Fig. 12f. Different material states at 100 ms in saturated limestone.

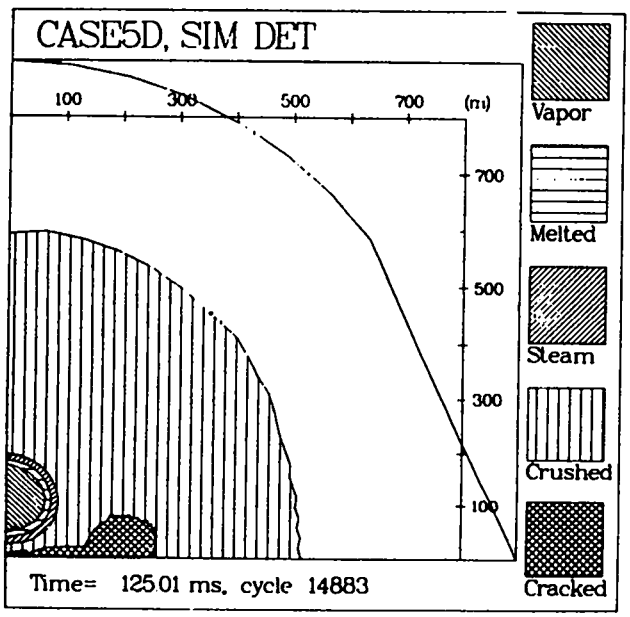

Fig. 12g. Different material states at 125 ms in saturated limestone. Cavity growth slows and tensile region expands.

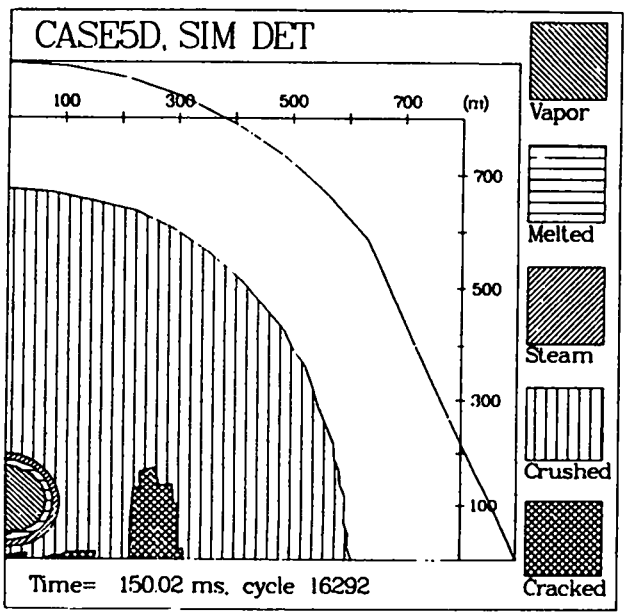

Fig. 12h. Different material states at 150 ms in saturated limestone. Region of tension is starting to form.

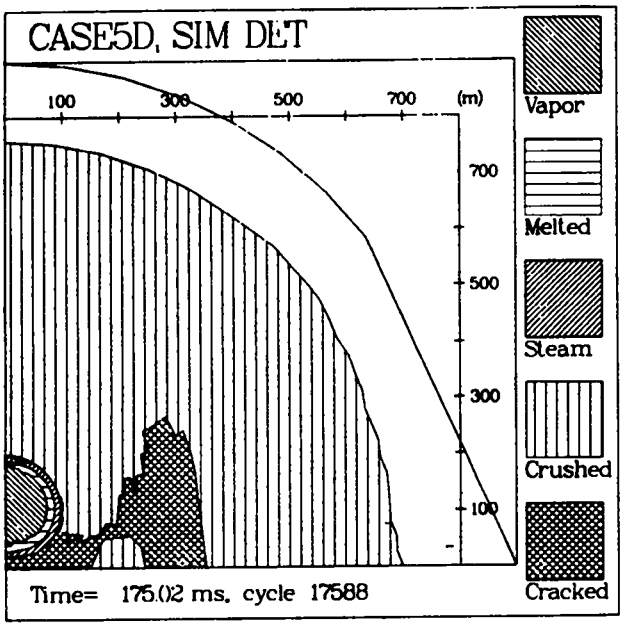

Fig. 12i. Different material states at 175 ms in saturated limestone. Cavity stops growing, and an island of compression appears.

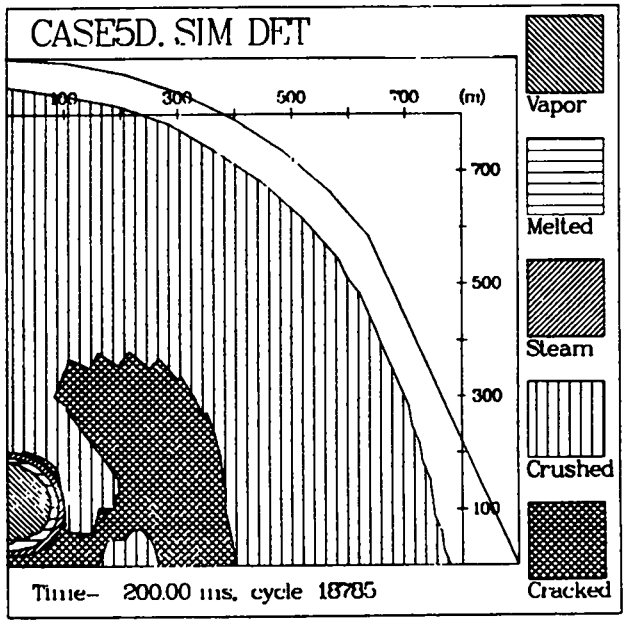

Fig. 12j. Different material states at 200 ms in saturated limestone. Tensile region expands as the front approaches the boundary.

Surface plots of pressure at 10 and 25 ms are shown in Figs. 13 and 14, respectively. Notice that the peak pressure in Fig. 14 of 5100 MPa (51 kbar) where the interaction is taking place is significantly higher than the pressure at the leading edge of either shock acting independently. A similar plot of pressure at 200 ms is shown in Fig. 15. Although the magnitude of the amplification effect is diminished from Fig. 14, it is still about 20% greater than the single source. Figure 16 is a contour plot of pressure at 200 ms where it is clearly seen that pressures greater than 100 MPa (1 kbar) extend well beyond 600 m. The density of the area near the sources is represented in Fig. 17 in a surface plot. The very low density region is where material has vaporized and melted. Notice the diminished density directly between the sources where intense reflections have extensively cracked the remaining solid material.

A revealing picture of what has happened is shown in Fig. 18. This is a surface plot of the maximum stress in the x-direction that has been experienced at a given location. An inner section with an approximate radius of 300 m has been omitted since the stresses in the vaporized and melted material are so great that they overwhelm the data of interest

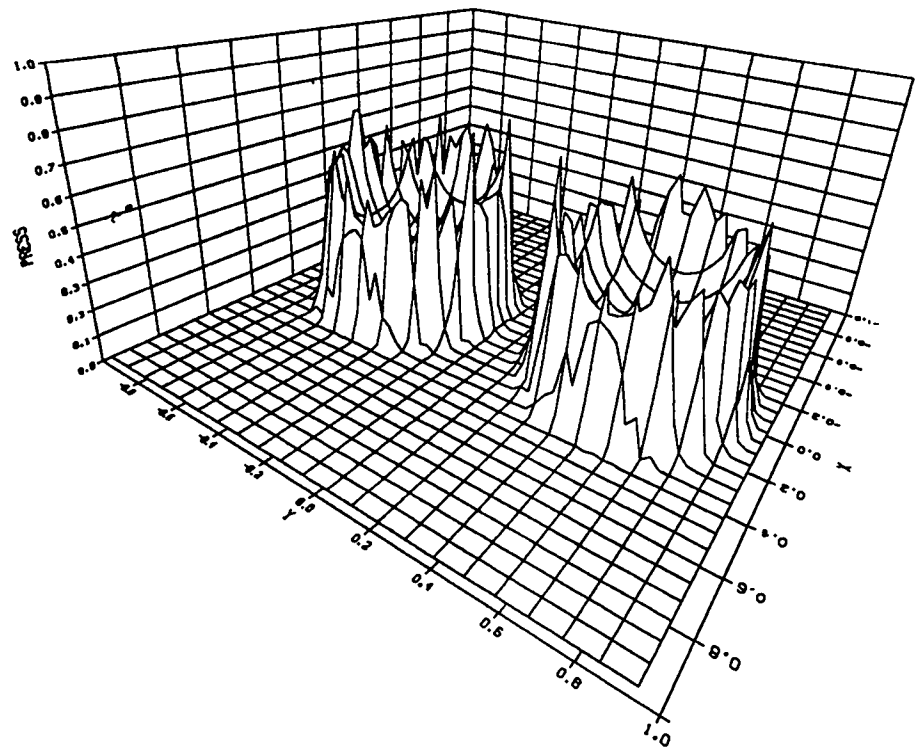

Fig. 13. Surface plot of pressure at 10 ms in saturated limestone. The area grid is 400 x 400 m, and the maximum pressure is 9269 MPa (92.69 kbar). Notice the two signals have not yet begun to interact.

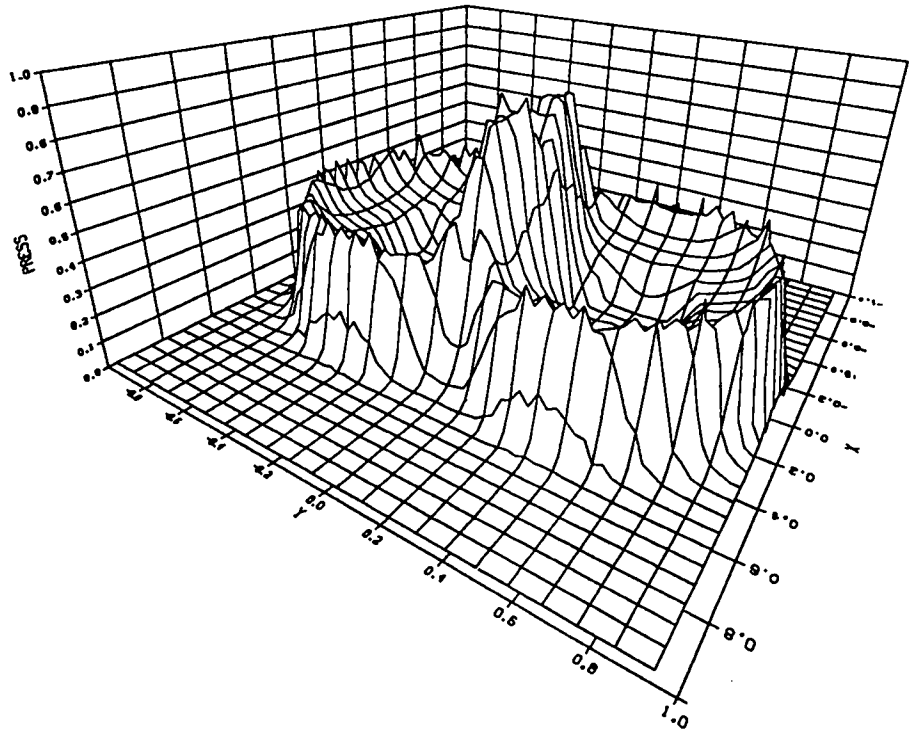

Fig. 14. Surface plot of pressure at 25 ms in saturated limestone. The area grid is 500 x 500 m, and the maximum pressure is 3360 MPa (33.6 kbar). The stagnation pressure is nearly twice as great as the one-dimensional pressure.

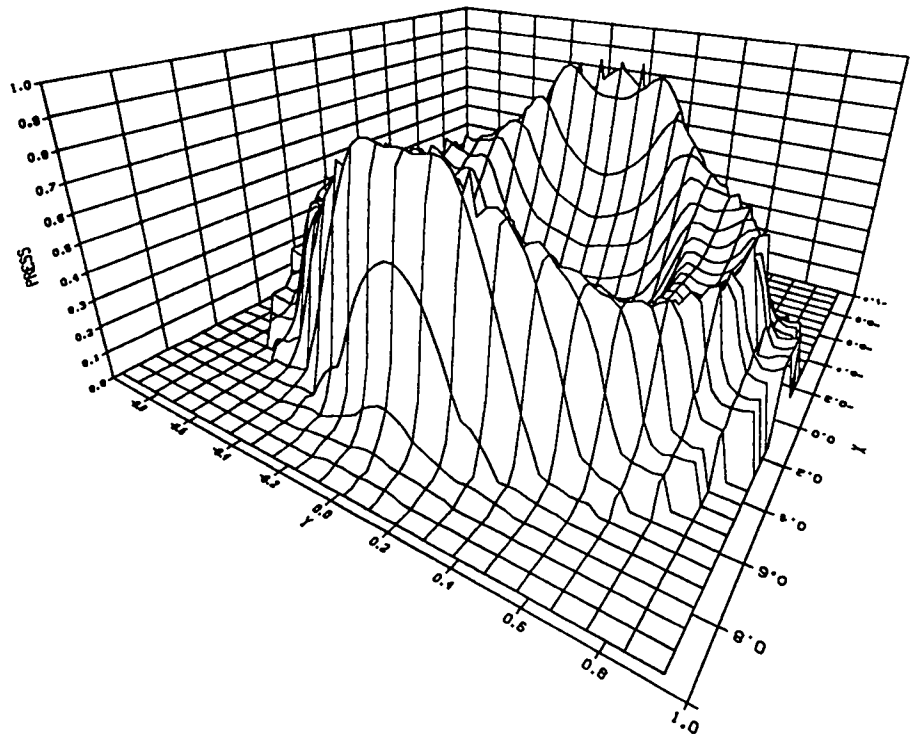

Fig. 15. Surface plot of pressure at 200 ms in saturated limestone. The area grid is 200 x 200 m, and the maximum pressure is 195 MPa (1.95 kbar). Notice the region of combined pressure and where the boundary is beginning to influence the calculation.

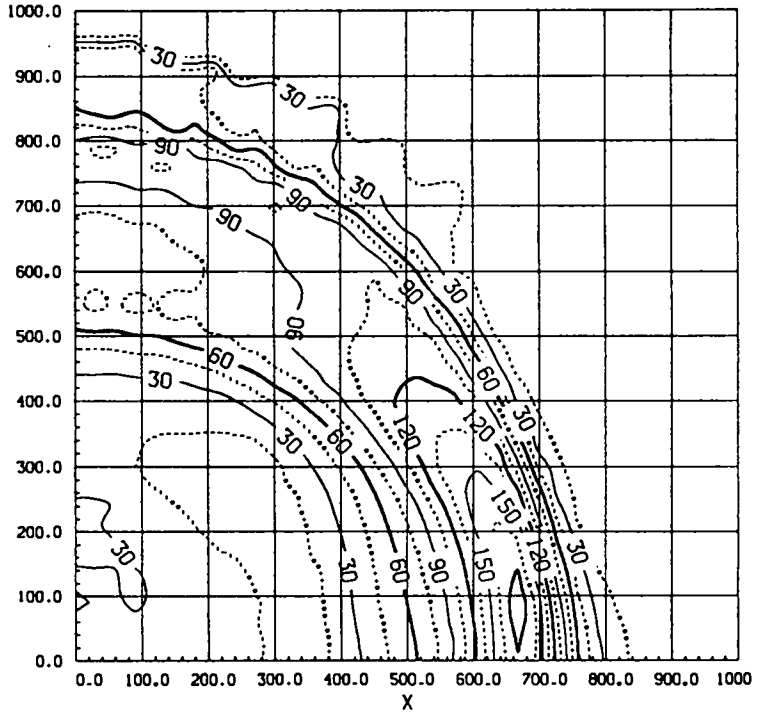

Fig. 16. Contour plot of pressure at 200 ms in saturated limestone. The area grid is 1000 x 1000 m, and the maximum pressure is 195 MPa (1.95 kbar). None of the image regions are represented here. The extent of significant amplification extends to the point (500 m, 400 m).

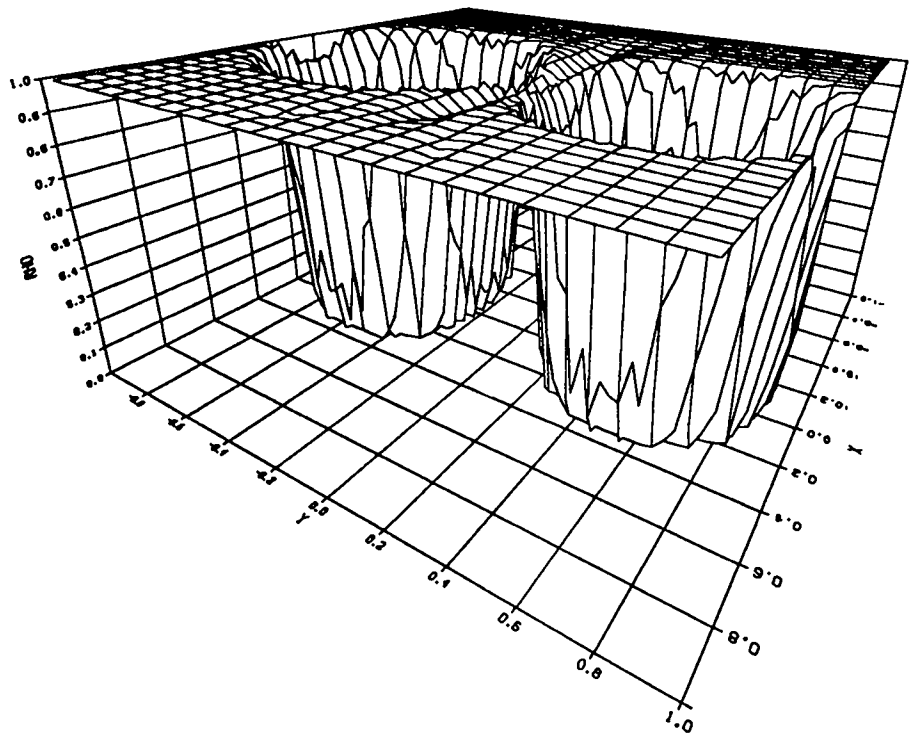

Fig. 17. Surface plot of density at 200 ms in saturated limestone. The area grid is 400 x 400 m, and the maximum density is 2.512 g/cc. This plot clearly shows the cavity regions since the vapor and melted material have very low densities.

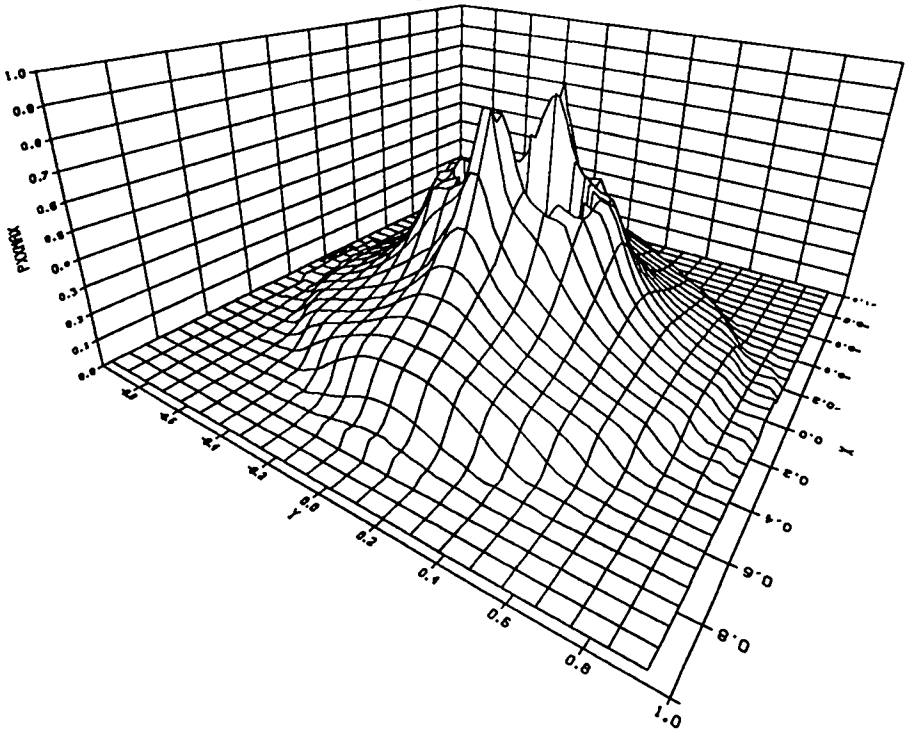

Fig. 18. Surface plot of maximum stress seen at any point in saturated limestone by 200 ms. The area grid is 2000 x 2000 m, and the maximum stress seen is 1047 MPA (10.47 kbar). Notice that the center portion is not plotted (to a radius of about 100 m) since the stresses inside are so great that they would overwhelm the rest of the data.

on a linear plot. Clearly, a nonsymmetric region exists near the source. The multiplication effect is diminished at greater ranges, but it is clear that even at 600 m the combined effect of both sources is substantial.

2. Limestone with One-Half Percent Air-Filled Voids. The physical properties of this material are given in Table I. Recall that this material is exactly the same as the saturated material except that a small amount of water volume has been removed. The most significant feature of the pressure time histories for this case is the compaction that takes place in the unsaturated material. The dashed lines in Figs. 8 to 11 represent the response of the unsaturated material. Figures 8a-f show the response along the reflection axis, i.e., where y = -900 m. They are histories for points spaced every 100 m from the point of double symmetry, not from one of the sources. The peak pressure is 95% of the saturated case at a range of 100 m and similarly resembles the saturated case at 200 m (the solid line in Fig. 8b). The peak pressure at 300 m along the reflection axis is only 90% of that for saturated material, and at 400 m the peak value has dropped to 77%. Notice in Fig. 8e that much flatter response is observed before the rapid rise to a peak of just over one-half the saturated peak. Notice also that at a range of 600 m the peak value has not yet been attained at 200 ms because of a decrease in effective (peak pressure) sound speed caused by pore crushing in the unsaturated case. The initial signals in both cases arrive at about 116 ms, but the saturated case shows the peak value at just over 170 ms (the solid line in Fig. 8f).

The response along the theta=zero line is given in Figs. 9a to 9f. The record at a range of 100 m shows the arrival of the signal from the second source at about 40 ms. The shape of the record in Fig. 9a is similar to the saturated case except the amplitude everywhere is slightly reduced. It is likely that most of this record represents the behavior of fully compacted material. The unsaturated record in Fig. 9b is also very similar in shape and magnitude to the saturated case. The arrival from the second source is clearly indicated, and the only difference seems to be a slightly lower amplitude caused by some pore crushing indicated by the leveling out of the precursor, shown in the early part of the record. This effect is more pronounced in Figs. 9c and 9d, but the significant feature of these two curves is that both signals have merged into a single waveform as in the

saturated case. As the peak amplitudes of pressure drop at distances of 500 and 600 m as shown in Figs. 9e and 9f, respectively, the magnitude of the onset of pore crushing becomes relatively more significant. Also notice the much later arrivals of peak pressure but identical times-of-arrival of the initial precursor.

The records for the response along the theta=45° line are given in Figs. 10a-f. These show similar relative behavior as previously discussed and are fairly unremarkable except to note the low-amplitude arrival pulse in Fig. 10a from the second source at about 75 ms. The second hump in Fig. 10b is again caused by the second source at a distance of 369 m.

The pseudo one-dimensional response (theta=90°) is shown in Figs. 11a-f. The history shown in Fig. 11b is for a source 200 m away and one at 400 m. Notice the small increase at 120 ms during the decline from peak stress. This is certainly the arrival of the second source. It may be significant that the peak pressure at a range of 500 m shown in Fig. 11e results from the addition of the signals from the two sources. Although the peak is much less than in the saturated case (the solid line in Fig. 11e), this qualitative feature of a relatively slow first signal compared with the arrival from the second source is unique to the unsaturated case. In the saturated case, almost no compaction takes place so the second signal never catches up with the first (nearer) signal.

The regions of different material states from 10 to 200 ms are shown in Figs. 19a-j. The corresponding times for the saturated case are given in Figs. 12a-j. The response looks very similar until about 50 ms, by which time the region of fully crushed material is noticeably smaller for the unsaturated case in Fig. 19d. Similar regions of tension develop, and by 125 ms the crushed region is significantly smaller. At 150 ms, this boundary no longer looks elliptical but has begun to bulge out along the reflection axis as a result of the influence from the stagnation pressures at the point of double symmetry. This effect continues to 175 ms at which point the stresses are low enough that the fully crushed region stops growing, as illustrated in Fig. 19j, which shows the same boundary at 200 ms. Notice that similar regions of tension have developed at 200 ms for both the saturated and unsaturated cases, shown in Figs. 12j and 19j, respectively.

A surface plot of the pressure at 150 ms is shown in Fig. 20 and shows the effect of the second burst in increasing the peak pressure to more than double the single burst

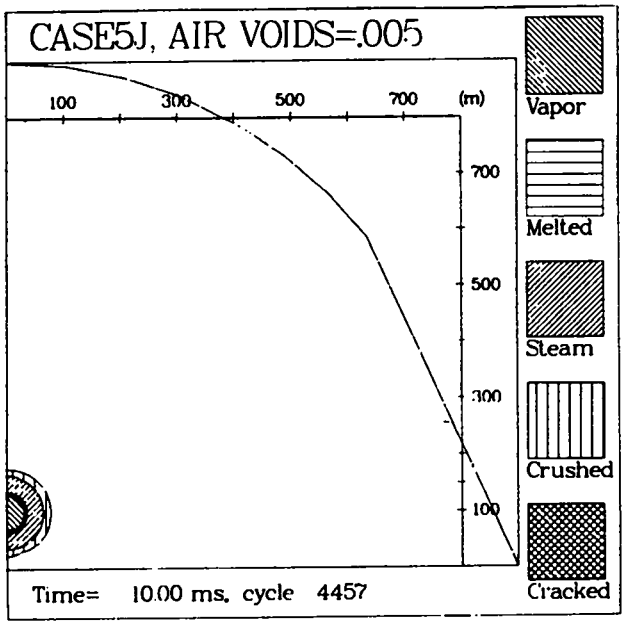

Fig. 19a. Different material states at 10 ms in unsaturated limestone. Each source is acting independently.

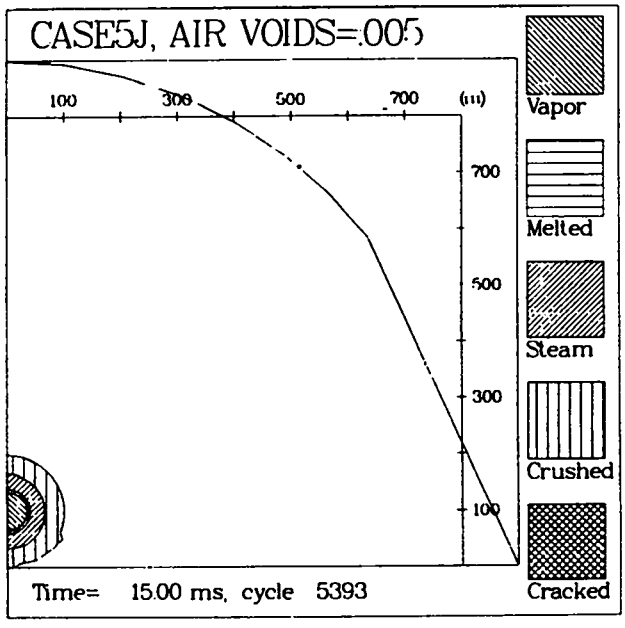

Fig. 19b. Different material states at 15 ms in unsaturated limestone. The stress waves have just started to interact.

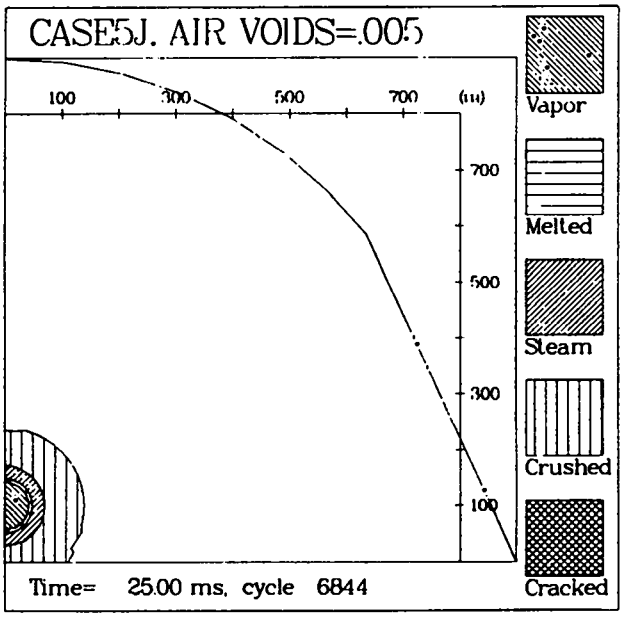

Fig. 19c. Different material states at 25 ms in unsaturated limestone. Influence from stagnation pressure is less obvious.

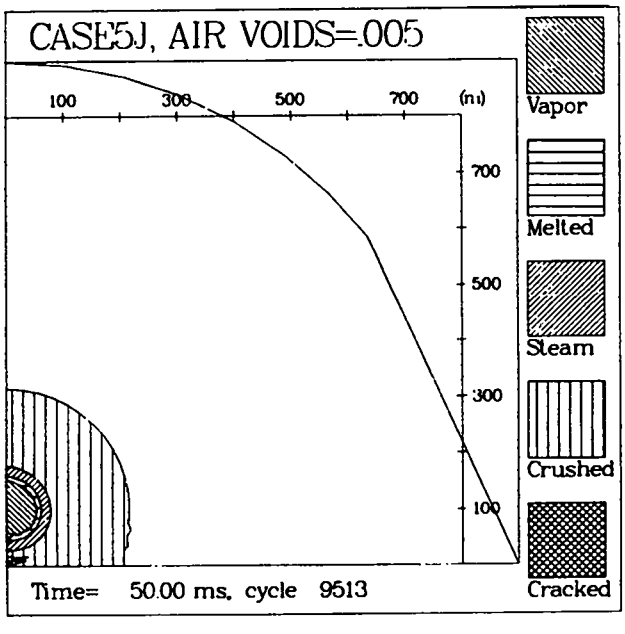

Fig. 19d. Different material states at 50 ms in unsaturated limestone. Region of tension is starting to form.

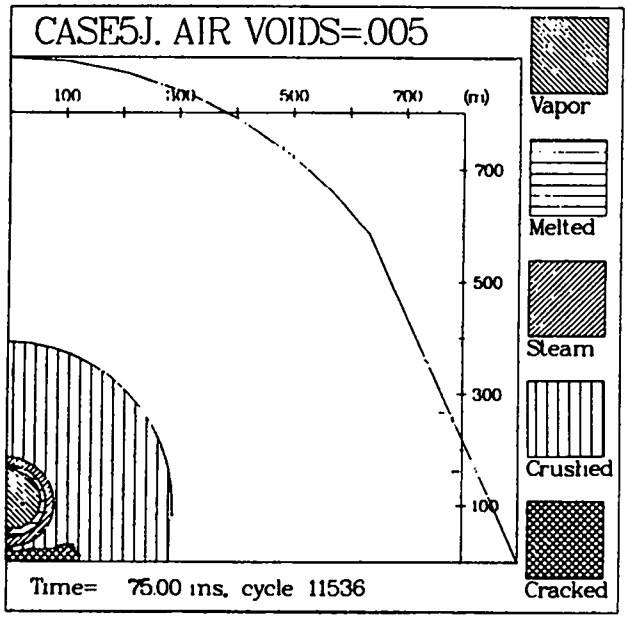

Fig. 19e. Different material states at 75 ms in unsaturated limestone. Crushed-out region is noticeably smaller than for the saturated case.

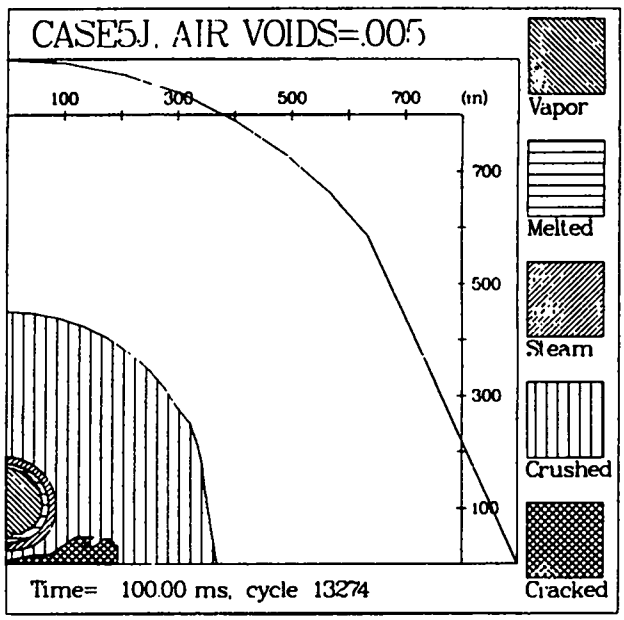

Fig. 19f. Different material states at 100 ms in unsaturated limestone.

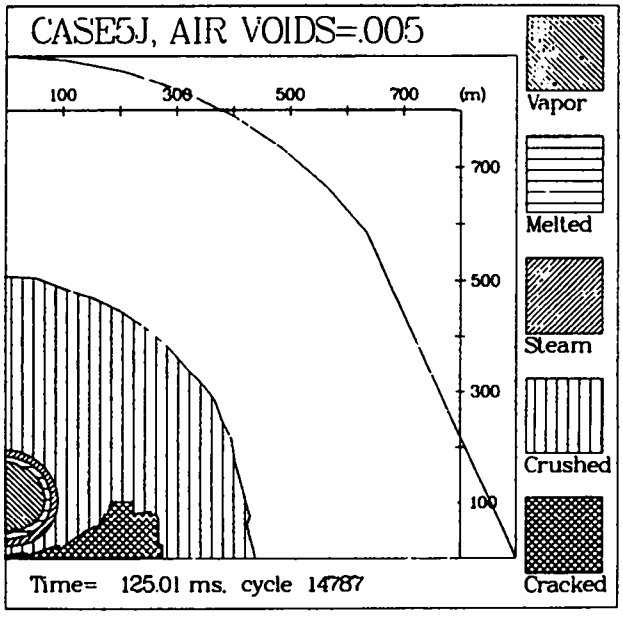

Fig. 19g. Different material states at 125 ms in unsaturated limestone. Crushed-out region appears more circular.

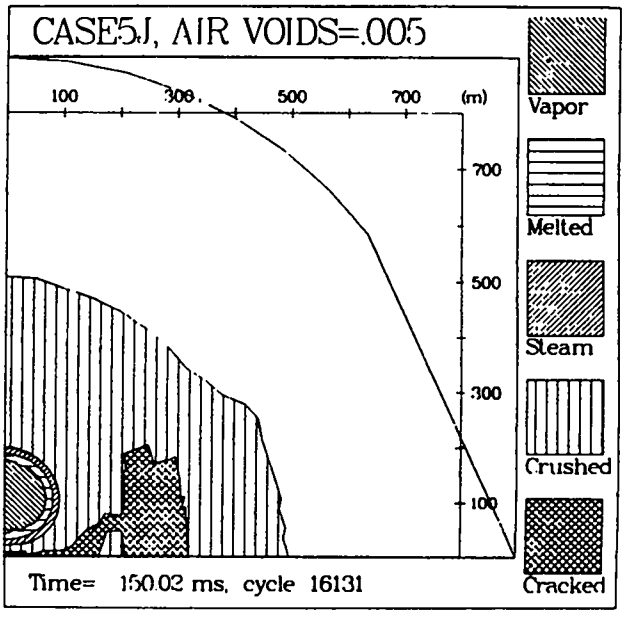

Fig. 19h. Different material states at 150 ms in unsaturated limestone. Influence from stagnation pressure shows more crushed material along the reflection axis.

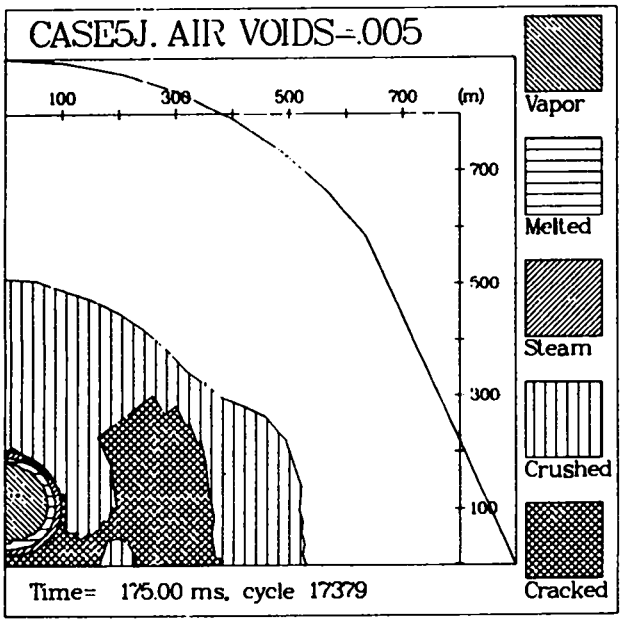

Fig. 19i. Different material states at 175 ms in unsaturated limestone. Crushed-out area stops growing as pressures drop.

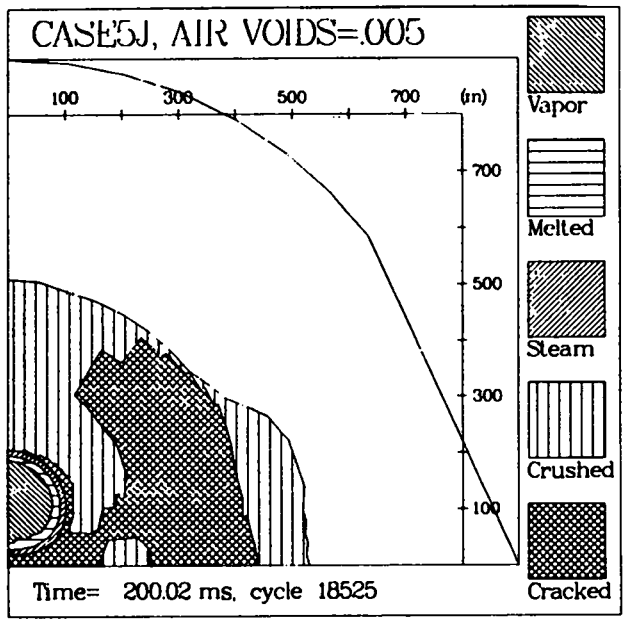

Fig. 19j. Different material states at 200 ms in unsaturated limestone. Tensile region touches the boundary of uncrushed material.

value along the reflection axis. Also note the low amplitude precursor followed by a much stronger pulse. The peak pressure of 180 MPa (1.8 kbar) at 500 m should be compared with the saturated case where a peak pressure of nearly 200 MPa (2 kbar) had been achieved at nearly 700 m by 200 ms (see Fig. 15). Figure 21 shows the peak stress attained at all points beyond a radius of about 100 m at 150 ms. Notice that the drop-off in peak stress is much more dramatic than in the saturated case, shown in Fig. 18. A plot of density is shown in Fig. 22 at 150 ms. It clearly shows the vaporized region and a peak density of 2.526 g/cc compared with a peak of 2.512 in the saturated case. Recall that the ambient density from Table I was 2.495 in both cases. Clearly, the void volume occupied by air in the unsaturated case allowed for higher compaction, resulting in greater energy losses and a subsequently diminished shock magnitude as a function of distance. Also notice where the density has decreased in the vicinity of the stagnation point, resulting from cracking and accumulation of void strain in this highly tensile region.

To summarize the numerical results of the simultaneous detonation of two contained nuclear bursts, the overwhelming conclusion is that the presence of one-half percent air-

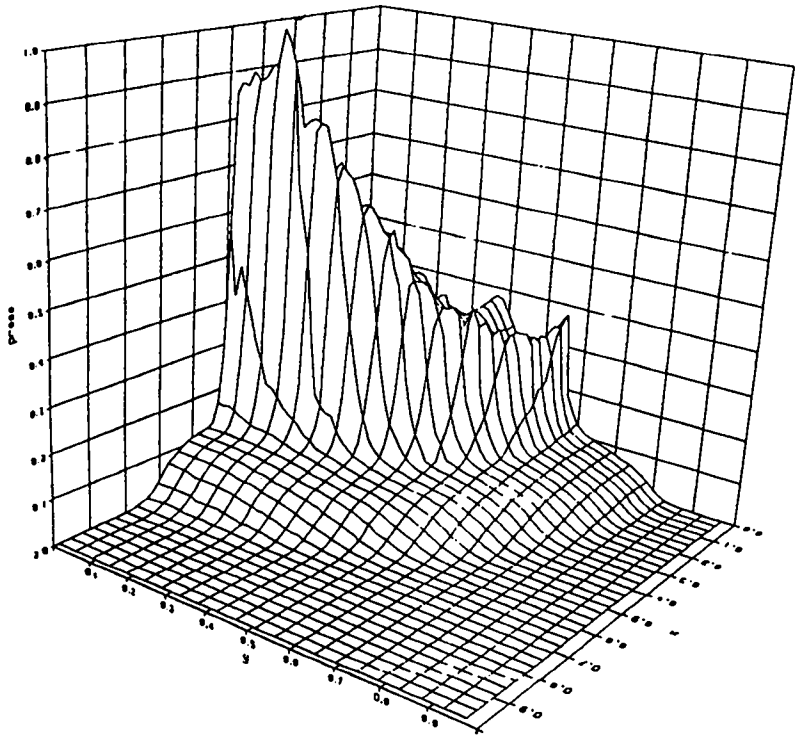

Fig. 20. Surface plot of pressure at 150 ms in unsaturated limestone. The area grid is 1000 x 1000 m, and the maximum pressure is 250 MPa (2.5 kbar). Notice the near doubling of the pressure amplitude along the reflection axis and the precursor.

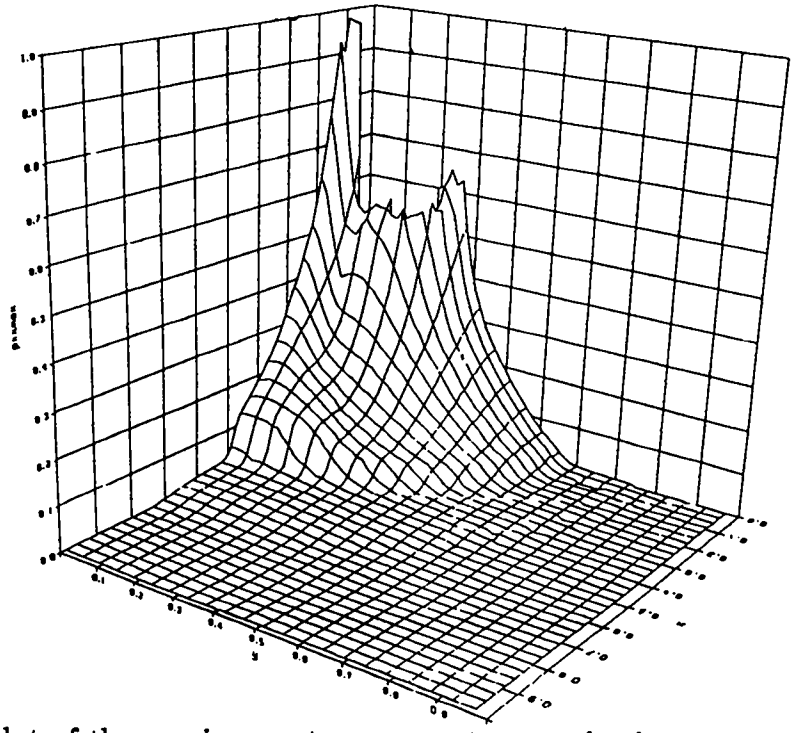

Fig. 21. Surface plot of the maximum stress seen at any point in unsaturated limestone by 200 ms. The area grid is 1000 x 1000 m, and the maximum stress seen is 2000 MPa (20 kbar). Notice that an interior portion is not plotted (to a radius of about 100 m) since the stresses inside are so great, they would overwhelm the rest of the data.

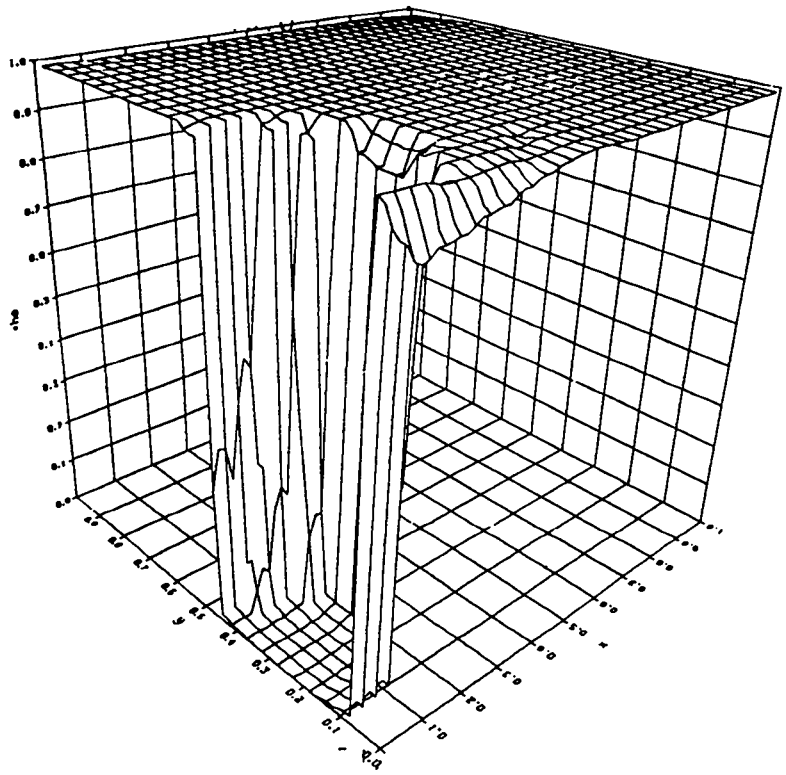

Fig. 22. Surface plot of density at 150 ms in unsaturated limestone. The area grid is 400 x 400 m, and the maximum density is 2.526 g/cc. Notice the cavity region and the lower density region along the reflection axis due to tensile cracking.

filled voids will significantly reduce the amplitude of the stress wave at ranges greater than 400 m. The size of the mesh used in this study limited the simulated time of the calculations. The saturated case provided meaningful information to 200 ms and indicated that the depth to 100 MPa (1 kbar) along the reflection axis should be well beyond 700 m. The unsaturated case had a much longer pulse width so that data obtained after 150 ms are less reliable since the amplitude of the boundary effects begins to approach the signal amplitude beyond this time. Still, the results were fairly conclusive that 100 MPa (1 kbar) will be seen at much shorter ranges than for the saturated case.

III. ONE-DIMENSIONAL SINGLE-SOURCE CALCULATIONS

The numerical results above illustrate the effect of stress wave interaction for two simultaneous detonations. One commonly used way of treating such simultaneous detonations is linear superposition. Clearly, material compaction and other energy-absorbing phenomena are highly nonlinear, especially near the source region. Still, much of the response of the geologic media is elastic or quasi-elastic, and it may be that at the ranges of

interest, i.e., at distances greater than 500 m from the source, superposition may not be too bad. This was the motivation for the execution of one-dimensional calculations for the saturated and unsaturated materials defined in Table I. Appropriate components of the stress tensor were transformed and summed to compare with the results in Figs. 8 to 11.

A. Definition of Linear Superposition (after Mase, 1970)

An elastic solution may be found for a homogeneous, isotropic body if the following three field equations are satisfied at all interior points:

1) the equations of motion, $\sigma_{ji,j} + \rho b_i = 0$ (elastostatic)
$= \rho \dot{v}$ (elastodynamic),
2) linear elasticity, $\sigma_{ij} = \lambda \delta_{ij} \epsilon_{kk} + 2\mu \epsilon_{ij}$, and
3) strain-displacement relations, $\epsilon_{ij} = 1/2(u_{ij} + u_{j,i})$.

The conditions must also be prescribed at the boundaries of the body, and initial conditions must be specified for the elastodynamic case. The theorem of superposition states that since all three equations above are linear equations, then two unique solutions may be summed together to obtain a third solution. For example, if σ^1_{ij}, u^1_i represent a solution with body forces, b^1_i and σ^2_{ij}, u^2_i are a solution with body forces b^2_i, then $\sigma^1_{ij} + \sigma^2_{ij}, u^1_i + u^2_i$ represent a solution with body forces $b^1_i + b^2_i$.

B. Application to the Present Problem

The numerical results of boundary value problems obtained with the SHALE code involve many nonlinear equations. In the sections that follow, a method will be described whereby superimposed stress time histories are obtained that agree reasonably well with the full two-source calculations, under certain circumstances. Recall that the components of two nonelastic stress tensors are being summed to obtain a third solution. It is a drastic step to take since uniqueness and energy conservation are sacrificed, but if reasonable solutions are obtained then it is a simple matter to determine the general effects of timing and of different yields, two parameters that are not varied in the SHALE calculations presented above. Another benefit from running the one-dimensional problem is that cube-root scaling may be used to determine the stress enhancement of the simultaneous detonation of two equal explosions in a homogeneous medium compared with a single burst with equivalent yield.

C. Numerical Results

Full two-dimensional SHALE calculations were performed even though the solution to a single burst in a homogeneous, isotropic medium is inherently one-dimensional. This was done to evaluate the boundary conditions and to confirm that SHALE gives truly one-dimensional results. The zoning for this problem was similar to that given in Fig. 6. From zero to 10 m, the initial spacing was uniform at 20-cm intervals. Then from 10 to 100 m, the spacing increased geometrically to 5 m. Then 5-m spacing was maintained to an outer boundary of 1000 m. This is much finer than would normally be required, but time histories were to be obtained at 10-m intervals for the superposition program explained below. The mesh is shown in Fig. 23. The time histories were obtained along the x-axis so as to minimize the axis effects at ranges from 100 m to 1000 m. The time histories obtained look very much like the initial portions of the two-source calculations before the arrival of the second signal. Typical time histories at 100, 200, and 500 m are shown in Figs. 24a-c. Figure 25 shows the pressure pulse at 200 ms. The signal peak is out to about 700 m, and the shape is still fairly uniform. A contour plot shows greater detail in Fig. 26. Similarly, the one-dimensional time histories for material with one-half percent air-filled voids resemble the early portions of the dashed lines in Figs. 8 to 11. Pressure time histories at ranges of 100, 250, and 500 m are given in Figs. 27a-c, respectively. The pressure at 200 ms for the unsaturated case shows a significantly broader shape, as illustrated in Fig. 28. The contour plot in Fig. 29 shows only slight boundary effects.

IV. LINEAR SUPERPOSITION OF THE ONE-DIMENSIONAL RESULTS

The initial comparisons of the superimposed results with the full two-source calculations will be a study of time histories of the pressure at equivalent locations. As mentioned previously, time histories were generated every 10 m from distances of 100 to 1000 m. As a result there are only certain locations that are available for comparisons, shown graphically in Fig. 30. Notice that the two sources are plotted along with concentric circles around each one beginning at 100 m (one-half the separation) and then at 10-m radial increments. Superimposed time histories are therefore only available at locations where the sets of circles intersect. The time histories shown in Figs. 8 to 11 were chosen for convenience.

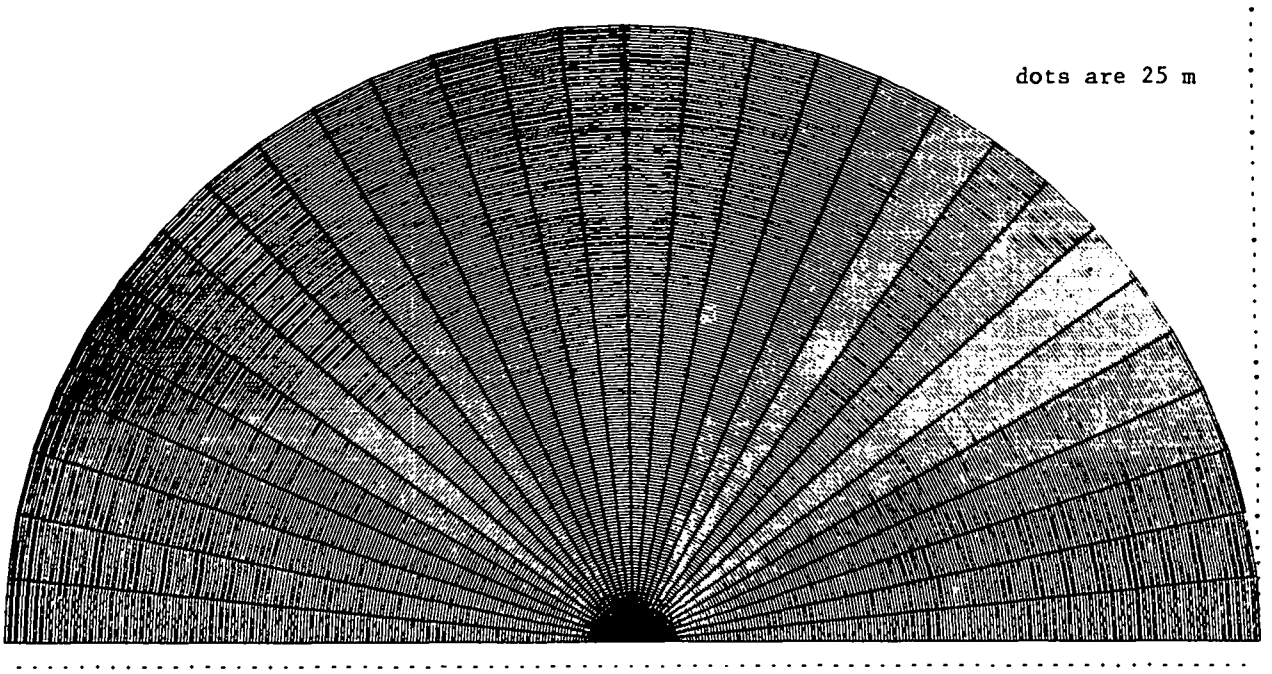

Fig. 23. Computational mesh for the one-dimensional calculations. The grid has 31 radial lines and 291 circumferential lines. The grid represents a sphere with a radius of 1000 m.

It was necessary to find the closest point in Fig. 30 to the corresponding location for the full two-source time history points. The orientation to each source must be determined so that the one-dimensional results may be properly transformed. This process is shown in Fig. 31.

It is important to recall from the definition of superposition that only equivalent components of tensors may be added. For this reason the orientation of the stress tensor is carefully determined in Fig. 31. Notice also that pressure, a scaler quantity, may not be simply added to get an accurate superimposed mean stress value.

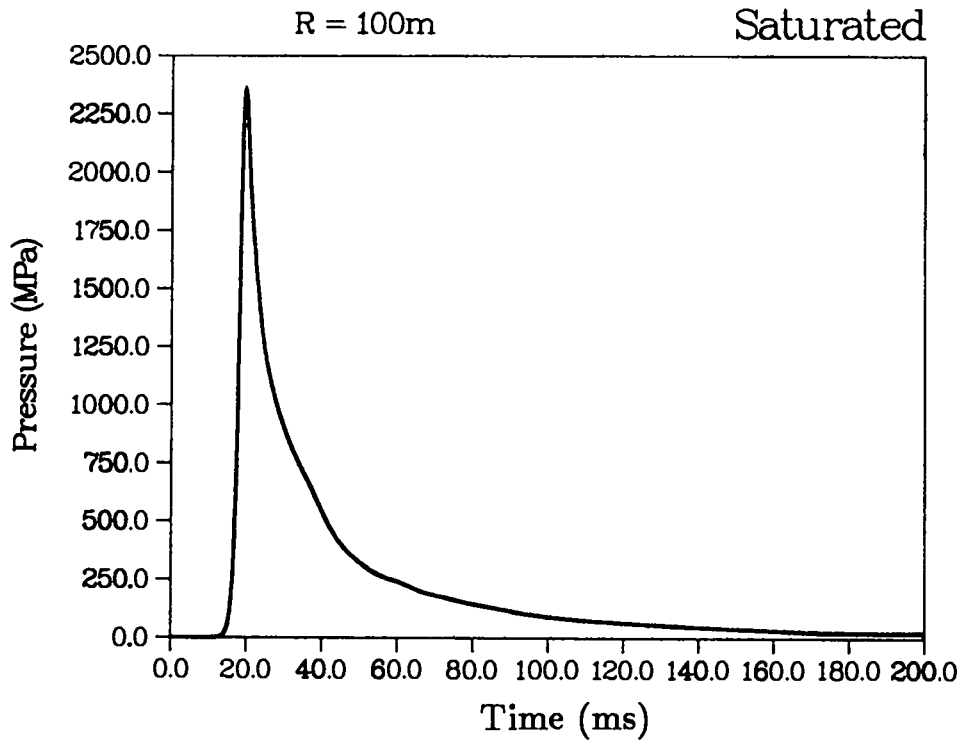

Fig. 24a. Time history of pressure at a range of 100 m in saturated limestone. Notice the rapid rise time and gradual decay.

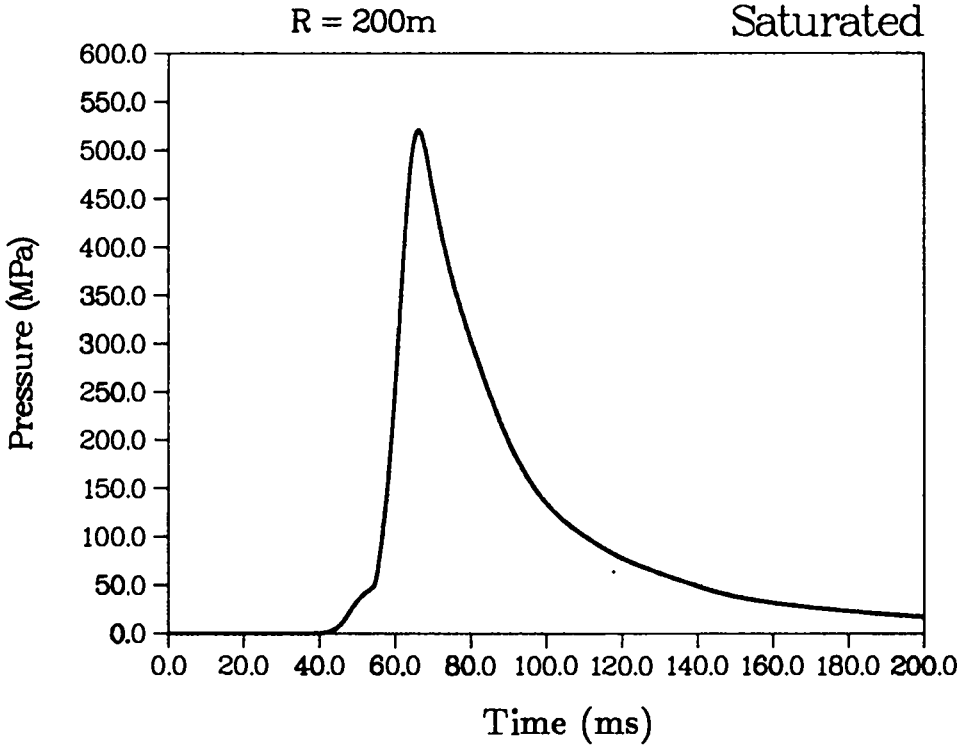

Fig. 24b. Time history of pressure at a range of 200 m in saturated limestone. The peak pressure is now only 540 MPa (5.4 kbar), and a slight precursor is observed.

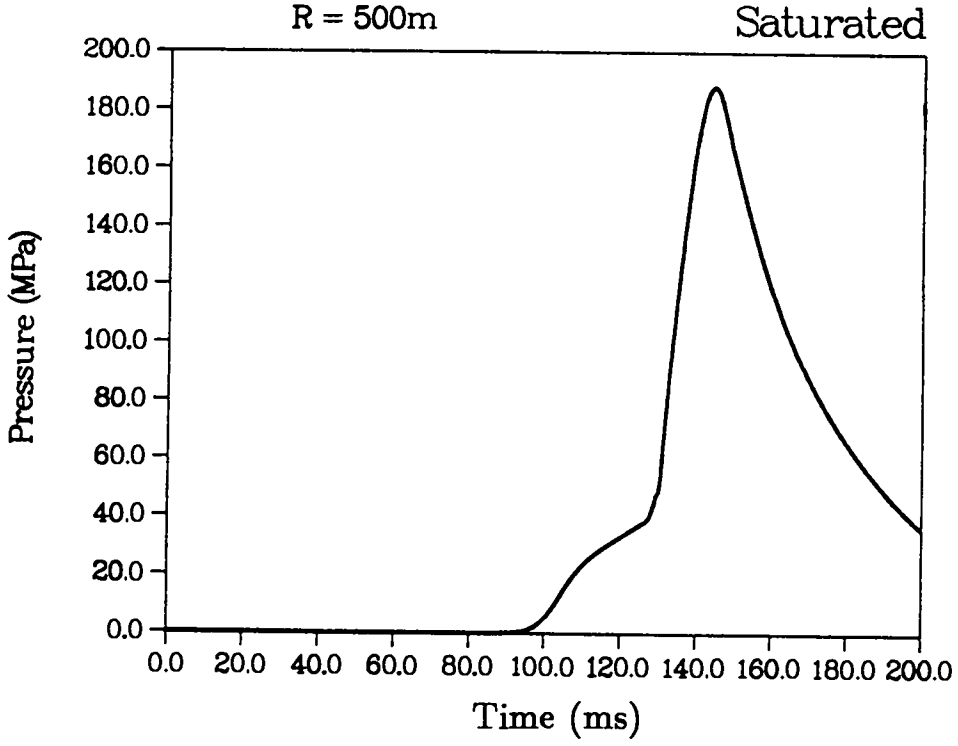

Fig. 24c. Time history of pressure at a range of 500 m in saturated limestone. The peak pressure is significantly diminished, and the pulse shape is more spread out.

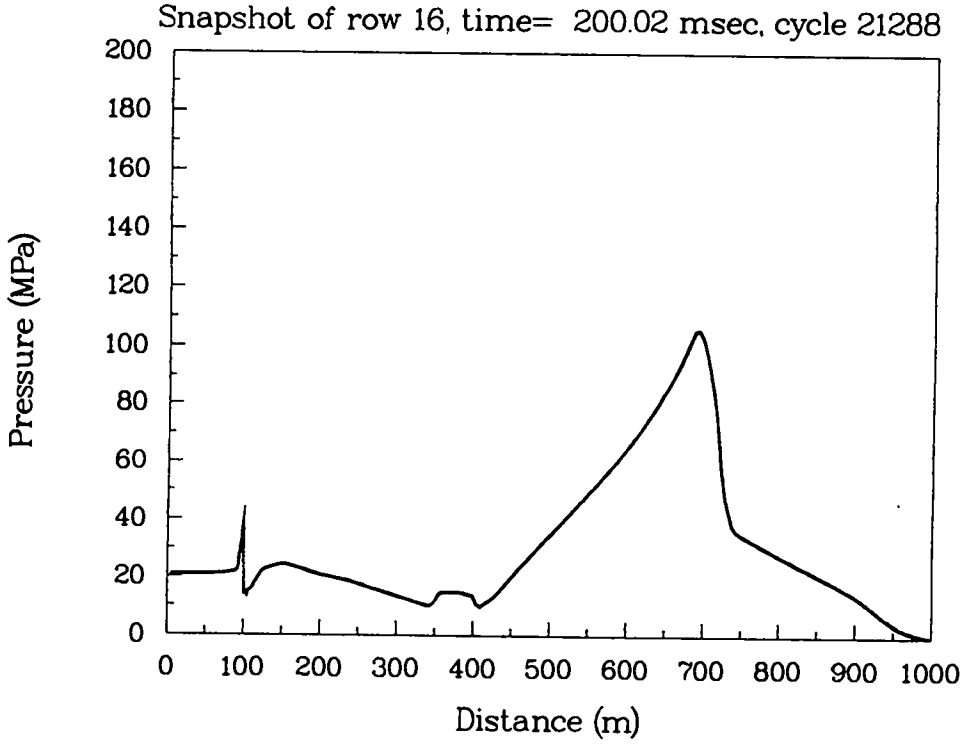

Fig. 25. Snapshot of pressure for a radial slice at 200 ms in saturated limestone. Notice the fairly sharp front and the cavity region and the lower pressures behind the front.

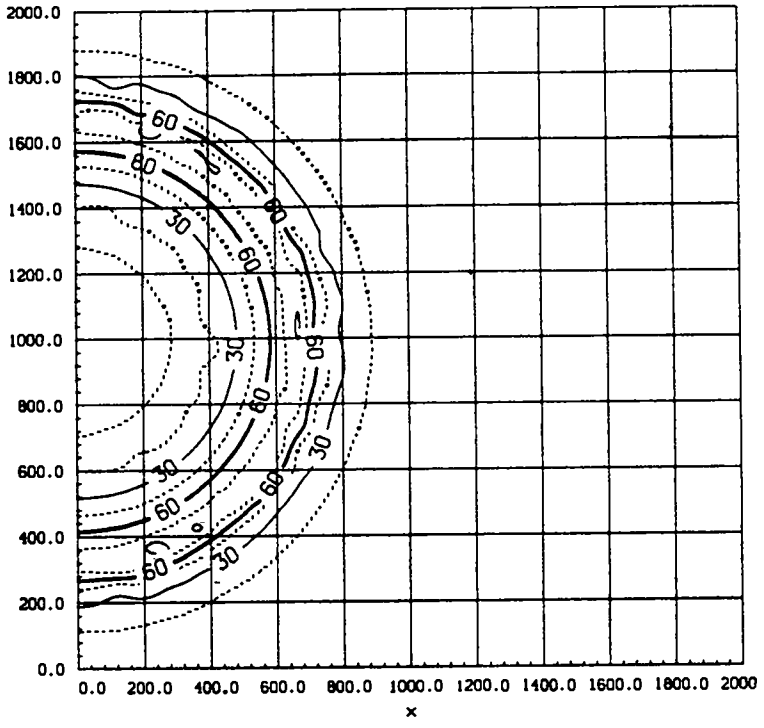

Fig. 26. Contour plot of pressure for the single-source calculation in saturated limestone at 200 ms. The area grid is 2000 x 2000 m, and the peak pressure is 109 MPa (1.09 kbar).

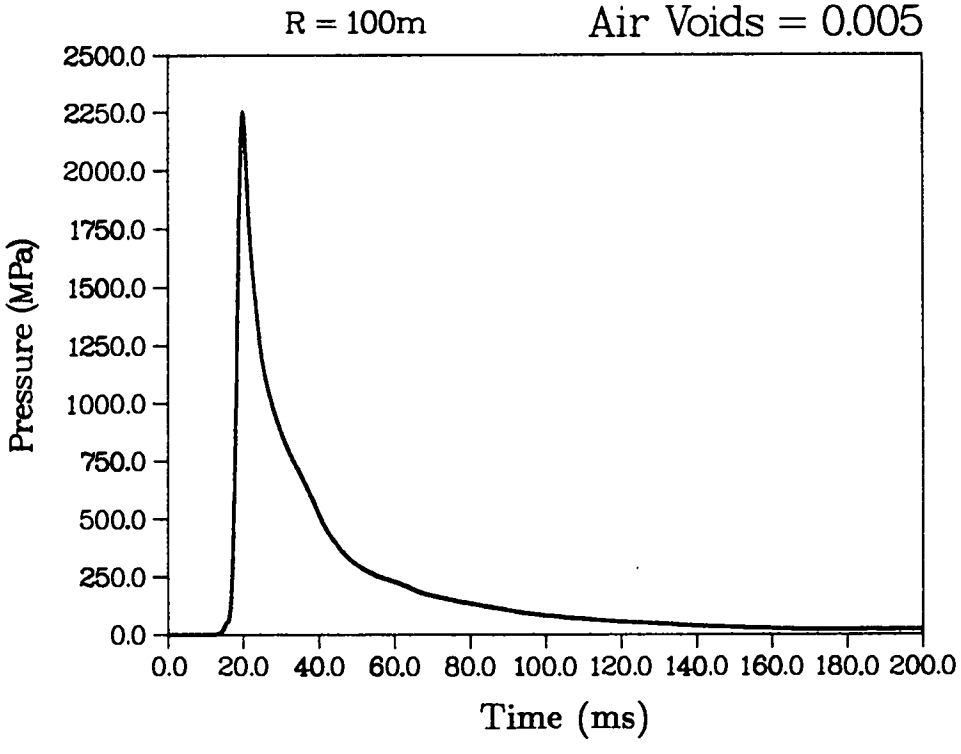

Fig. 27a. Time history of pressure at a range of 100 m in unsaturated limestone. Notice the rapid rise time and gradual decay. The peak pressure is nearly as great as the saturated case (see Fig. 24a.)

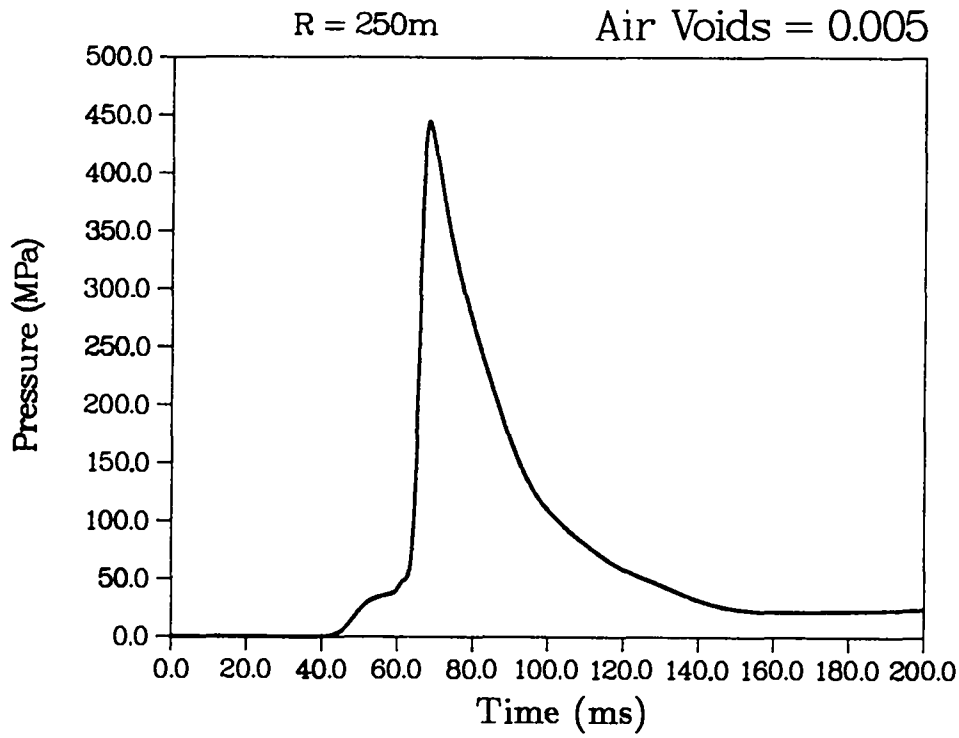

Fig. 27b. Time history of pressure at a range of 250 m in unsaturated limestone. The peak pressure is now only 450 MPa (4.5 kbar), and a more pronounced precursor is present.

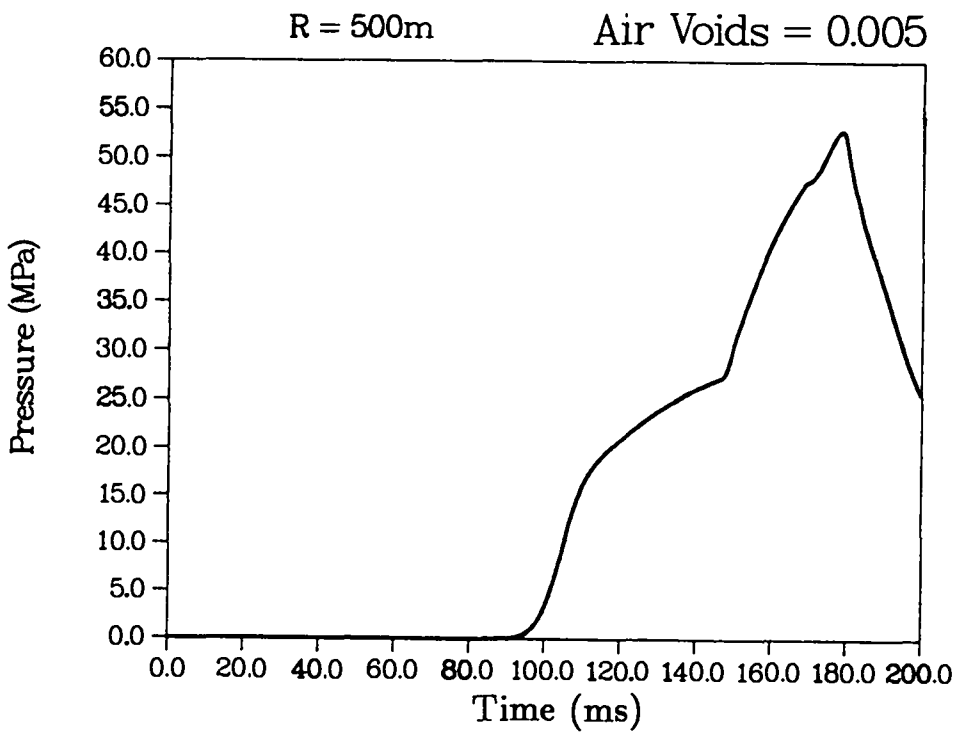

Fig. 27c. Time history of pressure at a range of 500 m in unsaturated limestone. The peak pressure is now only 30% of the saturated peak, and the precursor dominates the pulse shape.

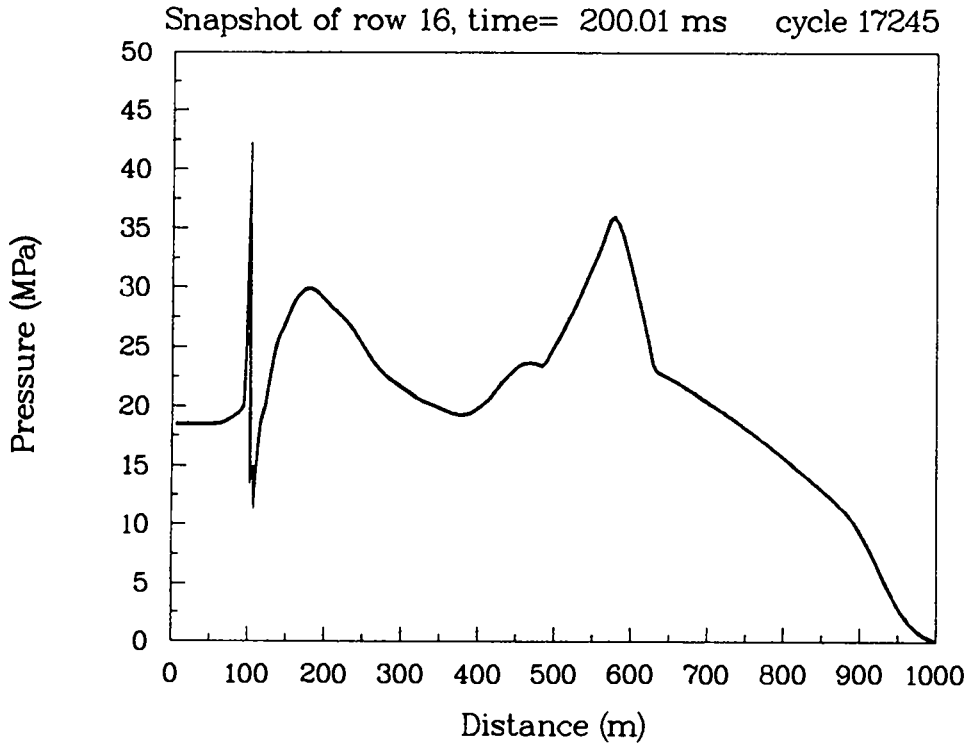

Fig. 28. Snapshot of a pressure for a radial slice at 200 ms in unsaturated limestone. The peak pressure is only nominally greater than the pressure behind the front and in the cavity.

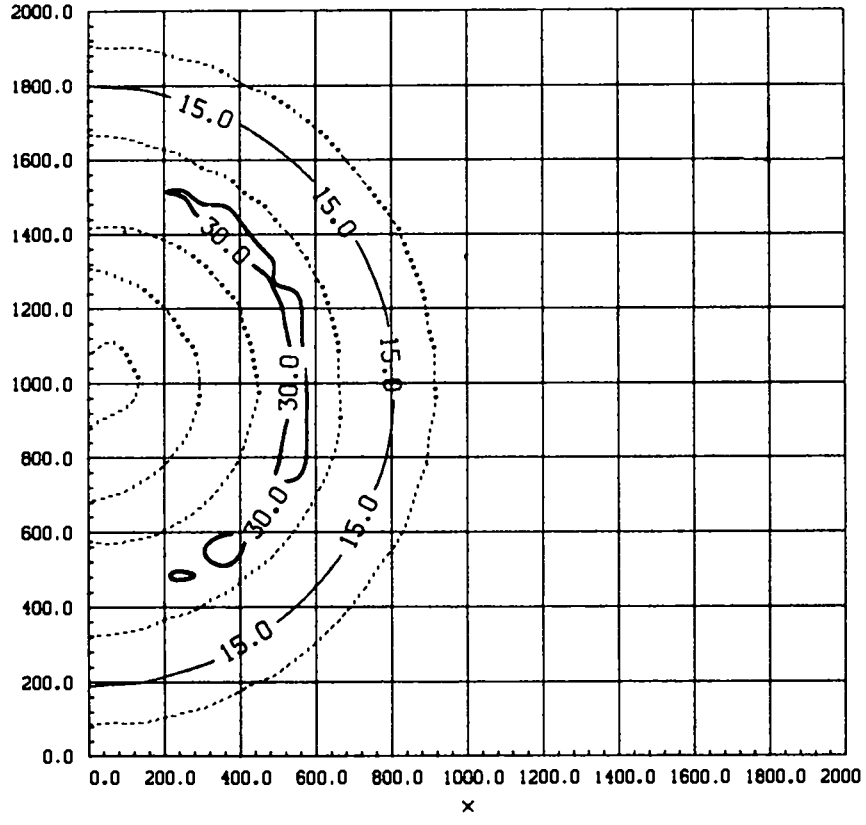

Fig. 29. Contour plot of pressure for the single-source calculation in unsaturated limestone at 200 ms. The area grid is 2000 x 2000 m, and the peak pressure is 53 MPa (0.53 kbar).

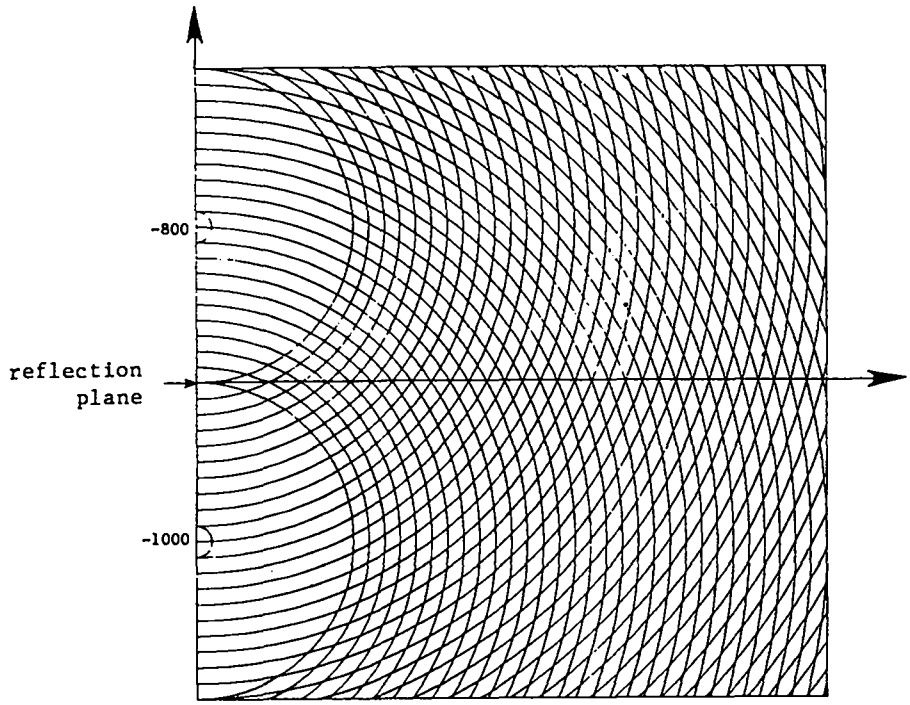

Fig. 30. Possible locations for superimposed time histories. Time histories were obtained from one-dimensional calculations at ranges from 100 to 1000 m, every 10 m. This plot shows those locations, assuming one source is at a depth of 1000 m and the other is at -800 m. The intersections of the concentric circles represent points where data from both sources may be summed. These locations are used to determine the time histories shown in Figs. 34, 35, 36, 39, 40, and 41, the surface plots in Figs. 37b, 38b, 42b, and 43b, and the footprint contour plots in Figs. 47b and 48b.

A. Description of the Superposition Program

The data structure is shown in Fig. 32, which represents 284 complete time histories as generated by the SHALE code. The order of these histories is determined from the code input. In a one-dimensional problem there are only two independent stress tensor components, the radial stress and two equal orthogonal values of the tangential stress. Since the calculation was performed with a two-dimensional code, four components were available. As expected, the in-plane and out-of-plane hoop stresses were essentially equal and the x-y shear stress along the x-axis was very nearly zero. Still, the program was made general and all four of these components were independently summed to give an accurate superimposed state of stress. The ordering was generated so that all 71 σ_{xx} histories were listed sequentially from 100 to 1000 m, then the σ_{yy}, σ_{th} and τ_{xy} results, respectively. For any x-y pair, two radial distances from each source may be calculated. Those radii have

corresponding time histories embedded within the data file as shown in Fig. 32. An index value indicates which history (1 to 284) relates to the required result.

A flow chart is given in Fig. 33, which shows how the proper histories are selected and how they are superimposed, resulting in four independent two-dimensional stress time histories at a point near the requested x-y pair. There are two parts to this process. First the closest point to the two-source location must be determined and the eight corresponding stress histories from the two radial distances must be loaded into memory. The orientations of the point in question (illustrated in Fig. 31) are then used to perform stress transformations at each time increment, and the contribution from each source is then summed to give the total stress component at that given time.

B. Numerical Results from Linear Superposition, Saturated Case

The superposition program described above was used to obtain complete time histories of each component of the stress tensor at selected locations. Once the stress tensor is known, the maximum principle stress and the mean stress (pressure) may be easily calculated. Pressure records along the reflection axis for the full two-source calculation are shown in Figs. 34a-c for x-values of 100, 200, and 500 m (also shown as solid lines in Figs. 8a, 8c, and 8e, respectively). Since these locations are equidistant from each source, the record appears as a single pulse. Notice the sharp rise and decline at all three locations. The records generated from the superposition program at nearly the same positions are shown as dotted lines. In general, the mean stress at a given point and a given time will not be equal to the sum of the mean stresses at the two radial distances from the two sources. For this reason, the full stress tensor is calculated and the individual components are added after transformation to the global x-y frame of reference. Only then can the pressure (or maximum stress) be calculated.

The records at 100 and 300 m show a longer tail than observed in the full two-source calculation. The initial pulse is modeled fairly well by superposition, but it is a bit higher in amplitude. In fact, the match is surprisingly good along the entire reflection axis for these first 200 ms. Comparisons are shown along the theta=zero line in Figs. 35a-d for radial distances of 100, 200, 300, and 500 m. Again, the peak pressures are fairly close,

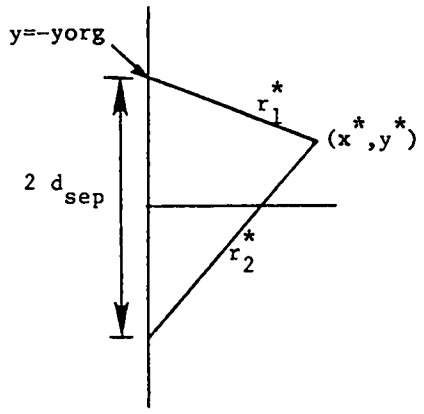

$dy1 = -yorg \quad \& \quad dy2 = -yorg - 2\, d_{sep}$

$$r_1^* = \left(x^{*2} + (y^* - dy1)^2 \right)$$

$$r_2^* = \left(x^{*2} + (y^* - dy2)^2 \right)$$

Closest radial distances are:

$$R_1 = 10 \left(\text{integer } (r_1^* + 5.) / 10 \right)$$

$$R_2 = 10 \left(\text{integer } (r_2^* + 5.) / 10 \right)$$

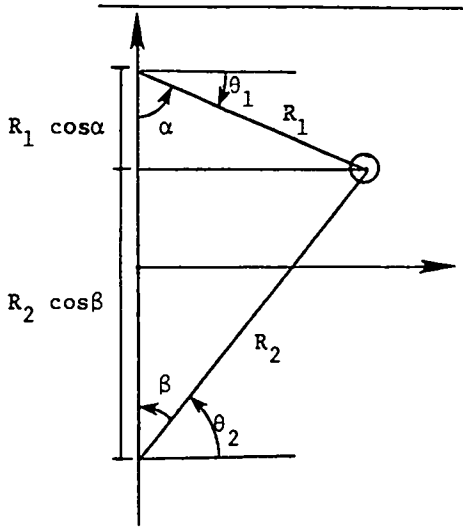

$$R_1 \cos\alpha + R_2 \cos\beta = 2\, d_{sep}$$

$$R_1 \sin\alpha = R_2 \sin\beta$$

$$\alpha = \arccos\left[\frac{(2\, d_{sep})^2 + R_1^2 - R_2^2}{2\, R_1\, (2\, d_{sep})} \right]$$

$$\beta = \arccos\left[\frac{(2\, d_{sep})^2 + R_2^2 - R_1^2}{2\, R_2\, (2\, d_{sep})} \right]$$

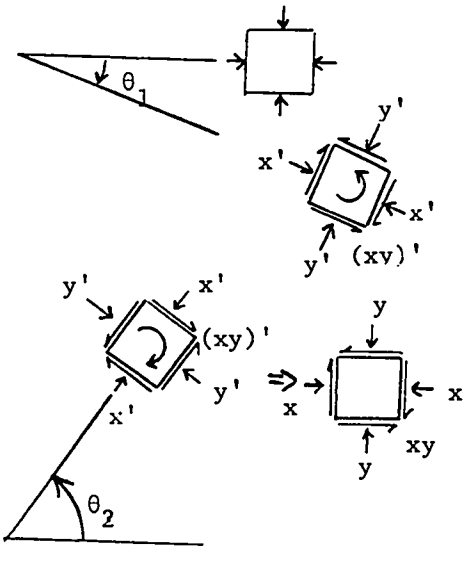

$\theta_1 = \pi/2 - \alpha$

so rotate <u>anti-clockwise</u> to get to global x-y-frame.

$\theta_2 = \pi/2 - \beta$

so rotate <u>clockwise</u> to get to global x-y-frame.

Fig. 31. Location of the requested point, calculation of the nearest point where superposition is possible (see Fig. 30), and orientation of the stress tensor from each source.

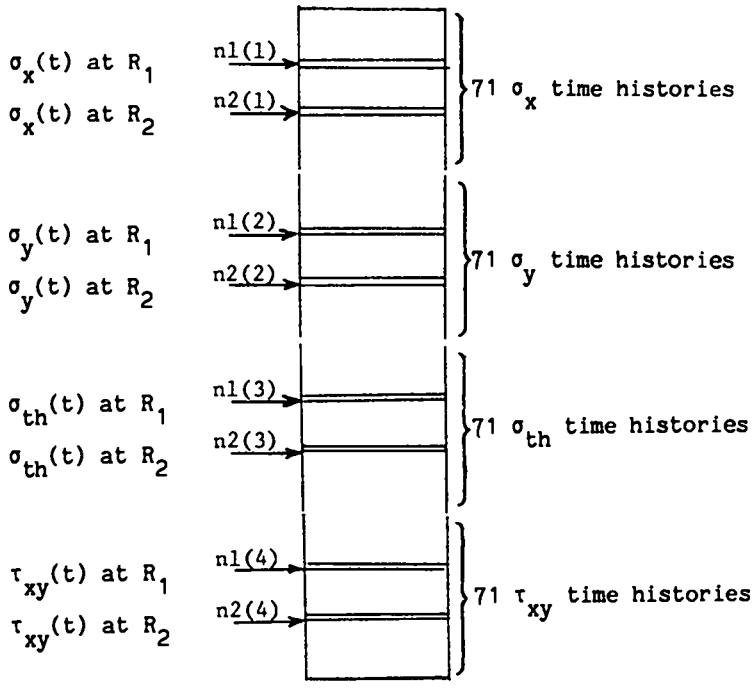

Fig. 32. Organization of the data file containing all the time history data from a one-dimensional SHALE calculation. Notice that all the time histories of a given type were loaded sequentially (zero to 200 ms) for each location (100 m to 1000 m) before the next stress component history group was written.

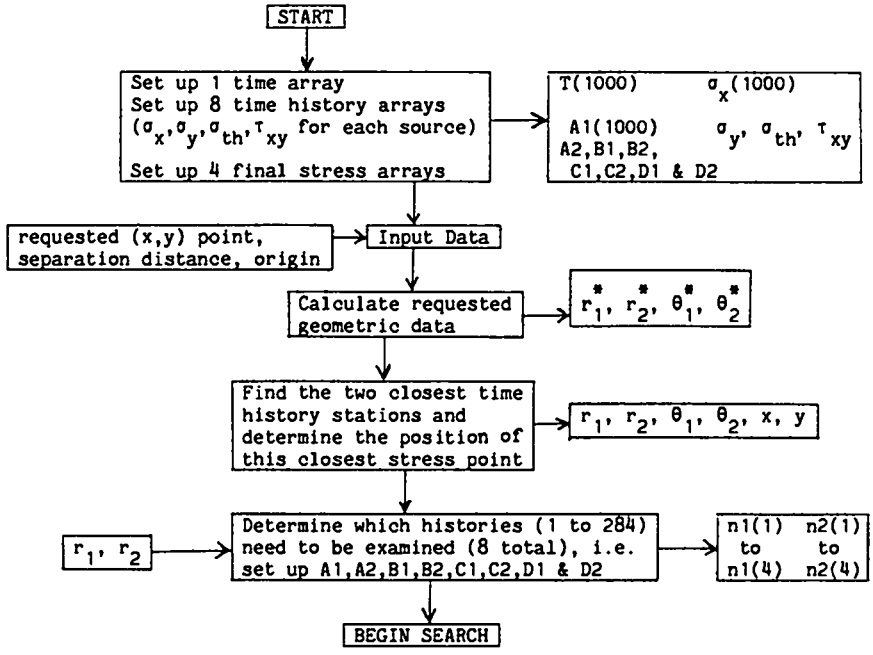

Fig. 33. Flow chart for the superposition program. (The data file is shown in Fig. 32.) There are three main parts of the program: a) setup and initialization; b) search for the required histories; and c) stress transformation and summation. This process must be followed for each (x,y) pair where a history is desired.

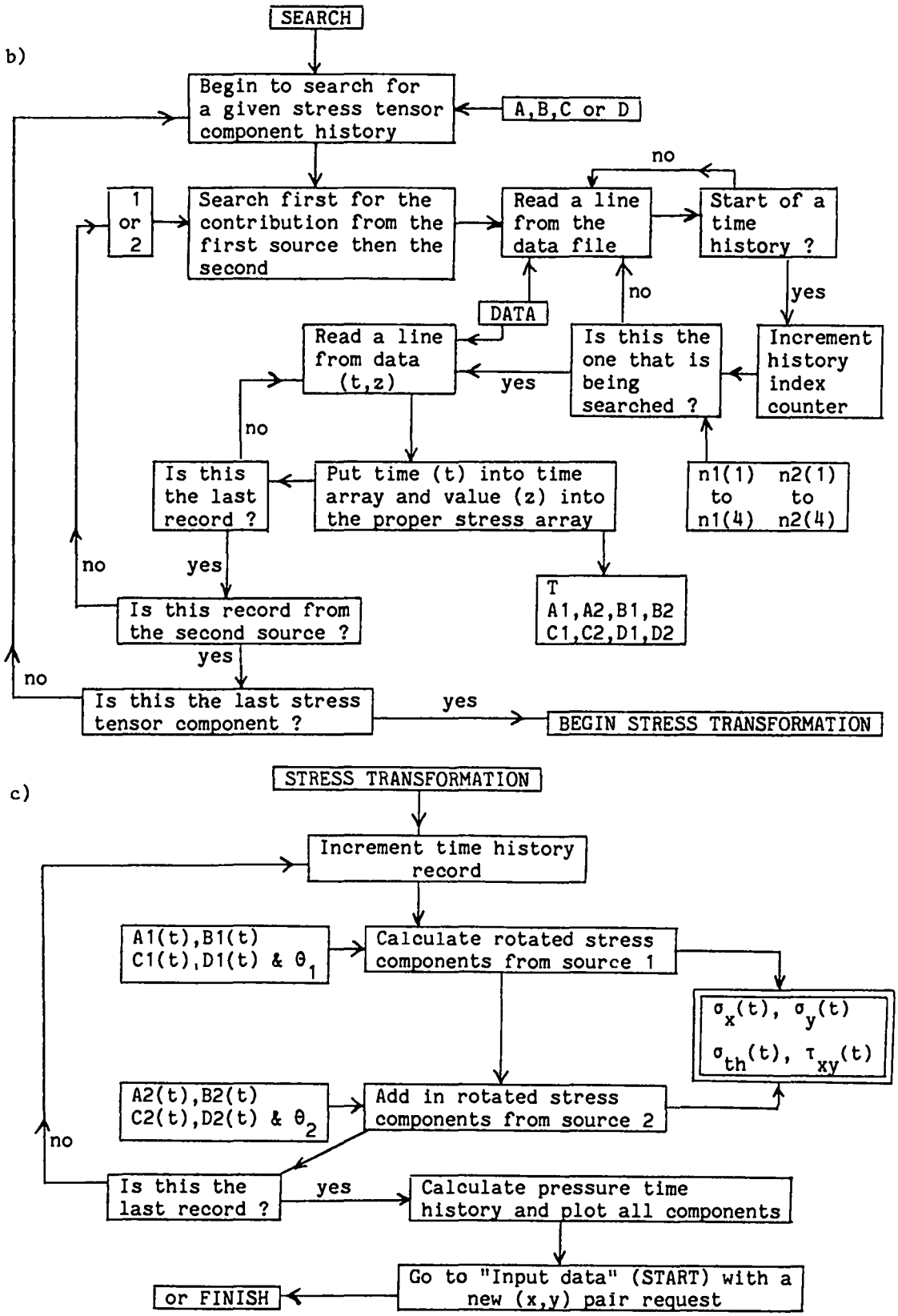
b)
SEARCH
Begin to search for a given stress tensor component history
A,B,C or D
1 or 2
Search first for the contribution from the first source then the second
Read a line from the data file
no
Start of a time history ?
yes
DATA
Read a line from data (t,z)
Is this the one that is being searched ?
no
yes
Increment history index counter
no
Is this the last record ?
Put time (t) into time array and value (z) into the proper stress array
n1(1) to n1(4)
n2(1) to n2(4)
no
yes
Is this record from the second source ?
T
A1,A2,B1,B2
C1,C2,D1,D2
yes
no
Is this the last stress tensor component ?
yes
BEGIN STRESS TRANSFORMATION
c)
STRESS TRANSFORMATION
Increment time history record
A1(t),B1(t) C1(t),D1(t) & θ1
Calculate rotated stress components from source 1
σx(t), σy(t)
σth(t), τxy(t)
A2(t),B2(t) C2(t),D2(t) & θ2
Add in rotated stress components from source 2
no
Is this the last record ?
yes
Calculate pressure time history and plot all components
Go to "Input data" (START) with a new (x,y) pair request
or FINISH

Fig. 33 (cont)

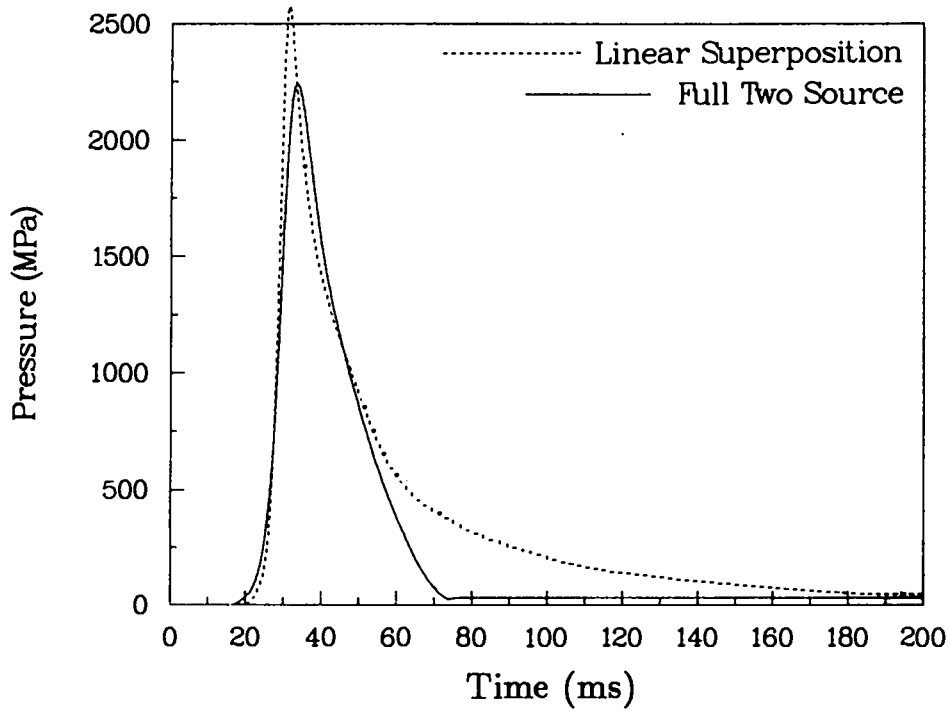

Fig. 34a. Pressure time histories at a location of x = 100 m and y = -900 m (along the reflection axis) for fully saturated limestone: full two-source calculation and linear superposition. The two curves are roughly equivalent.

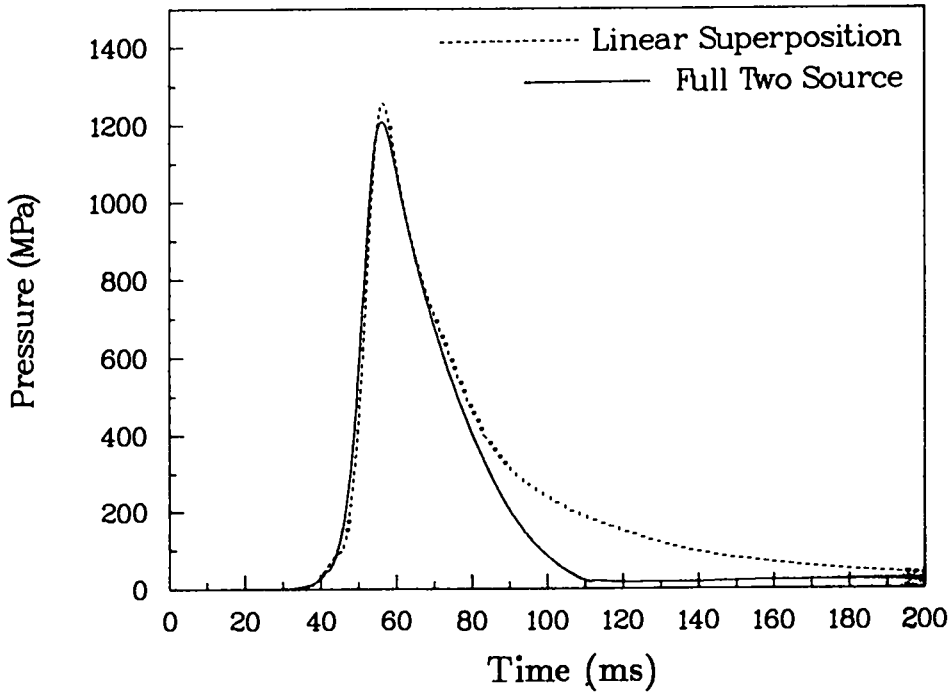

Fig. 34b. Pressure time histories at a location of x = 200 m and y = -900 m (along the reflection axis) for fully saturated limestone: full two-source calculation and linear superposition. The superimposed tail is a bit longer.

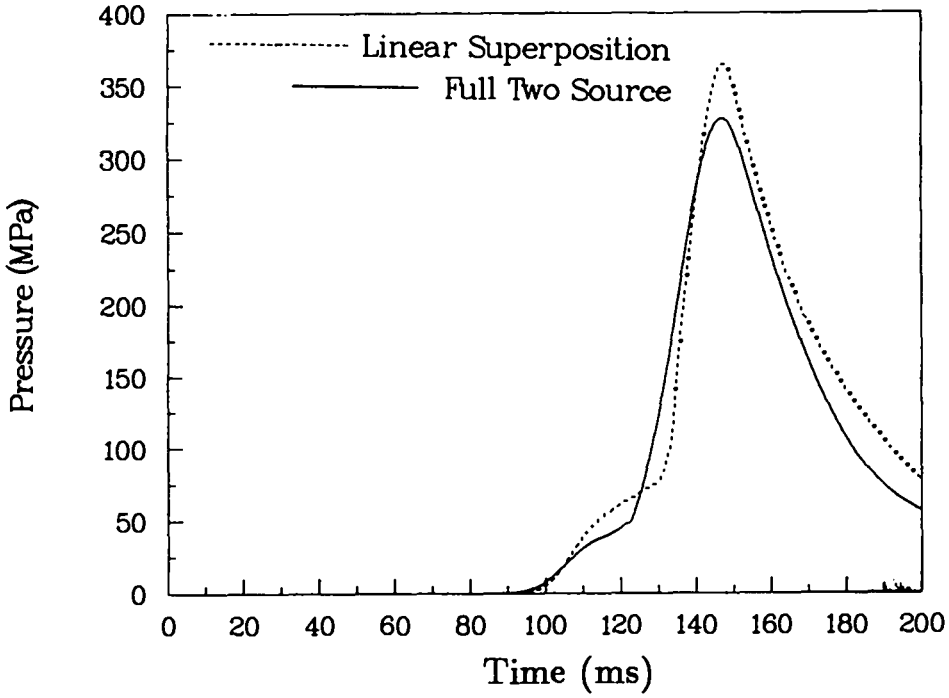

Fig. 34c. Pressure time histories at a location of x = 500 m and y = -900 m (along the reflection axis) for fully saturated limestone: full two-source calculation and linear superposition. Slightly different precursor positions.

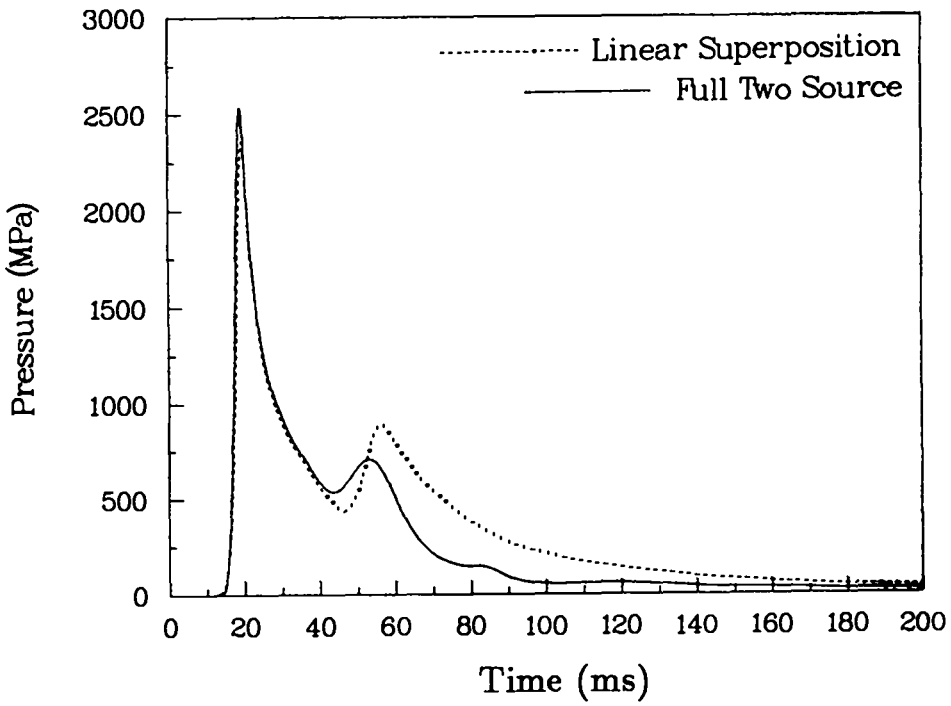

Fig. 35a. Pressure time histories at a location of x = 100 m and y = -800 m (theta=zero) for fully saturated limestone: full two-source calculation and linear superposition. Notice later arrival of second superimposed signal.

but the second pulse arrives noticeably later in the superposition case. This is presumably because some preconditioning, or compaction of the geologic material, is done by the closest source so that the signal from the more distant source travels at a higher velocity and thus arrives a bit sooner. At 200 m both curves show the second arrival clearly, but the full two-source case indicates some merging of the signals, and by 300 m they are essentially a single pulse. The amplitude of the second superimposed source at this range actually appears larger since it is simply adding the fairly high amplitude declining signal from the very recent first pulse. Finally, by 500 m both cases have merged into a single pulse waveform whose amplitudes are essentially equal. The time histories along the theta=45° line are shown in Figs. 36a-c for ranges of 100, 200, and 500 m. The peak amplitudes agree fairly well as before, but the the second signal is more distinct and arrives even later because of the greater distances it must travel in material compacted by the nearer source. At 500 m, the full two-source calculation shows both signals merged together. Notice that in Fig. 34a the superimposed signal has a slower decay than the signal from the full two-source calculation. This accounts for the relatively higher peak of the second signal as it rides up on the more slowly decaying tail of the nearer source signal in Figs. 36a-c.

Another method of determining the relative effect of superposition is to compare the state of stress for the entire region at a given time. These "snapshots" show the extent of agreement or disagreement that cannot be evaluated from individual time histories. Figure 37a shows a surface plot of pressure for the full two-source calculation in saturated material at 150 ms. The two axes of symmetry have been used to get a complete picture. The amplification along the reflection axis is clearly visible. The vertical axis is scaled such that the maximum is 350 MPa (3.5 kbar). The length scale is 1400 x 1400 m (-700 to +700 m in each direction, double symmetry). Notice along the axis of cylindrical symmetry, the shock front appears to be from a single source. The enhancement along the other axis is about 60%. If two sources are superimposed as described above, the resulting pressure field is shown in Fig. 37b. Essentially, the steps in Fig. 33 had to be followed for enough x-y pairs (about 2500) to obtain a smooth surface. Notice the peak amplitudes along the reflection axis are nearly equal. Two significant differences may be observed, however. First, the peak drops off much more quickly in this case than in Fig. 37a. This

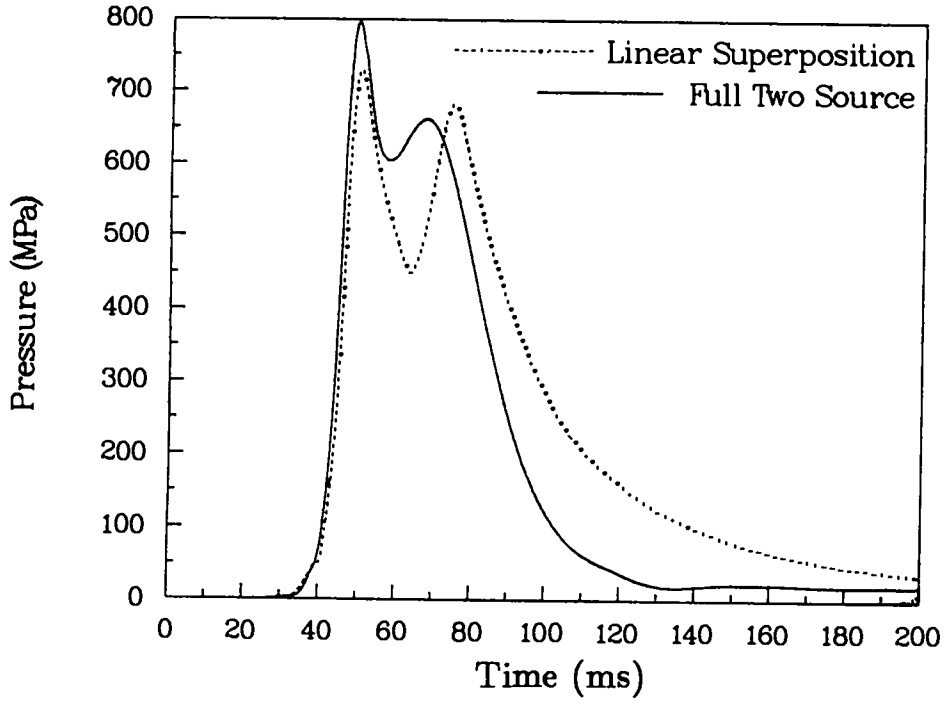

Fig. 35b. Pressure time histories at a location of x = 200 m and y = -800 m (theta=zero) for fully saturated limestone: full two-source calculation and linear superposition. The peak pressures are governed by the initial signals.

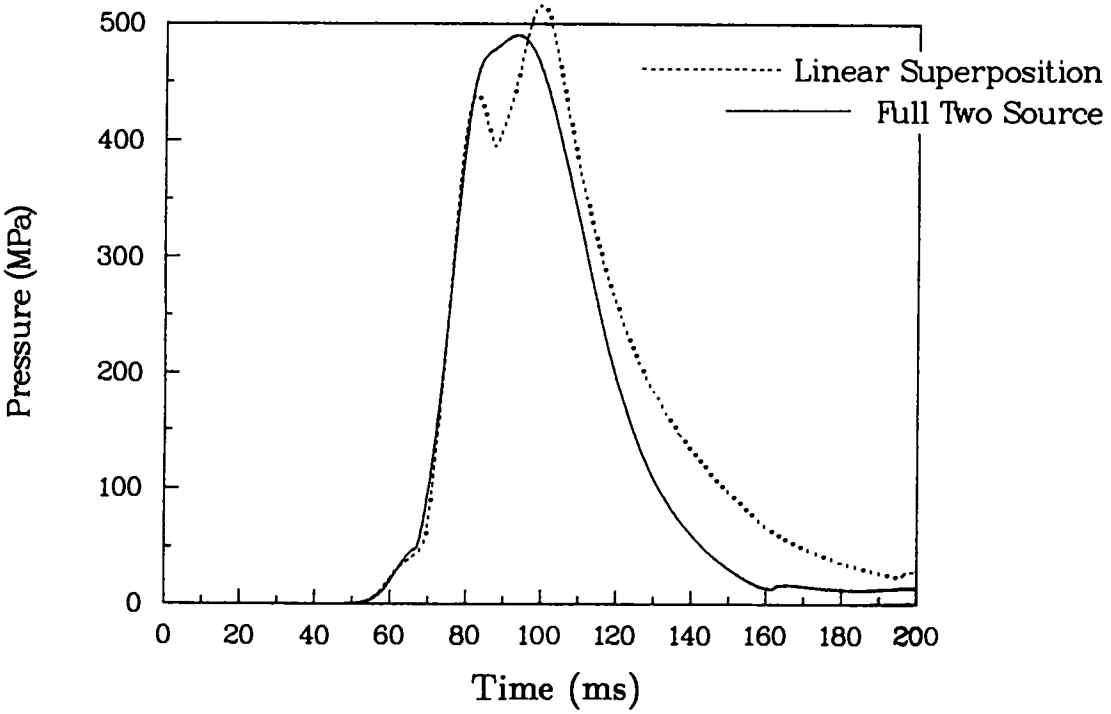

Fig. 35c. Pressure time histories at a location of x = 300 m and y = -800 m (theta=zero) for fully saturated limestone: full two-source calculation and linear superposition. The full two-source signals have merged into a single pulse.

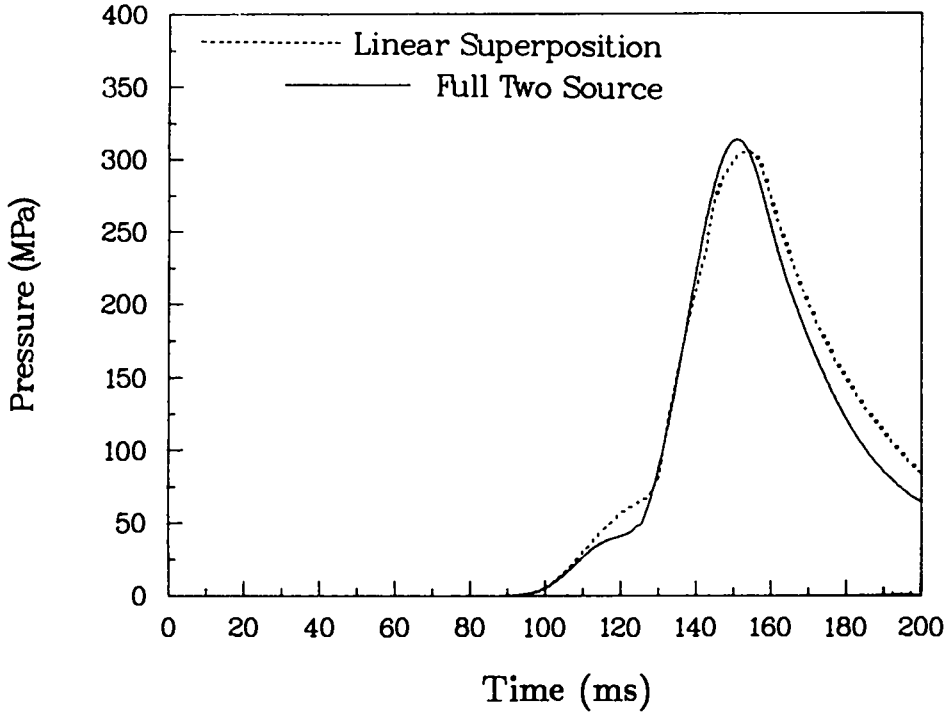

Fig. 35d. Pressure time histories at a location of x = 500 m and y = -800 m (theta=zero) for fully saturated limestones: full two-source calculation and linear superposition. Both signals are virtually indistinguishable at this range.

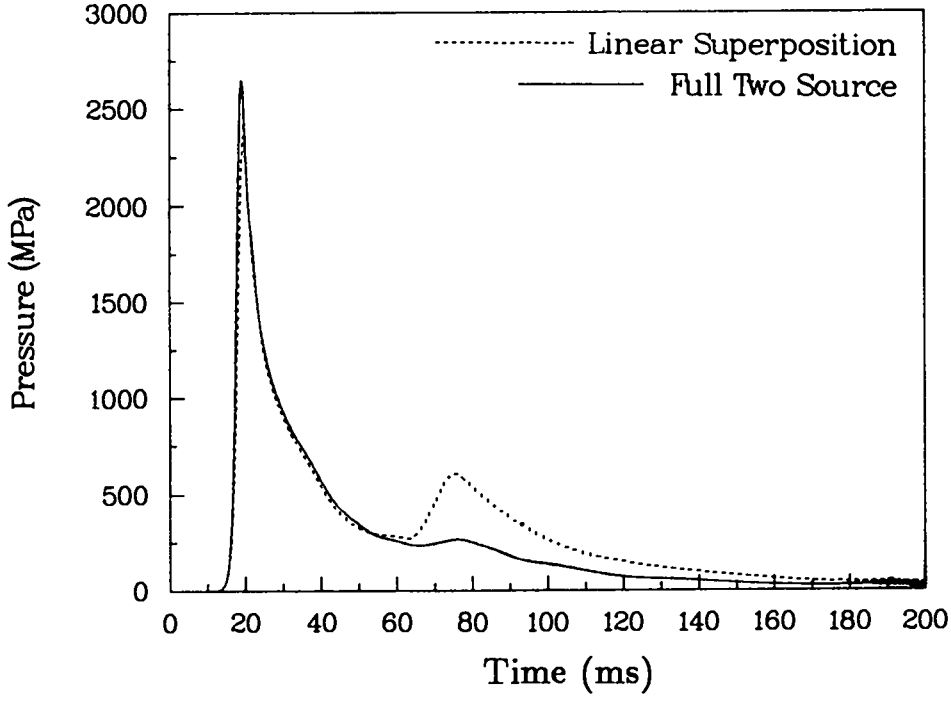

Fig. 36a. Pressure time histories at a range of 100 m and along the theta=45° line for fully saturated limestone: full two-source calculation and linear superposition. There is a more pronounced superimposed signal.

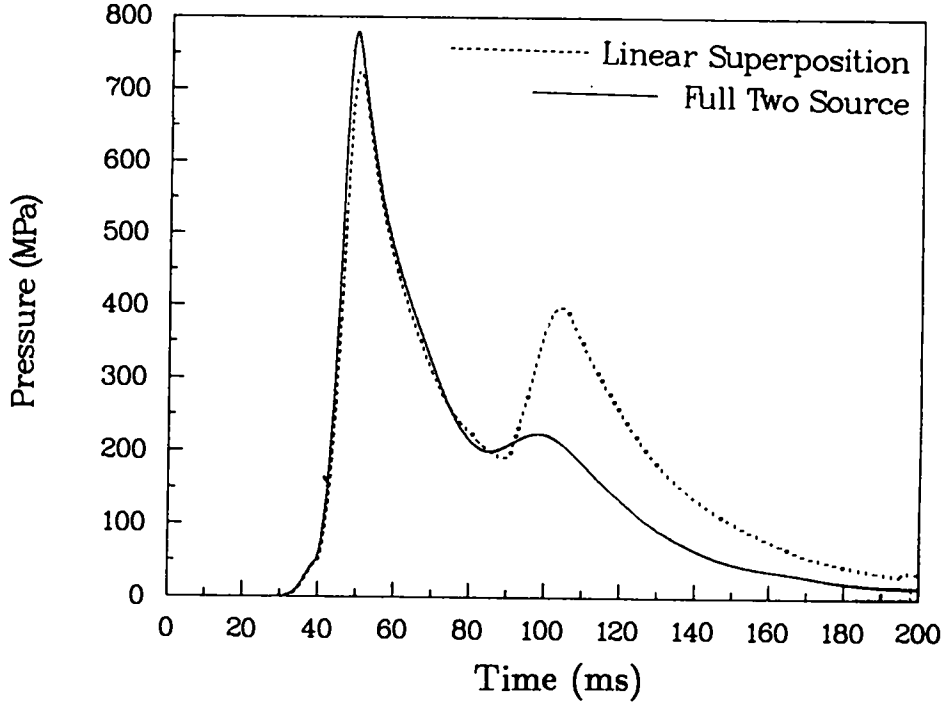

Fig. 36b. Pressure time histories at a range of 200 m and along the theta=45° line for fully saturated limestone: full two-source calculation and linear superposition. The peak signal in both cases is still from the first source.

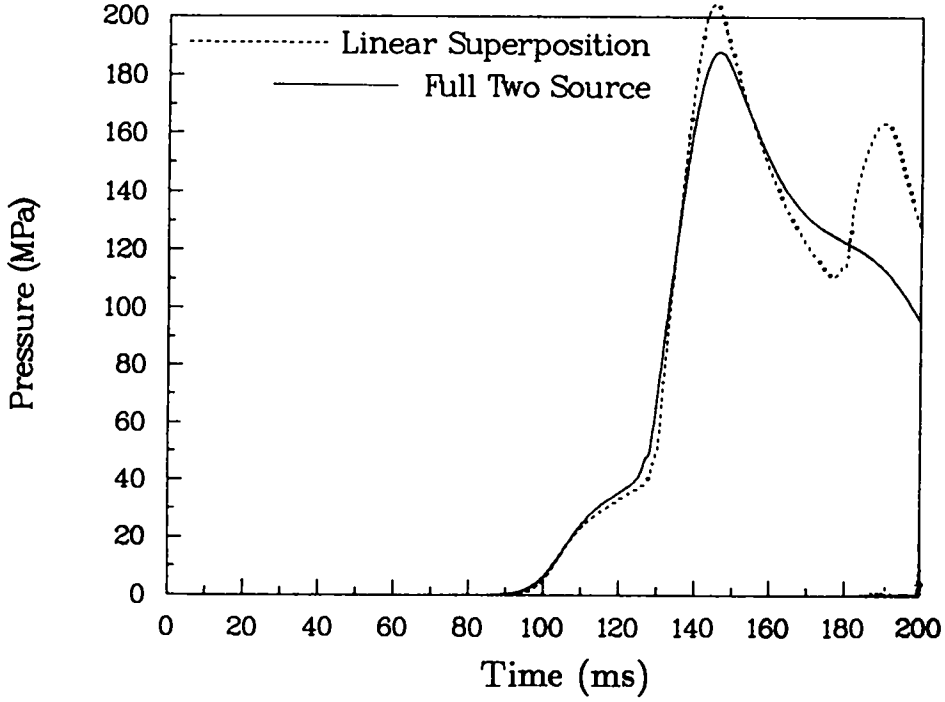

Fig. 36c. Pressure time histories at a range of 500 m and along the theta=45° line for fully saturated limestone: full two-source calculation and linear superposition. The second superimposed signal arrives too late to add to the peak.

would result in a diminished "footprint" of an area exceeding a stress of a given magnitude. The second feature is that the two stress waves can be clearly seen along the other axis, whereas they had merged into a single, "spread-out" pulse in Fig. 37a, the full two-source calculation. Again, the reason for the difference is that the superposition case does not allow for precompaction of material in the path of the second signal. Thus it travels more slowly and can be seen more clearly.

Surface plots of maximum principle stress for the full two-source and superimposed calculations are shown in Figs. 38a and 38b, respectively. All the scales are the same as in Figs. 37a and 37b. Notice that the peak mean stress is only about 10% less than the peak maximum stress at this time since the stress state is nearly hydrostatic at this time. The superimposed case actually shows a slightly higher peak along the reflection axis but again drops off much too quickly along the azimuth when compared with the full two-source calculation. Also, the two distinct fronts are much more visible in Fig. 38b than in Fig. 38a.

C. Numerical Results from Linear Superposition, Unsaturated Case

Except for the sharper drop-off in pressure in the azimuthal direction for the superimposed case, the comparison to the full two-source calculation in most other respects was fairly good. A second full-source calculation was run in which the water content and bulk density were slightly reduced so that the gas porosity represented one-half of 1% of the total volume. It has been suggested that this may be a reasonable upper limit for a generic limestone below the water table. Although the mass water content only changed from 5.830 to 5.646% and the bulk density changed from 2.4950 to 2.4901 g/cc, the resulting propagation and interaction of the shock waves were dramatically affected. Moreover, the superposition technique is much less accurate in virtually all aspects for this case.

Pressure time histories for this unsaturated case along the reflection axis are shown in Figs. 39a-d for ranges (from the point of double symmetry) of 100, 300, 400, and 500 m, respectively. They may be compared to similar plots for the saturated case in Figs. 35a-d. Notice the response at 100 m is similar, but the signal has been strongly attenuated at greater distances. The linearly superimposed results are shown as dashed

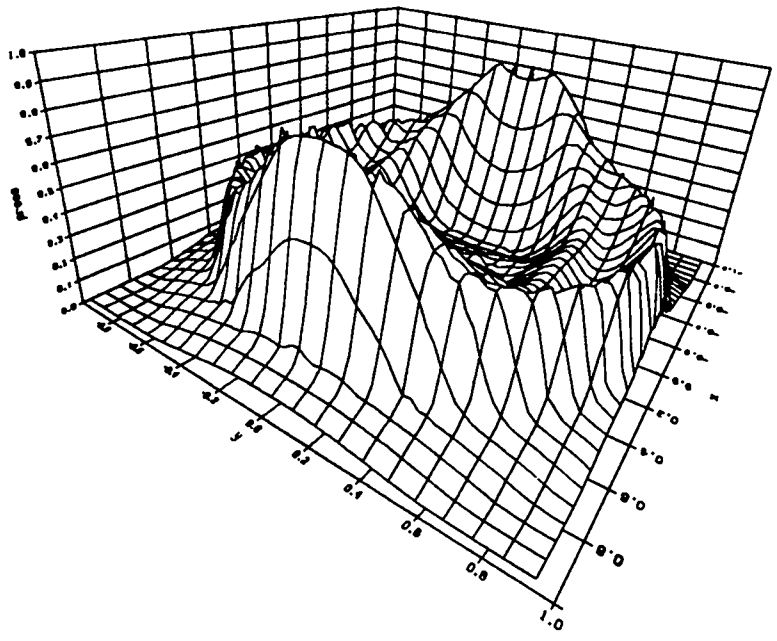

Fig. 37a. Surface plot of pressure at 150 ms in fully saturated limestone for the full two-source calculation. This plot shows all the symmetry with an area of 1400 x 1400 m. The maximum z-axis value is 350 MPa (3.5 kbar). Notice the region of pressure addition and the other areas of essentially one-dimensional peak behavior.

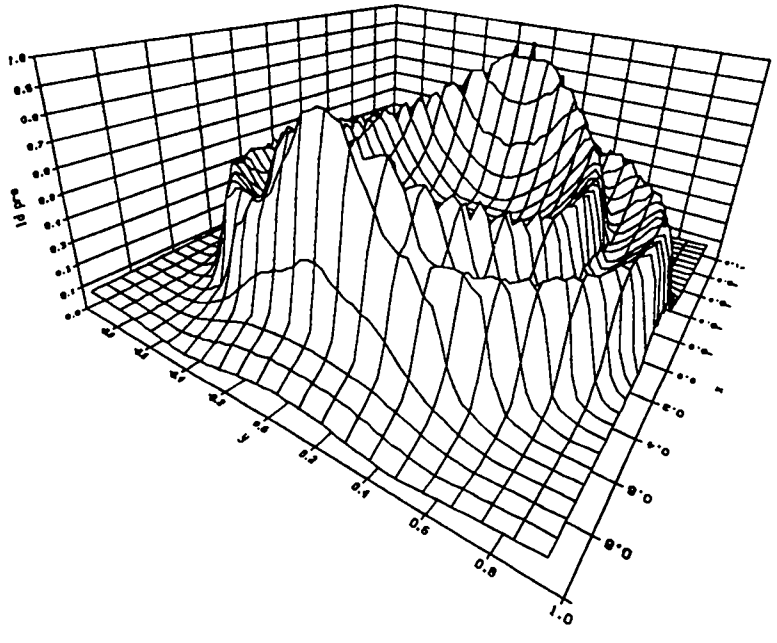

Fig. 37b. Surface plot of pressure at 150 ms in fully saturated limestone using linear superposition. This plot shows all the symmetry with an area of 1400 x 1400. The maximum z-axis value is 350 MPa (3.5 kbar). Although the peak pressure along the reflection axis is similar to Fig. 35a, the magnitude drops off more rapidly along the azimuth. Also notice the more prominent second signal following the initial pulse.

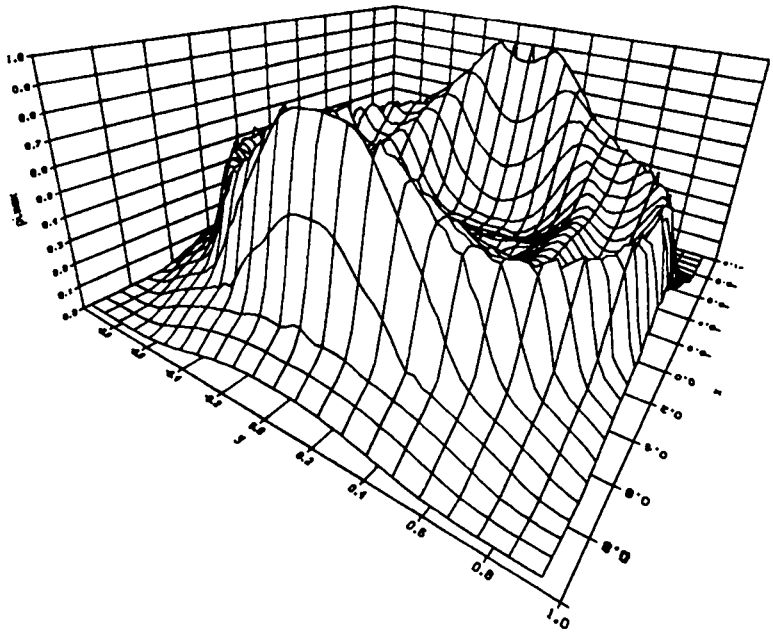

Fig. 38a. Surface plot of maximum stress at 150 ms in fully saturated limestone for the full two-source calculation. This plot show all the symmetry with an area of 1400 x 1400 m. The maximum z-axis value is 350 MPa (3.5 kbar). Notice the maximum stress in all locations is only slightly greater than the pressures in Fig. 37a.

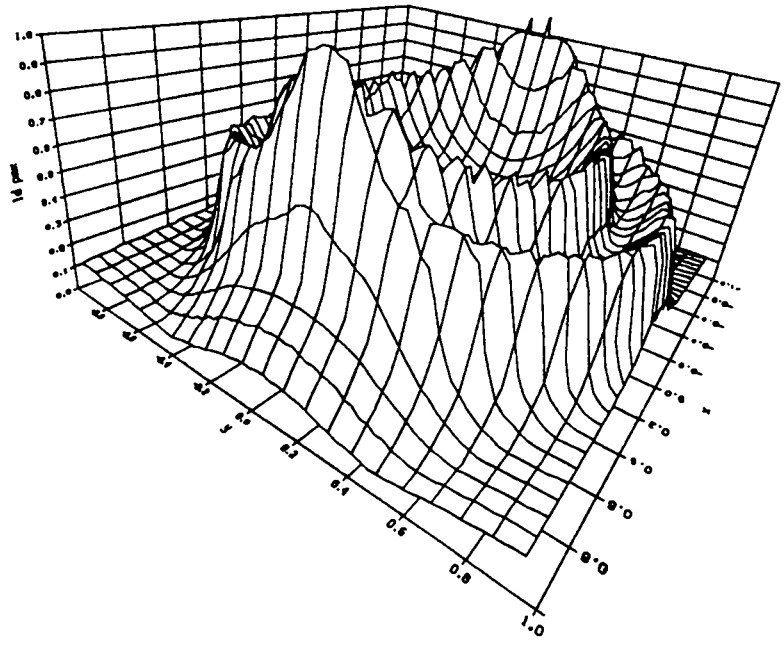

Fig. 38b. Surface plot of maximum stress at 150 ms in fully saturated limestone using linear superposition. This plot shows all the symmetry with an area of 1400 x 1400 m. The maximum z-axis value is 350 MPa (3.5 kbar). The maximum stresses are slightly higher than the pressures, but notice that the peak values fall off away from the reflection axis as in Fig. 37b.

lines in Fig. 39. Although both curves match fairly well up to 300 m, the peak amplitudes of the superimposed curves are significantly less at greater ranges, even along this axis of symmetry. Notice in particular the formation and evolution of the precursor signal, which seems to have stabilized for the full two-source calculation but looks completely different and more dominant for the superimposed case. The response along the theta=zero line is shown in Figs. 40a-e for distances of 100 to 500 m. These time histories, more than any other series of figures, show the limitations of linear superposition. The main feature of all these plots is the significantly delayed arrival of the second signal for linear superposition. The cause is the same as before, i.e., precompaction and thus velocity enhancement, but it is much more influential in the case with some air-filled voids. The response at 100 m is not too bad, but even by 200 m (Fig. 40b) the second signal has nearly been completely merged into the first. Since the full two-source calculation is then essentially a single pulse signal at greater distances, the peak pressure is nearly double at ranges beyond 400 m (see Figs. 40d and 40e). This has profound effect on the dimensions of the peak stress "footprint" as explained below. The time histories along the theta=45° line are shown in Figs. 41a-e. The signal from the second source is delayed even more since more precompacted material is in between the second source and each time history location. The peak pressures are not significantly different between the full two-source and superimposed histories since that quantity is governed only by the arrival of the nearest (first) source signal. Still, the tendency of the two signals to merge into a single pulse in the two-source calculation is significant.

Surface plots showing the spatial extent of pressure at a given time are shown in Figs. 42a and 42b for the full two-source and superposition cases at 150 ms, respectively. The x- and y-axes both go from -700 to +700 m as before, but the maximum pressure is 200 MPa (2 kbar), reflecting the decreased amplitude resulting from compaction. Clearly, the full two-source calculation gives a significantly higher pressure along the reflection axis as well as a much larger "footprint" of material, which has seen a pressure of a given level. Notice also that in the superimposed case (Fig. 42b), the amplitude is significantly less and the peak pressure drops off rapidly away from the reflection axis in this case as in the saturated material as shown in Fig. 37b. Figures 43a and 43b show similar surface plots of

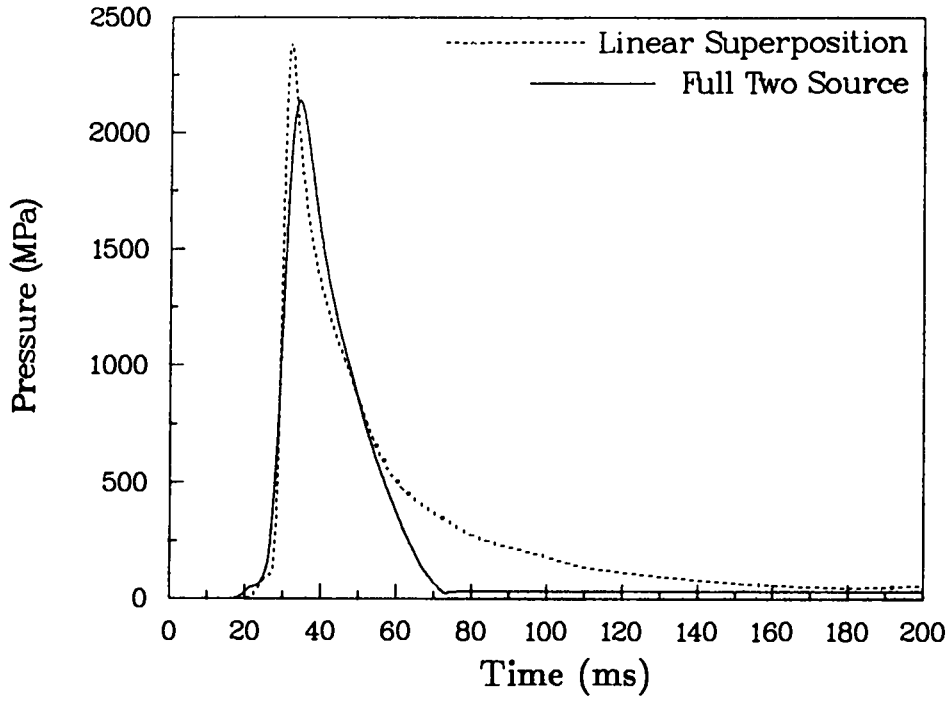

Fig. 39a. Pressure time histories at a location of x = 100 m and y = -900 m (along the reflection axis) for 0.005 air voids limestone: full two-source calculation and linear superposition. The two curves are roughly equivalent.

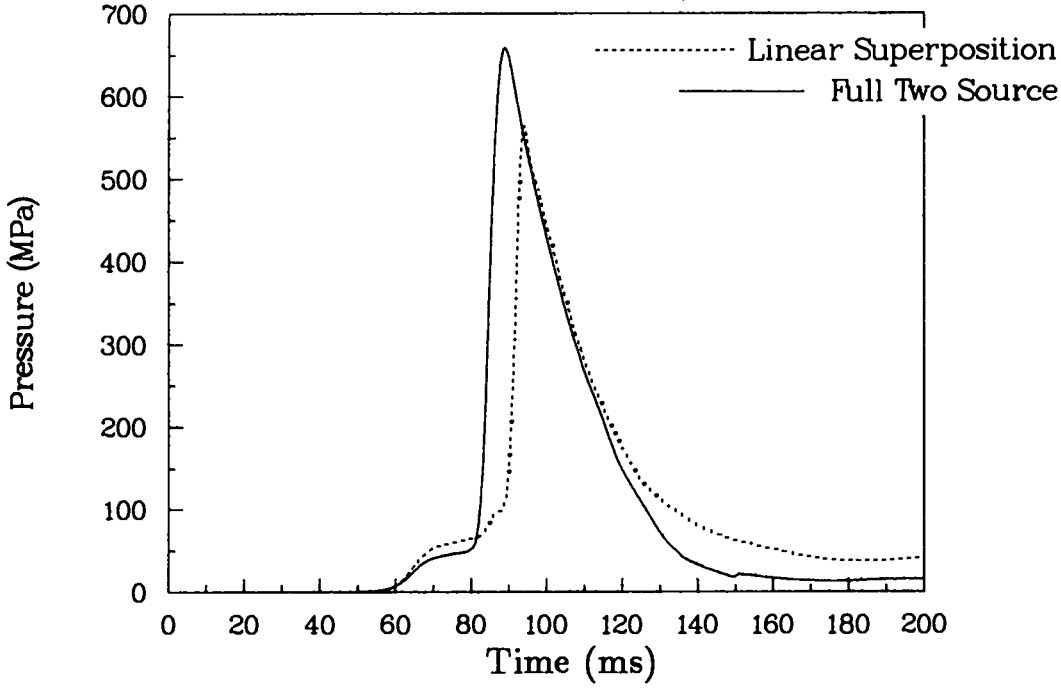

Fig. 39b. Pressure time histories at a location of x = 300 m and y = -900 m (along the reflection axis) for 0.005 air voids limestone: full two-source calculation and linear superposition. The superimposed peak is lower and later.

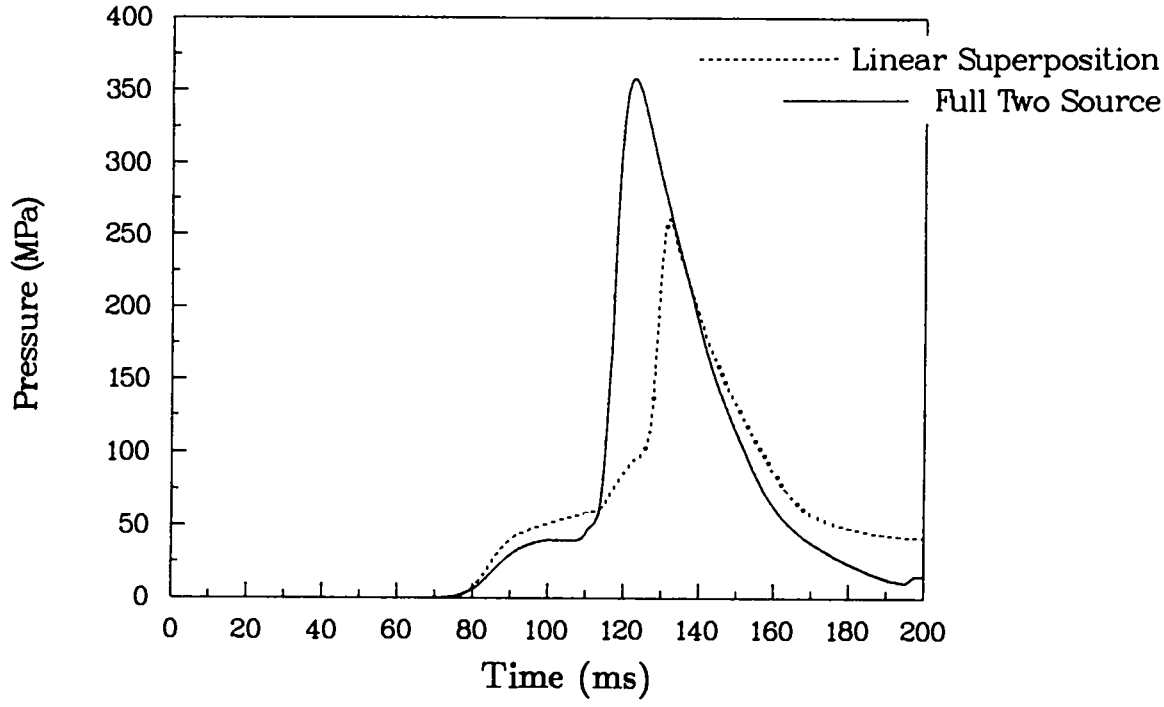

Fig. 39c. Pressure time histories at a location of x = 400 m and y = -900 m (along the reflection axis) for 0.005 air voids limestone: full two-source calculation and linear superposition. The superimposed signal is much weaker.

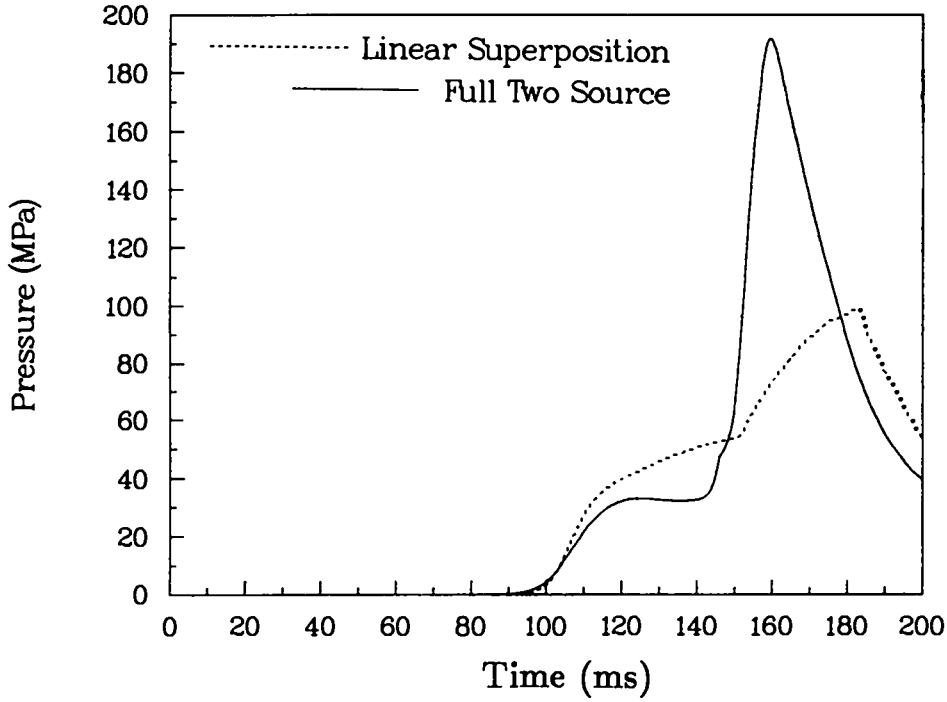

Fig. 39d. Pressure time histories at a location of x = 500 m and y = -900 m (along the reflection axis) for 0.005 air voids limestone: full two-source calculation and linear superposition. Strongly attenuated superimposed signal.

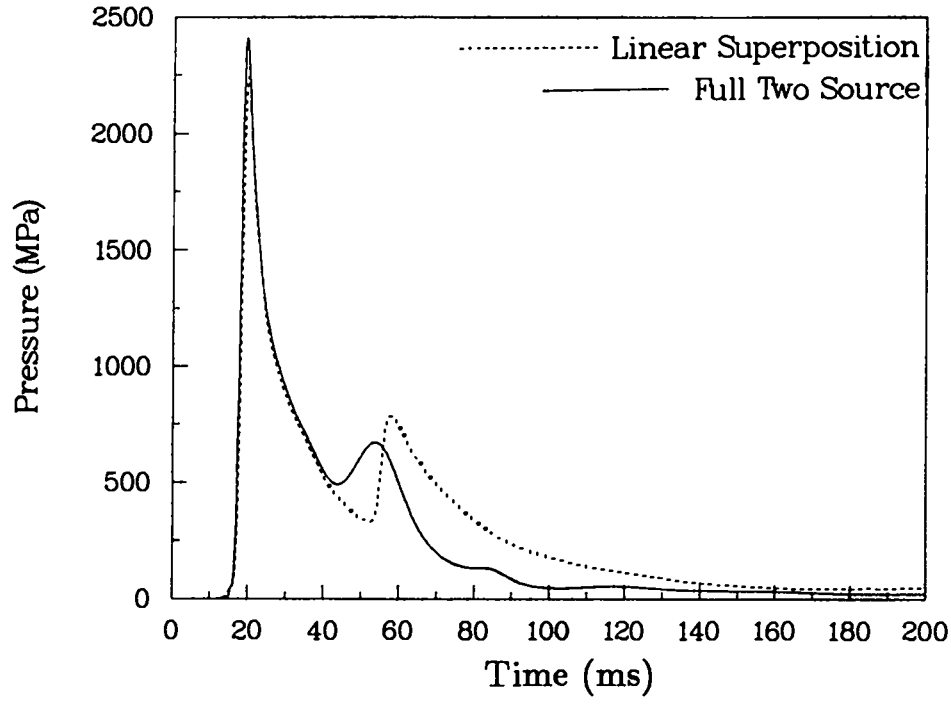

Fig. 40a. Pressure time histories at a location of x = 100 m and y = -800 m (theta=zero) for 0.005 air voids limestone: full two-source calculation and linear superposition. Notice later arrival of second superimposed signal.

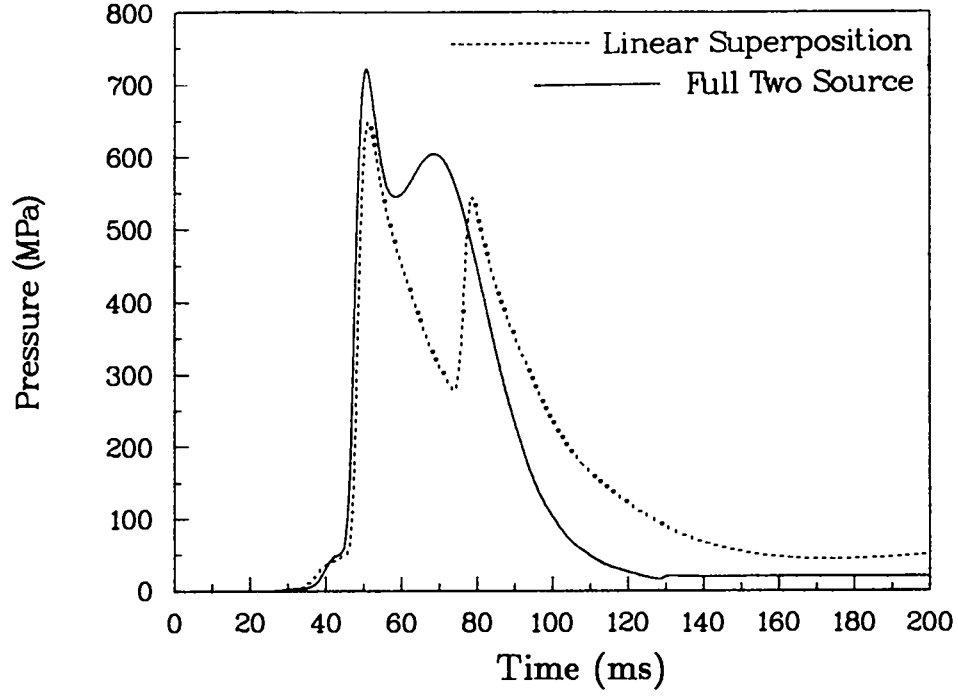

Fig. 40b. Pressure time histories at a location of x = 200 m and y = -800 m (theta=zero) for 0.005 air voids limestone: full two-source calculation and linear superposition. The peak pressures are governed by the initial signals.

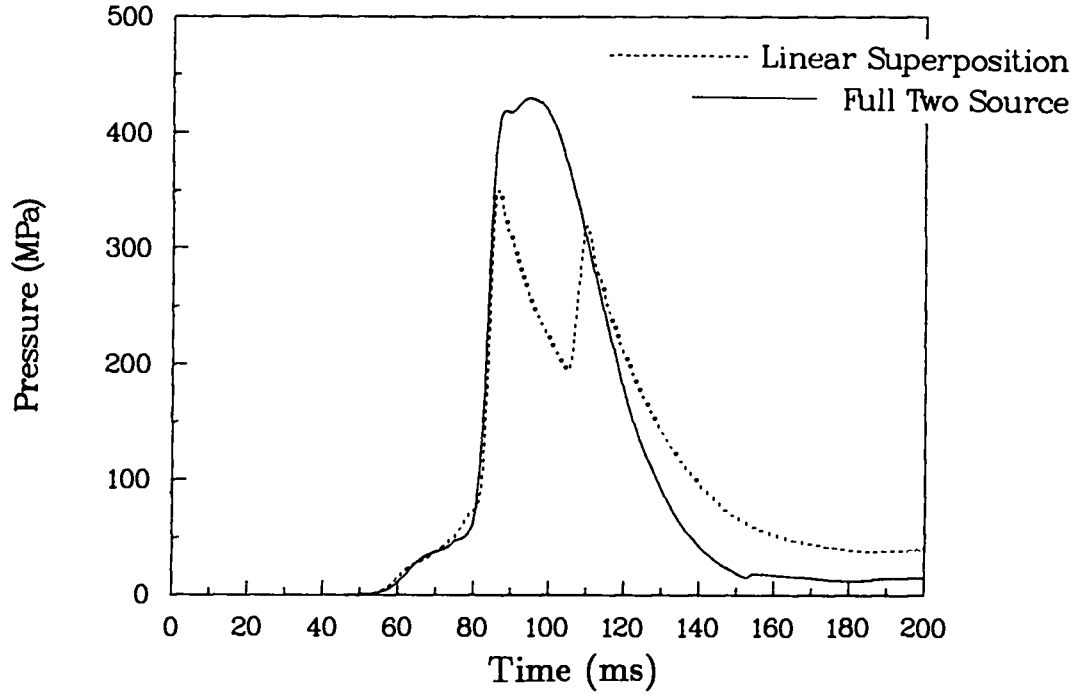

Fig. 40c. Pressure time histories at a location of x = 300 m and y = -800 m (theta=zero) for 0.005 air voids limestone: full two-source calculation and linear superposition. Superimposed signal is no longer a good predictor of peak value.

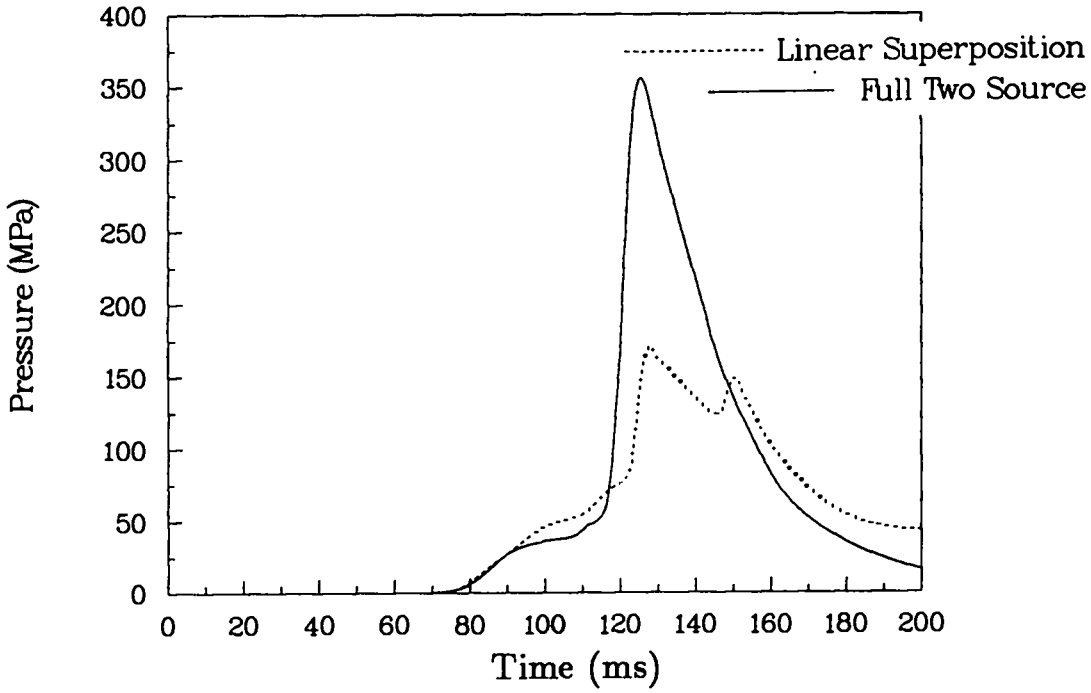

Fig. 40d. Pressure time histories at a location of x = 400 m and y = -800 m (theta=zero) for 0.005 air voids limestone: full two-source calculation and linear superposition. Second superimposed signal arrives too late to add to the peak.

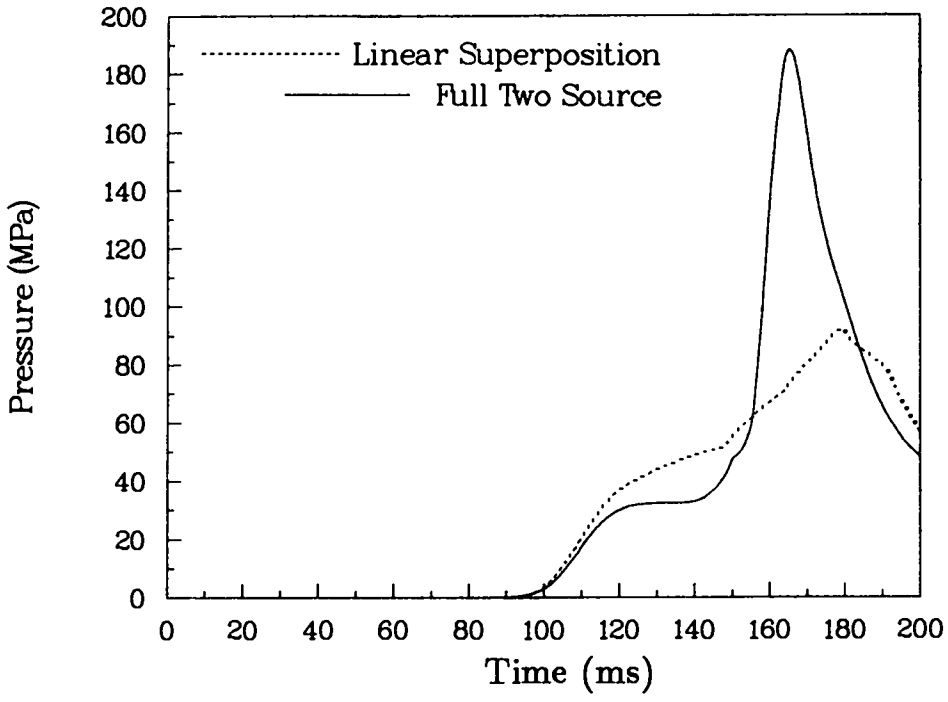

Fig. 40e. Pressure time histories at a location of x = 500 m and y = -800 m (theta=zero) for 0.005 air voids limestone: full two-source calculation and linear superposition. Note the significantly different response curves.

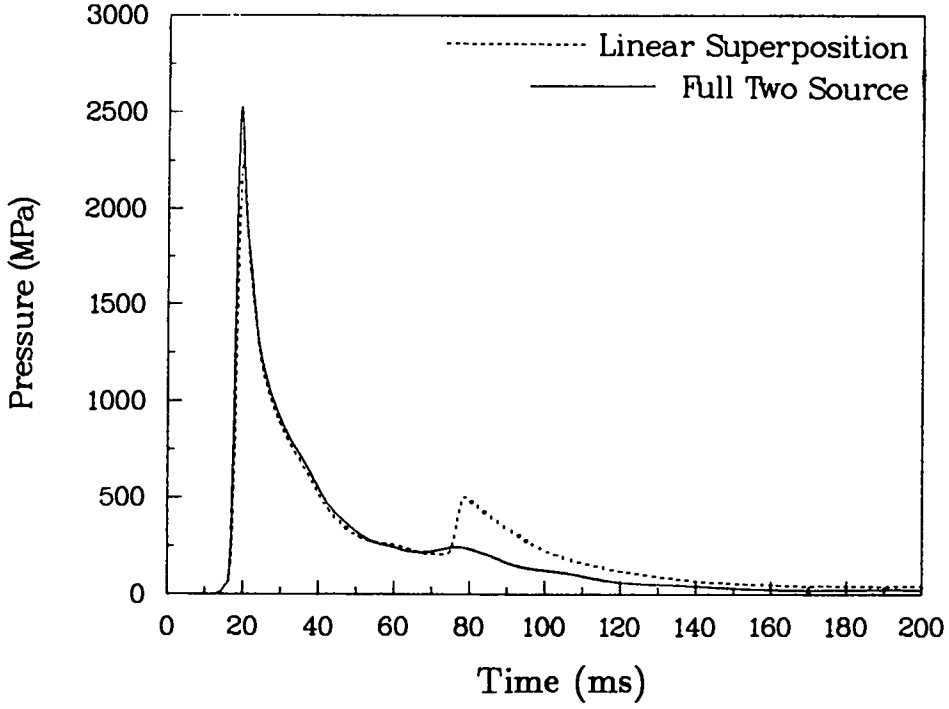

Fig. 41a. Pressure time histories at a range of 100 m and along the theta=45° line for 0.005 air voids limestone: full two-source calculation and linear superposition. There is a more pronounced superimposed signal.

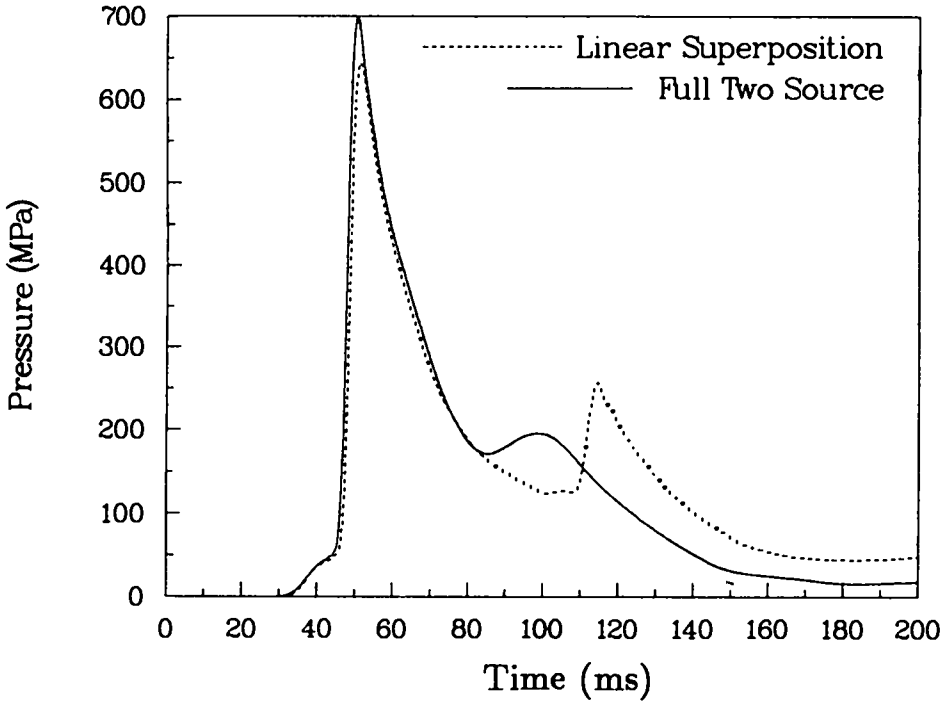

Fig. 41b. Pressure time histories at a range of 200 m and along the theta=45° for 0.005 air voids limestone: full two-source calculations and linear superposition. The second superimposed signal is arriving much later.

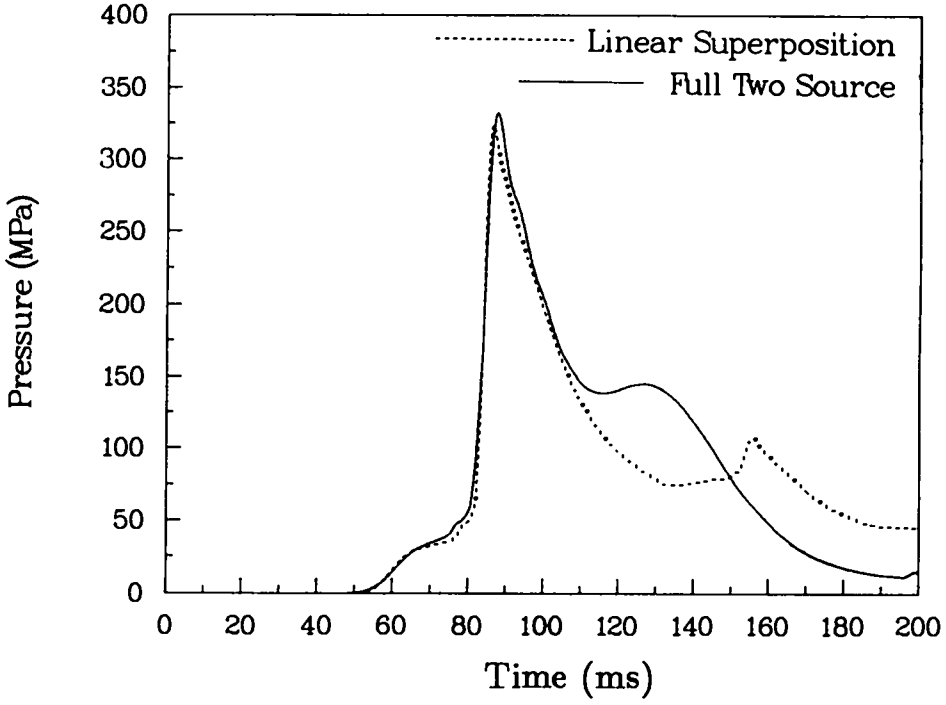

Fig. 41c. Pressure time histories at a range of 300 m and along the theta=45° line for 0.005 air voids limestone: full two-source calculation and linear superposition. The peak signal in both cases is still from the first source.

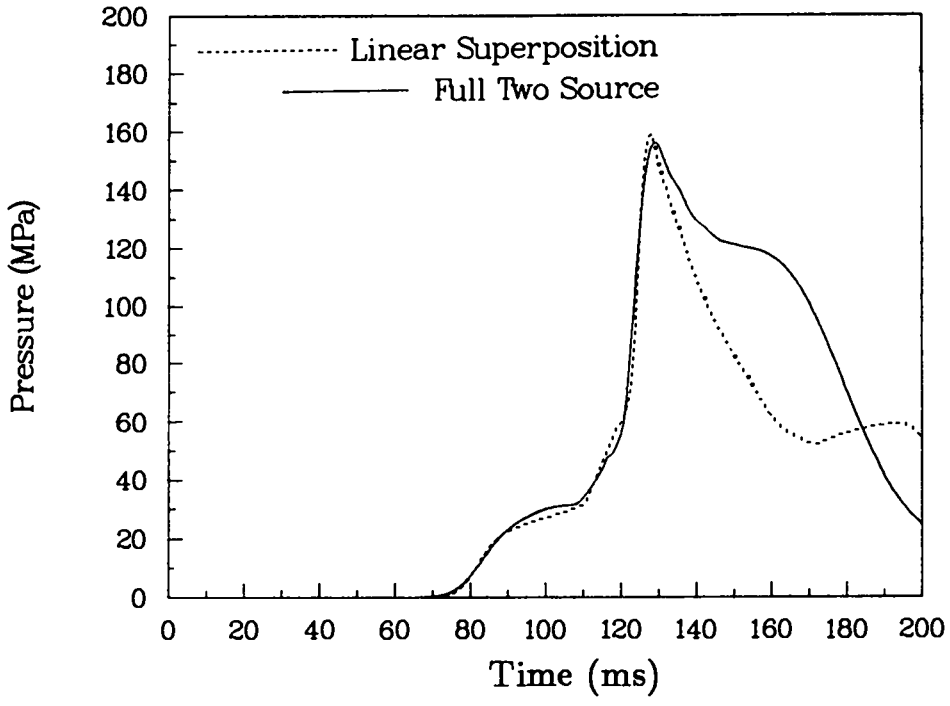

Fig. 41d. Pressure time histories at a range of 400 m and along the theta=45° for 0.005 air voids limestone: full two-source calculations and linear superposition. The peaks are both one-dimensional and of equivalent magnitude.

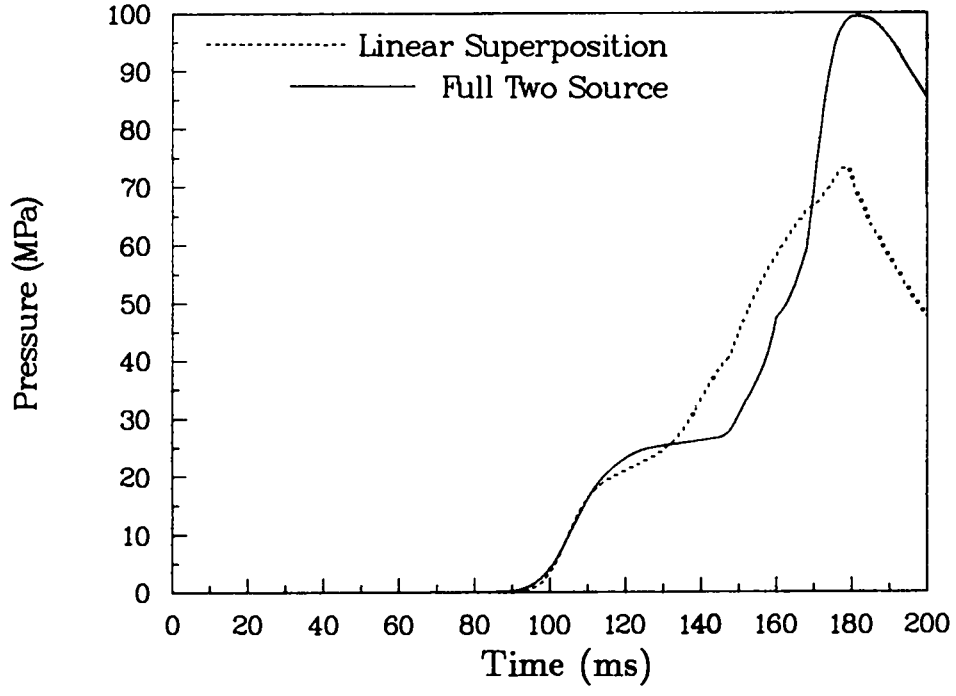

Fig. 41e. Pressure time histories at a range of 500 m and along the theta=45° line for 0.005 air voids limestone: full two-source calculation and linear superposition. Here the full two-source signals have combined into a single pulse.

the peak stress for the full two-source and superimposed solutions in unsaturated material. There is a bigger difference between the pressure and the maximum stress (generally in the radial direction) in this unsaturated case than when comparing Figs. 37 and 38 since the absolute stresses are lower and thus less likely to experience inelastic behavior, thus leading to a more isotropic stress state.

V. STRESS WAVE ENHANCEMENT WITH RESPECT TO A SINGLE BURST

All the calculations presented in this report have been performed entirely within a uniform material with no free surface effects. As a result, the calculations may be scaled to estimate the effects of different yields. For the full two-source calculations, the distance between the sources would scale with the cube root of the yield. Here, the one-dimensional calculations were scaled up from 500 kt to 1 Mt in order to determine the advantages and disadvantages of stress wave propagation of two separated 500-kt explosions with respect to a single burst of equivalent aggregate yield.

The scaling law allows for time and radial distance to scale with the cube root of the yield, while all other parameters remain the same. This technique has been used routinely in containment phenomenology. This means that the calculational variables from a 500-kt explosion at a given time are the same as for a 1-Mt explosion at a later time and at a greater distance, the magnitudes of which differ by a factor of the cube root of 2 over the 500-kt time and distance, respectively. Figure 44a shows a surface plot of pressure at 150 ms for a 1-Mt detonation in the saturated limestone. Since a comparison was to be made at 150 ms, these data are from 119 ms (150/ 1.26) and the x and y positions have been multiplied by 1.26 (cube root of 2). The scaled dimensions of the plot are therefore 700 x 700 m. The vertical axis maximum is 350 MPa (3.5 kbar) as before. This figure may be compared directly with Fig. 44b, which is the pressure distribution from the simultaneous detonation of two 500-kt bursts, separated by 200 m. This is one-fourth of the surface plot shown in Fig. 37b. The location of the 1-Mt explosion is at the point of double symmetry, i.e., the stagnation point. Several interesting observations may be made. Both signal peaks have traveled along the reflection axis (x-axis) about 525 m, but Fig. 44b shows

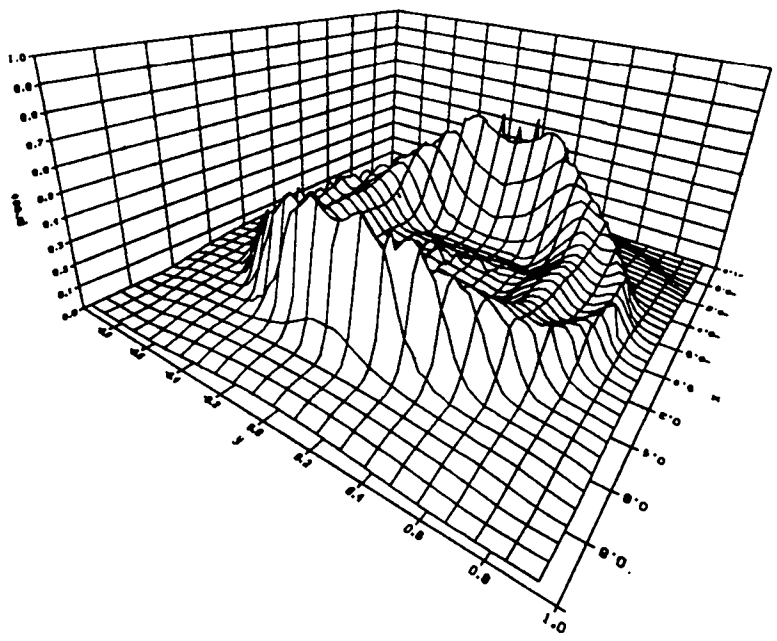

Fig. 42a. Surface plot of pressure at 150 ms in 0.005 air voids limestone for the full two-source calculation. This plot shows all the symmetry with an area of 1400 x 1400 m. The maximum z-axis value is 350 MPa (3.5 kbar). Notice the region of pressure addition and the other areas of essentially one-dimensional peak behavior. Compare this figure with Fig. 37a for the higher-magnitude saturated case.

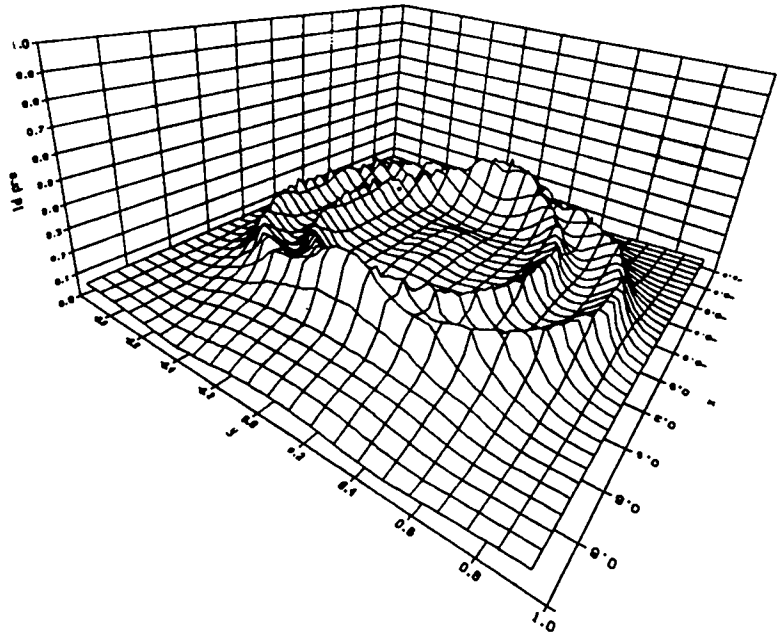

Fig. 42b. Surface plot of pressure at 150 ms in 0.005 air voids limestone using linear superposition. This plot shows all the symmetry with an area of 1400 x 1400 m. The maximum z-axis value is 350 MPa (3.5 kbar). Although the peak pressure along the reflection axis is similar to Fig. 35a, the magnitude drops off more rapidly along the azimuth. Also notice the more prominent second signal following the initial pulse. Compare this figure with Fig. 37b for the higher-magnitude saturated case.

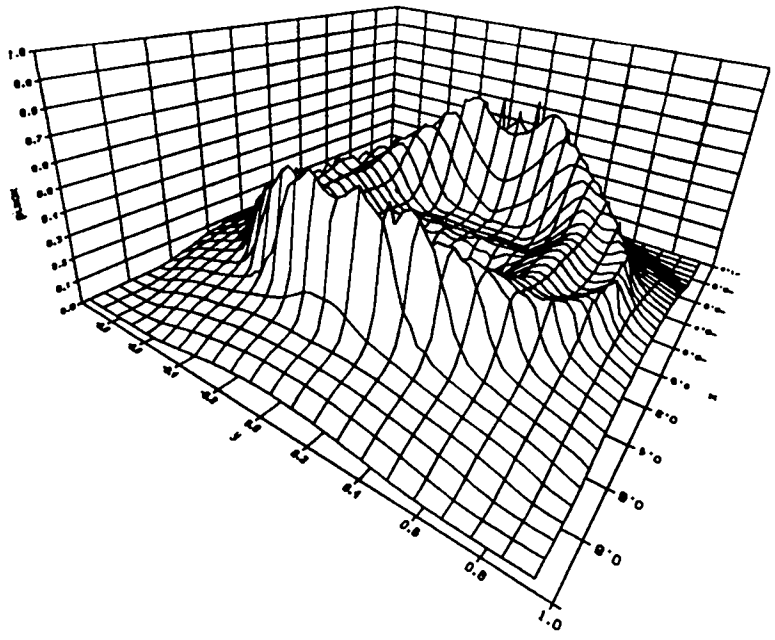

Fig. 43a. Surface plot of maximum stress at 150 ms in 0.005 air voids limestone for the full two-source calculation. This plot shows all the symmetry with an area of 1400 x 1400 m. The maximum z-axis value is 350 MPa (3.5 kbar). Notice the maximum stress in all locations is only slightly greater than the pressures in Fig. 42a.

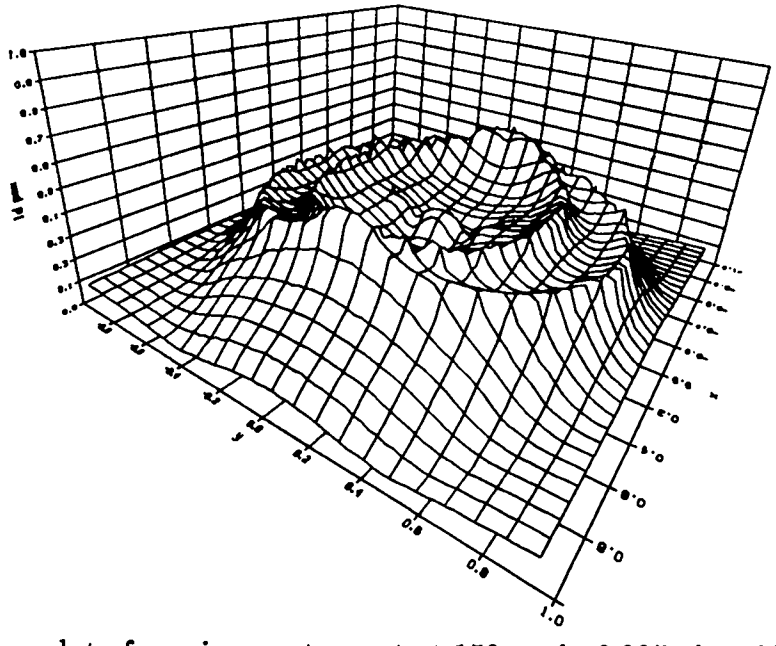

Fig. 43b. Surface plot of maximum stress at at 150 ms in 0.005 air voids limestone using linear superposition. This plot shows all the symmetry with an area of 1400 x 1400 m. The maximum z-axis value is 350 MPa (3.5 kbar). The maximum stresses show more of an increase over the pressures than in the saturated cases in Figs. 37b and 38b. Still, the maximum stress falls off away from the reflection axis.

approximately 30% greater amplitude. Along the axis of cylindrical symmetry (y-axis), the signal is significantly diminished (by about 30%) since the second 500-kt signal is well behind the shock front of the nearer source. Also notice that the 1-Mt signal is about 100 m behind the (essentially one-dimensional) 500-kt signal. This is because the large single burst was detonated midway between the 200-m-separated, smaller, simultaneous burst points.

A similar analysis was performed for material with one-half percent air-filled voids; the pressure distribution is shown in Fig. 45a at a scaled time of 150 ms. The scaled dimensions of the plot are 700 m as before. The equivalent simultaneous burst plot is in Fig. 45b. Although the magnitudes in this case are all smaller than for the saturated case, similar observations may be made. The peak pressure is now about 40% greater along the reflection axis but is only about 60% of the single burst value (but has traveled 100 m farther) along the axis of symmetry. Notice the location of the peak for the single burst is midway between the signals from the separated sources along this axis.

These plots clearly show where the signal is enhanced by separating the total yield and where there may be an advantage for a single large burst. This is a "snapshot" at a given time (150 ms), and different times will show variations but similar trends. Also, the advantage gained by the simultaneous detonation of two identical explosions may be strongly diminished by small differences in timing.

SUMMARY

The preceding sections have shown the results of the simultaneous detonation of two equal bursts in saturated material and material with one-half percent air-filled voids. In addition, a technique for the linear superposition of the stress tensor components was presented and utilized to determine the applicability of this approach for the two different materials. All calculations were fully contained, and there was no free surface and no gravity.

The properties of the two uniform materials are described in Table I, and the effect on compressibility is shown in Figs. 46a and 46b for saturated and one-half percent air-filled voids material, respectively. Generally, there were significantly enhanced pressures along

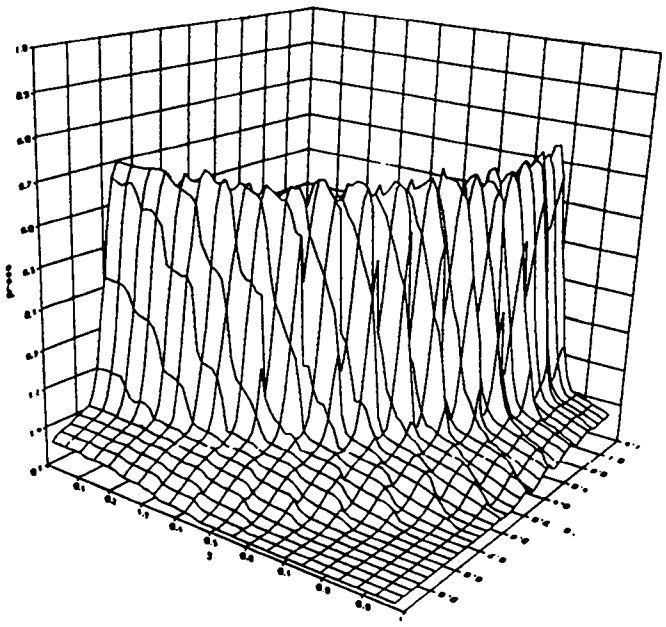

Fig. 44a. Surface plot of pressure from a scaled 1-Mt explosion in saturated limestone. The scaled area is 700 x 700 m and the scaled time is 150 ms. The maximum z-axis value is 350 MPa (3.5 kbar).

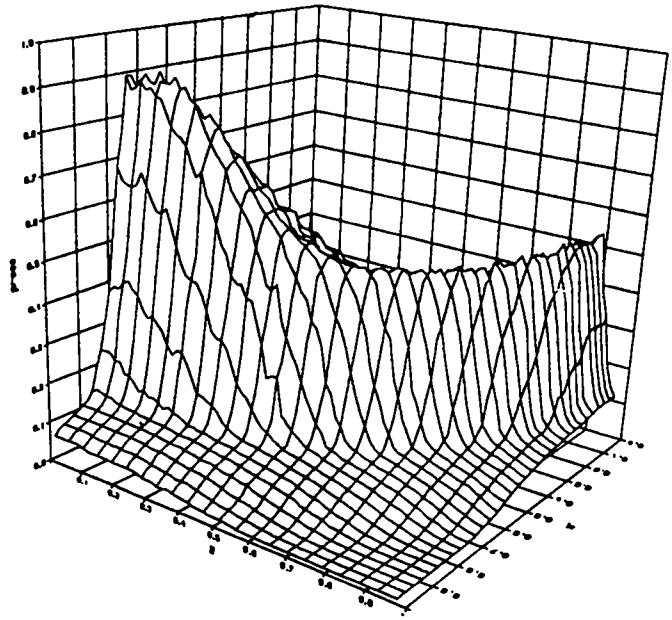

Fig. 44b. Surface plot of pressure from the two-source calculation presented earlier (see Fig. 37a). The area is 700 x 700 m and at a time of 150 ms. The maximum z-axis value is 350 MPa (3.5 kbar). Notice where the multiburst signal has greater amplitude along the reflection axis and where the combined single burst has higher pressures along the other axis. Notice also that the pressure front is about 100 m farther along the y-axis for the two-source calculation, reflecting one-half of the separation distance.

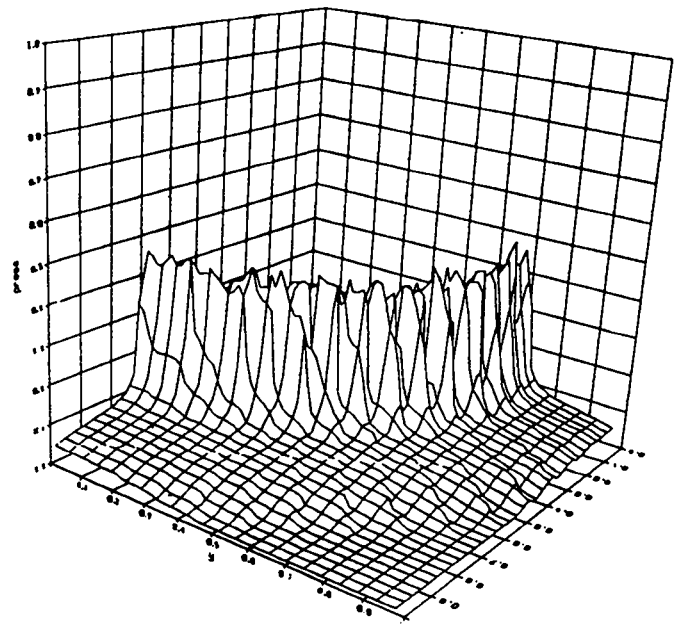

Fig. 45a. Surface plot of pressure from a scaled 1-Mt explosion in limestone with 0.005 air-filled voids. The scaled area is 700 x 700 m and the scaled time is 150 ms. The maximum z-axis value is 350 MPA (3.5 kbar).

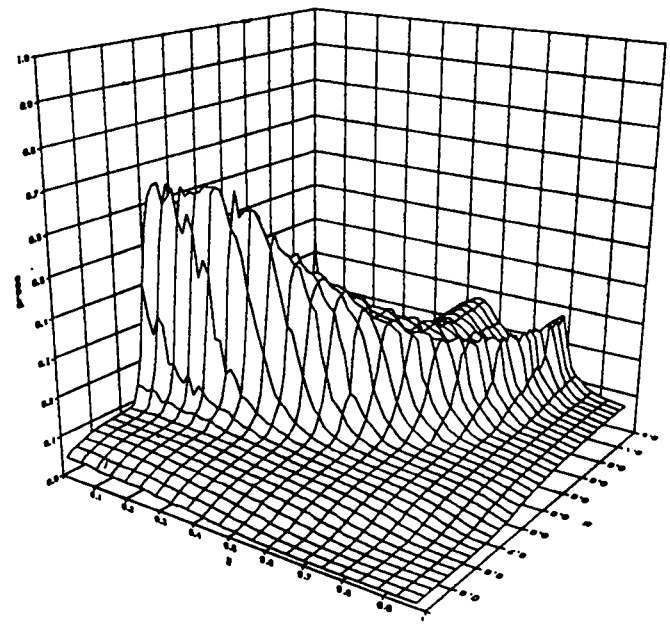

Fig. 45b. Surface plot of pressure from the two-source calculation in 0.005 air voids limestone. The area is 700 x 700 m and at a time of 150 ms. The maximum z-axis value is 350 MPa (3.5 kbar). Notice where the multiburst signal has greater amplitude along the reflection axis and where the combined single burst has higher pressures along the other axis. Compare Figs. 45a and 45b with Figs. 44a and 44b to see the effect of the air voids.

the reflection axis between the two sources, the relative magnitude of which diminished with range (time) from the point of double symmetry. The peak pressure was about 350 MPa (3.5 kbar) at 600 m in the saturated case and 200 MPa (2 kbar) at 600 m for the unsaturated case. Although both calculations were run to 200 ms, boundary effects were beginning to influence the calculation. A larger mesh or smaller yields would be required to determine the distance to 100 MPa (1 kbar).

The results from one-dimensional calculations were superimposed to determine if this method could reproduce the full two-source results. The results were mixed. For the saturated case this technique worked reasonably well. Peak pressures and stresses were predicted with reasonable accuracy and time histories at selected locations were quite similar. At selected times, the peak stress and pressure fields were in reasonable agreement, although the peak values dropped off too rapidly in the azimuthal direction from the reflection axis toward the other axis of symmetry. The superposition of one-dimensional results from an explosion in material with one-half percent air-filled voids did not match the two-source calculation well at all except at very early times, at short ranges from the point of double symmetry along the reflection axis. This was because the signal from the nearer source compacted material as the shock front moved radially away in the full two-source calculation. The signal from the second source traveled at a faster velocity for significant distances, and it was not attenuated because very little additional compaction was possible. As a result, the second signal traveled faster and was able to merge with the first signal to form a single pulse of much higher amplitude. When the one-dimensional results were superimposed, by the time the second signal arrived, the first had nearly dropped to zero at ranges beyond 300 m. The peak pressure at 600 m at 150 ms was only 100 MPa (1 kbar) as predicted by superposition.

Contours of peak overstress show the footprint, or regions subjected to constant levels of a given stress amplitude. Figures 47a and 47b show footprints of peak maximum principle stress at 150 ms in saturated material as determined by the full two-source calculation and linear superposition, respectively. The latter was generated by using the single source time histories at 10-m intervals (described earlier) to create areal distributions of maximum principle stress at 5-ms intervals. Time was incremented up to 150 ms, and the

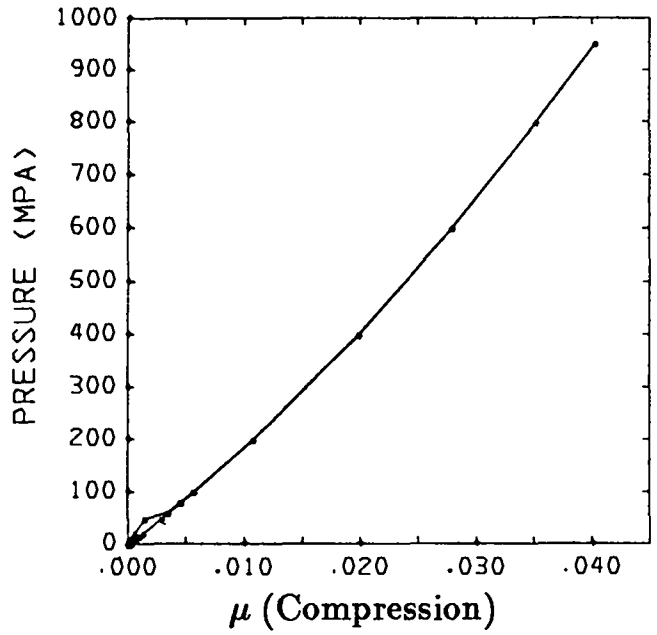

Fig. 46a. Crush curve for saturated limestone up to 1000 MPA (10 kbar). The compression μ is related to the initial density, $\mu = \rho/\rho_o$ - 1. Notice the initial slightly higher slope during loading at low stress levels.

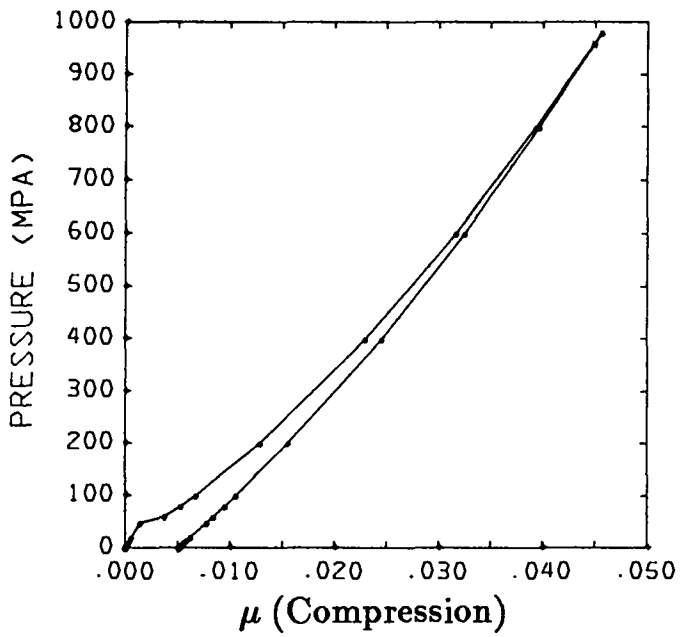

Fig. 46b. Crush curve for limestone with one-half percent air-filled voids up to MPa (10kbar). The compression μ is related to the initial density, $\mu = \rho/\rho_o$ - 1. Notice the slightly higher slope during initial loading, a merge pressure of about 900 MPa (9 kbar) and an unrecoverable volumetric strain of 0.5%.

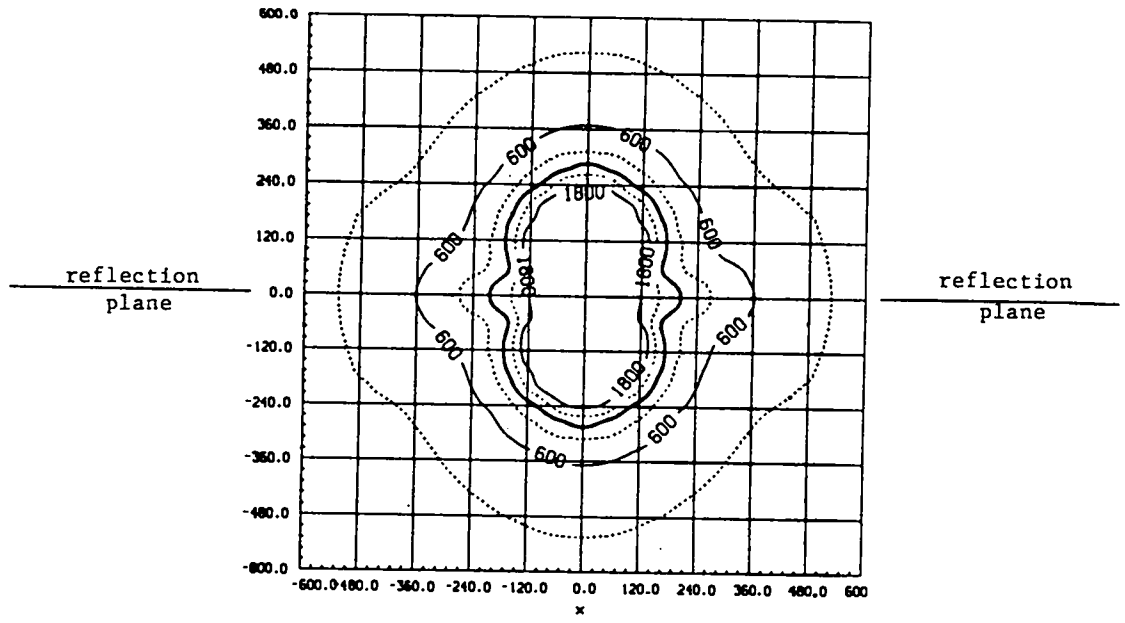

Fig. 47a. Footprint contours of peak maximum principle stress for detonation in saturated limestone by 150 ms as generated by the full two-source calculation. Maximum plotted values are 2000 MPa (20 kbar). Notice the higher stress contours are elliptical, and the lower values look more circular as if they were from a single source.

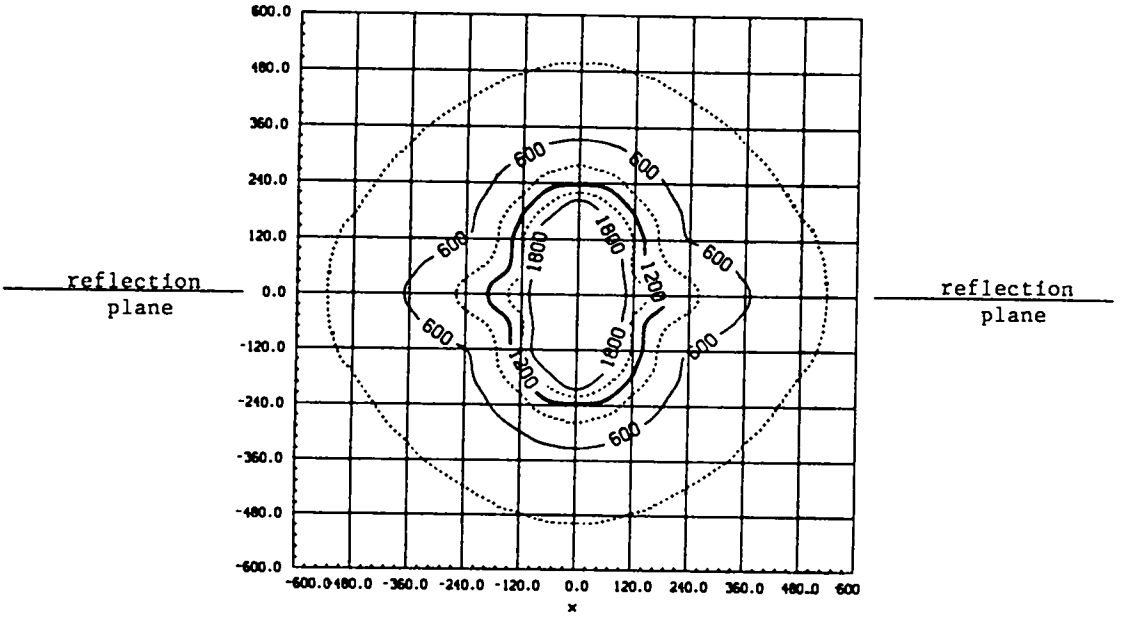

Fig. 47b. Footprint contours of peak maximum principle stress for detonation in saturated limestone by 150 ms as generated by linear superposition. Maximum plotted values are 2000 MPa (20 kbar). Notice the similarity in size and shape to the full two-source results in Fig. 47a.

value at each concentric intersection (see Fig. 30) was either updated with a higher value or maintained at a previous peak for each 5-ms time step. The maximum value allowed was 2000 MPa (20 kbar). Notice that the contour levels in Figs. 47a and 47b are similar in size and shape, particularly at lower values. This indicates that while superposition does slightly underpredict the footprint, the agreement is good in saturated material.

Equivalent footprint contours are plotted for detonation in unsaturated material in Figs. 48a and 48b. Notice that the linear superposition contour levels (Fig. 48b) show substantially smaller bounded areas. Also notice that the full two-source calculation shows a much wider region of influence along the 300-MPa (3-kbar) contour line along the reflection axis. These plots clearly show that linear superposition is less reliable for predicting response in material with one-half percent air-filled voids.

For comparison, peak maximum principle overstress is plotted for scaled 1-Mt explosions at the point of double symmetry by 150 ms. Figures 49a and 49b show the contour levels for the response in saturated material and one-half percent air-filled voids material, respectively.

CONCLUSIONS

There are two general conclusions. First, significant enhancement may be obtained from the simultaneous detonation of two equal bursts. Second, linear superposition may be used with some confidence to determine the effects of timing and different yields but only in saturated material. Further numerical calculations are anticipated to do exactly that and also to run the full two-source calculations out to distances to determine the range and footprint of material exposed to stresses in excess of 100 MPa (1 kbar).

The advantage of simultaneous detonation of two identical bursts over a single large burst was shown to extend significantly beyond the reflection axis. The magnitude of the advantage seems to be slightly greater in material with one-half percent air-filled voids, although the absolute magnitudes of the stresses are significantly lower than in saturated material. The effect of timing on the stress enhancement should be addressed before any final conclusions are drawn.

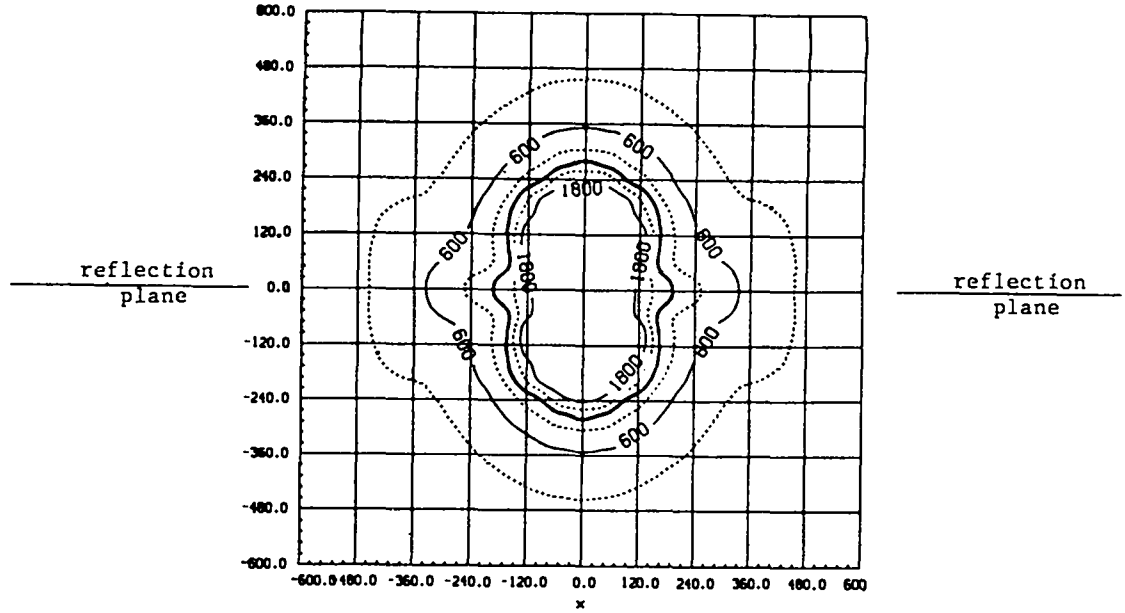

Fig. 48a. Footprint contours of peak maximum principle stress for detonation in limestone with 0.5% air-filled voids by 150 ms as generated by the full two-source calculation. Maximum plotted values are 2000 MPa (20 kbar). Notice the extent of the 300-MPa (3-kbar) contour in the vicinity of the reflection axis and the resulting noncircular shape.

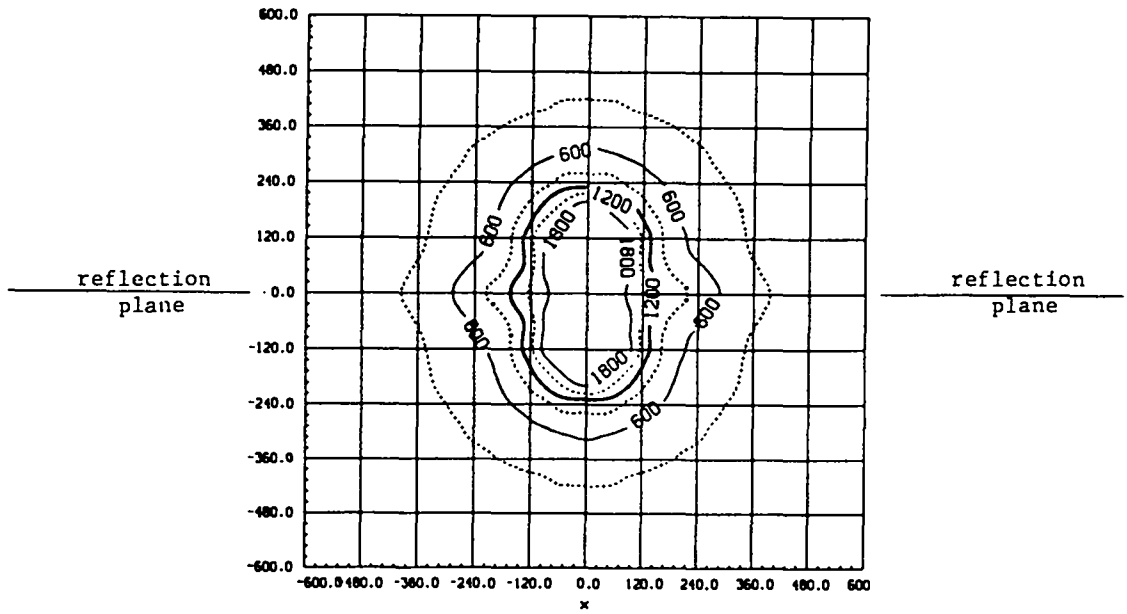

Fig. 48b. Footprint contours of peak maximum principle stress for detonation in limestone with 0.5% air-filled voids by 150 ms as generated by linear superposition. Maximum plotted values are 2000 MPa (20 kbar). Notice that the contours at every level bound significantly smaller areas than the full two-source results in Fig. 48a. The 300-MPa (3-kbar) level significantly underestimates the extent when compared with the full two-source calculation, particularly in the vicinity of the reflection axis.

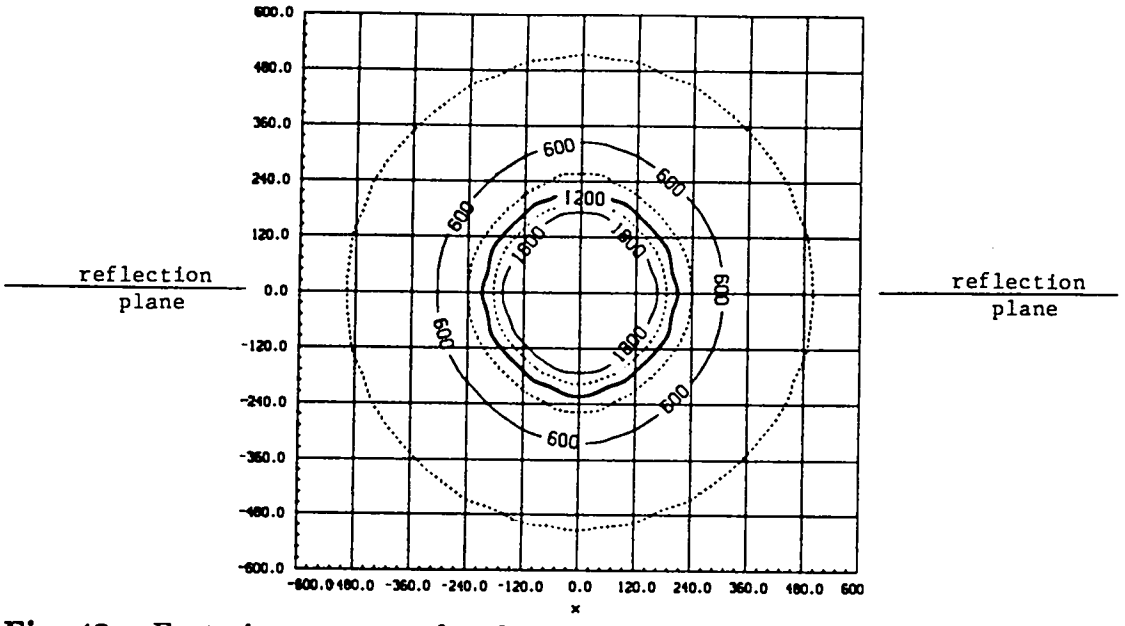

Fig. 49a. Footprint contours of peak maximum principle stress for detonation in saturated limestone by 150 ms as generated by a scaled 1-Mt single source. Maximum plotted values are 2000 MPa (20 kbar). Notice the circular shape of all contours and compare with the results shown in Figs. 47a and 47b.

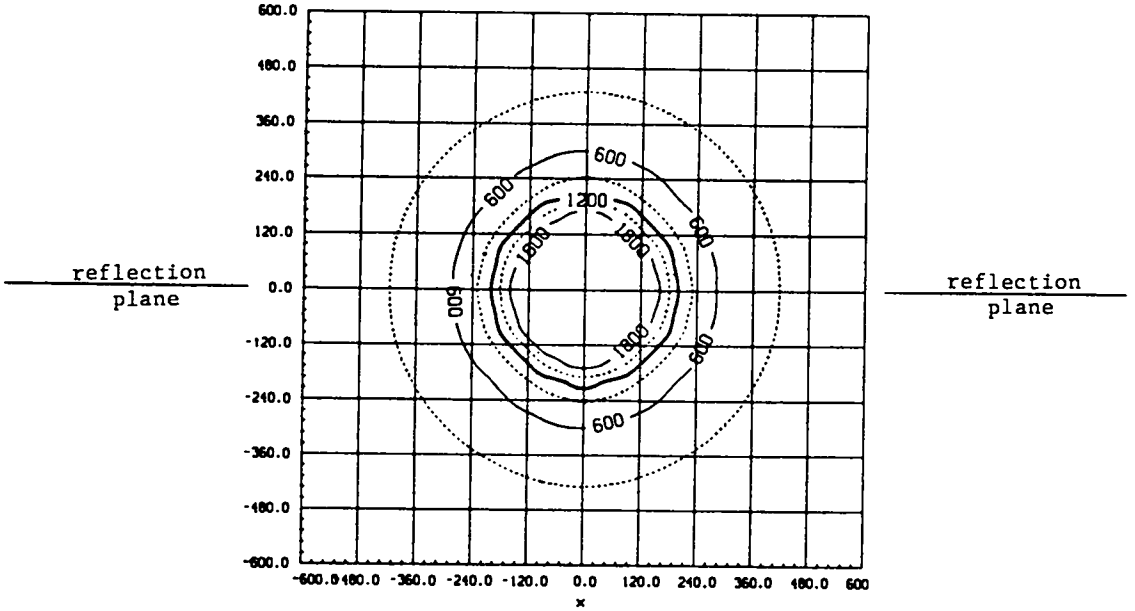

Fig. 49b. Footprint contours of peak maximum principle stress for detonation in limestone with 0.5% air-filled voids by 150 ms as generated by a scaled 1-Mt single source. Maximum plotted values are 2000 MPa (20 kbar). Notice the circular shape of all contours and compare with the results shown in Figs. 48a and 48b.

ACKNOWLEDGMENTS

I would like to thank the other members of the SHALE team for their contributions to the SHALE code: Robert Deupree, Tom Dey, Hunter DeVault, and Norris Nickols. This work was supported by the U.S. Department of Energy.

REFERENCES

Demuth, R.B., L.G. Margolin, B.D. Nichols, T.F. Adams, and B.W. Smith, "SHALE: A Computer Program for Solid Dynamics," Los Alamos National Laboratory report LA-10236 (May 1985).

DeVault, G. P., "Preliminary Surface Ground Motion Calculations of Underground Nuclear Explosions," Proceedings of the Fourth Symposium on Underground Nuclear Explosions, Colorado Springs, Colorado (1987).

Margolin,L. G., and B.W. Smith, "A Criterion for Quasibrittle Crack Growth, "Proceedings of the 24th U.S. Symposium on Rock Mechanics," American Institute of Mining, Metallurgical, and Petroleum Engineers, New York (1984).

Margolin, L. G., D. E. Burton, W. P. Crowley, and B. C. Trent, "Computer Simulation of Nuclear Weapons Effects," Proceedings of the Second Military Computing Conference, Anaheim, California (1988).

Mase, G.E, *Continuum Mechanics* (McGraw-Hill, New York, 1970).

Page Range	NTIS Price Code	Page Range	NTIS Price Code	Page Range	NTIS Price Code	Page Range	NTIS Price Code
001–025	A02	151–175	A08	301–325	A14	451–475	A20
026–050	A03	176–200	A09	326–350	A15	476–500	A21
051–075	A04	201–225	A10	351–375	A16	501–525	A22
076–100	A05	226–250	A11	376–400	A17	526–550	A23
101–125	A06	251–275	A12	401–425	A18	551–575	A24
126–150	A07	276–300	A13	426–450	A19	576–600	A25
						601-up*	A99

*Contact NTIS for a price quote.

Los Alamos National Laboratory
Los Alamos, New Mexico 87545